Title

An optimized differentiation protocol produces robust endothelial cells essential for a physiologically relevant 3D in vitro angiogenesis model

Author

Natividad, Sylvia Lucia

Publication Date

2017

Peer reviewed|Thesis/dissertation

An optimized differentiation protocol produces robust endothelial cells essential for a physiologically relevant 3D *in vitro* angiogenesis model

By

Sylvia Lucia Natividad

A dissertation submitted in partial satisfaction of the

requirements for the degree of

Joint Doctor of Philosophy
with the University of California, San Francisco

in

Bioengineering

in the

Graduate Division

of the

University of California, Berkeley

Committee in charge:

Professor Kevin Healy, Chair
Professor Tejal Desai
Professor Helen Bateup

Fall 2017

An optimized differentiation protocol produces robust endothelial cells essential for a physiologically relevant 3D *in vitro* angiogenesis model

By
Sylvia Lucia Natividad

University of California, Berkeley

Abstract

An optimized differentiation protocol produces robust endothelial cells essential for a physiologically relevant 3D *in vitro* angiogenesis model

By

Sylvia Lucia Natividad

Doctor of Philosophy in Bioengineering

University of California, Berkeley

Professor Kevin Healy, Chair

Human induced pluripotent stem cell (hiPSC) derived angiogenesis models present a unique opportunity for patient-specific platforms to study the complex process of angiogenesis and the endothelial cell response to biochemical and biophysical changes in a defined microenvironment. This dissertation presents a robust method for differentiating hiPSCs into a CD31+ endothelial cell population (hiPSC-ECs) using a chemically defined basal medium from the pluripotency stage to the final stage of differentiation and the development of a physiologically relevant *in vitro* angiogenesis model. The endothelial cell differentiation was validated through phenotype characterization, gene expression studies, and lineage-specific function assays. This protocol produced robust, functional endothelial cells in a shorter period of time relative to current reports since a maturation period was not required. Subsequently, the hiPSC-ECs were incorporated into a tunable, growth factor sequestering hyaluronic acid (HyA) matrix that formed stable, capillary-like networks that responded to environmental stimuli in a physiologically relevant manner. An *in vitro* angiogenesis model containing the HyA matrix and hiPSC-ECs was then developed within a tri-chamber microfluidic device that demonstrated perfusion of the capillary networks. Finally, an *in vitro* cardiovascular tissue model was developed by culturing hiPSC derived cardiomyocytes (CMs) in the HyA hydrogel with the hiPSC-ECs. The hiPSC-CMs demonstrated a limited ability to survive, function, and support angiogenesis within the hydrogel.

Chapter 3 presents a novel endothelial cell differentiation method from human pluripotent stem cells that was developed and validated in this study. The phenotype and gene expression of the total differentiated population and the purified CD31+ population were characterized for endothelial lineage with phase contrast microscopy, flow cytometry, fluorescence microscopy, and RT-qPCR analysis. The purified endothelial cell population was further validated with functional assays including Ac-LDL uptake and network formation within a Matrigel angiogenesis assay.

Chapter 4 presents a study to assess the behavior of the hiPSC-ECs (from chapter 3) in a growth factor sequestering hyaluronic acid (HyA) matrix, which promoted cell survival and maintenance of lineage-specific function. The system's ability to respond to biochemical and biophysical cues was demonstrated through characterization of changes in tube formation with confocal microscopy and measurement of nitric oxide production using a fluorescence-based Griess assay. The dependence of network formation on proangiogenic signaling was further demonstrated by treatment with a small-molecule VEGFR2/FGFR inhibitor, which eliminated network formation and permitted the calculation of an IC_{50} value. An *in vitro* angiogenesis model containing the HyA matrix and hiPSC-ECs was then developed within a tri-chamber microfluidic device that demonstrated perfusion of the hollow capillary tube networks. A fluid dynamics analysis of the HyA flow through the microfluidic device's capillary burst valve (CBV) system during sample loading is also discussed.

Chapter 5 demonstrates the study of an *in vitro* cardiovascular tissue model that is developed by culturing hiPSC-CMs in the HyA hydrogel alone and with the hiPSC-ECs. The hiPSC-CMs ability to survive, function, and support angiogenesis within the hydrogel was analyzed through live/dead fluorescence staining, beat rate analysis with motion tracking software, and confocal microscopy characterization of the cellular morphology, organization, and sarcomere structure.

Dedicated to my amazing and inspiring husband, Nathan M. Diaz

Table of Contents

List of Figures

List of Tables

List of Abbreviations

AcHyA (Hya)	Acrylated hyaluronic acid
ADH	Adipic acid dihydrazide
bFGF (FGF2)	Basic fibroblast growth factor
bpm	Beats per minute
BSA	Bovine serum albumin
bsp-RGD	Bone sialoprotein-RGD [arginine (R), glycine (G), aspartic acid (D)]
CBV	Capillary burst valve
CM	Cardiomyocyte
EC	Endothelial cell
ECM	Extracellular matrix
EDC	1-ethyl-3-(3-dimethylaminopropyl) carbodiimide hydrochloride
HyA-850 R	3wt% AcHyA +WTC hiPSC-EC+RPMI B27 complete media
HyA-850 E	3wt% AcHyA +WTC hiPSC-EC+EGM2 media
HyA-850 ET	3wt% AcHyA +WTC hiPSC-EC+EGM2 media + TGFβ1 (gel)
HyA-850 EV	3wt% AcHyA +WTC hiPSC-EC+EGM2 media + VEGFA165 (gel)
HyA-170 E	2wt% AcHyA +WTC hiPSC-EC+EGM2 media
FC	Flow cytometry
FGFR	Fibroblast growth factor receptor
GF	Growth factor
IF	Immunofluorescence
hESC	Human embryonic stem cell
hiPSC	Human induced pluripotent stem cells
HyA	Hyaluronic acid
MW	Molecular weight
MMP	Matrix metalloproteinase
NMR	Nuclear magnetic resonance
PBS	Phosphate-buffered saline
ΔP_d	Driving pressure difference
ΔP_{max}	Maximum pressure difference
PCR	Polymerase chain reaction
RT-qPCR	Reverse Transcription-quantitative polymerase chain reaction
TEOA	Triethanolamine buffer
TGF-β1	Transformation growth factor beta 1
v_{AcHyA}	loading velocity for AcHyA
$v_{e,AcHyA}$	Equilibrium loading velocity for AcHyA
$v_{e,water}$	Equilibrium loading velocity for water
v_{water}	loading velocity for water
VE-CAD (VCAD)	Vascular endothelial cadherin
VEGF-A	Vascular endothelial growth factor A
VEGFR2	Vascular endothelial growth factor receptor 2
WTC	Wilde type C (hiPSC line)

Acknowledgements

I am very grateful for having the opportunity to obtain my doctoral education and training at U.C. Berkeley. I would like to thank my advisor, Professor Kevin Healy, for giving me the opportunity to work in his lab and pursue a project that not only aligned with my research interests but also allowed me to learn important technical skills that will help advance my scientific career. I'm also very appreciative of all his support throughout graduate school; his advice and guidance were essential components to the successful completion of my doctoral degree. I would also like to thank the members of my dissertation and qualifying exam committee, Professor Tejal Desai, Professor Helen Bateup, Professor Song Li, and Professor Niren Murthy. I really appreciate the time they took to meet with me and provide insight and advice on my dissertation project.

During my doctoral training, I met and got to work with so many interesting and intelligent scientists, engineers, and students in the Healy Lab. I would like to especially thank Amit Jha, Shane Browne, and Zhen Ma for being my mentors during their postdoctoral training in the Healy lab and teaching me essential skills for my research project. I want to also thank Brian Siemons, our lab manager, for all his help and assistance with lab matters and experiments. I'm also thankful to Mary West, who manages the U.C. Berkeley Stem Cell Center, for training me on several biological characterization instruments and for being so supportive of my work. I also want to acknowledge Felipe Montiel, Felicia Svedlund, Naomi Kohen, and all the Healy lab members I had the opportunity to meet for their advice, friendship, and scientific discussions.

Additionally, I'm immensely grateful to my funding sources throughout graduate school. The National Science Foundation Graduate Research Fellowship Program (NSF GRFP) helped me get started and established at U.C. Berkeley. The National Institute of Health T32 Stem Cell Engineering Training program provided me with so many great opportunities to meet scientists outside my department and field. I also got the opportunity to learn more about ethics and regulations regarding stem cell research. Finally, the Siebel Scholars Foundation fellowship supported me during my last year of graduate school and allowed me to focus on the rigor of finishing my dissertation.

I'm incredibly fortunate to have such a loving and supportive husband who came with me on this journey to pursue a doctoral degree. I am so grateful for all his love, patience, encouragement, advice, and friendship throughout graduate school. Nathan created a home for us in a completely new place where we didn't know anyone and he helped me stay focused. I also want to thank my brother and my parents for their support and encouragement during my doctoral work. Despite our challenging circumstances, they encouraged and nurtured my aptitude for science and math from a young age and taught me to be resilient. I also want to thank my mother and father in-law, who are like second parents to me. They were extremely supportive in my pursuit of a doctoral degree and their unwavering encouragement helped keep Nathan and me moving forward. I am extremely grateful to all my family and friends for their support and encouragement.

CHAPTER 1:
MOTIVATION, SPECIFIC AIMS, AND DISSERTATION OUTLINE

1.1 Motivation

Pathological angiogenesis and vascular diseases are the underlying problem in many life-threatening illnesses. The pathological growth and proliferation of blood vessels, termed the "activated aniogenic switch", is one of the six hallmarks of tumor growth and cancer progression[1]. The WHO reports the global burden of cancer deaths in 2015 to be 8.8 million people and estimates the total annual economic cost of cancer in the U.S. to be $1.16 billion[2]. Cardiovascular disease refers to damaged, narrowed, or blocked blood vessels composed of dysfunctional endothelial cells that can cause a stroke or myocardial infarction [3,4]. According to the 2017 Heart Disease and Stroke Statistics Update by the American Heart Association, Cardiovascular Diseases (CVD) including atherosclerosis, myocardial infarction, stroke, peripheral artery disease, and venous disease collectively remain the leading causes of death in the United States [5]. Additionally, the World Health Organization cites CVD as the leading cause of death worldwide and expects the death rate to continue rising within the next 15 years regardless of socioeconomic backgrounds [6].

Angiogenesis is a complex process that is involved in disease progression and tissue repair, yet it is not fully understood. The multifaceted mechanisms of angiogenesis along with the relatively high cost and technical skill level associated with *in vivo* studies make it difficult to efficiently evaluate the efficacy of therapies intended to promote angiogenesis [7-9]. *In vitro* models provide a less expensive, more controlled, and reproducible platform for better quantification of isolated angiogenic processes in response to a biochemical or biophysical stimulus [9-13].

Current *in vitro* angiogenesis models have provided insight into this process; however, many continue to rely on primary endothelial cells or immortalized cell lines (HUVEC, HMEC, HAEC, etc) [9,14-16]. This limits the genetic diversity of the test samples so that patients from different backgrounds (gender, age, race/ethnicity, etc) are not represented in the studies. Furthermore, primary cell lines are limited in supply and are notoriously difficult to culture and expand, so they are not a sustainable source for *in vitro* studies. Additionally, HUVECs have a tendency to form unstable capillary structures *in vitro* that quickly and spontaneously regress. Many studies include secondary stromal cells, often from a different source, to stabilize these capillary-like networks [15-18]. However, this approach adds a confounding factor since it is unclear if the ECs are directly affected by the treatment in question or if they are reacting to the fibroblast response.

In contrast to primary endothelial cells, human induced pluripotent stem cell (**hiPSC**) derived endothelial cells (**hiPSC-ECs**) have the potential to provide a limitless supply of patient-specific vascular cells to research pathological angiogenesis, vascular diseases, and regeneration of ischemic tissues. Incorporating hiPSC-ECs into angiogenesis models provides a unique, patient-specific platform to study *in vitro* the complex process of

angiogenesis and endothelial cell response to biochemical and biophysical changes in their microenvironments [19-23].

Toward this end, significant progress has been made in directed differentiation protocols for human pluripotent stem cell monolayers to the endothelial cell lineage. However, many issues remain with total differentiation time, late stage expression of mature endothelial cell markers, and the use of several different culture medias for a single differentiation. Total differentiation time is a significant problem and needs to be decreased, since most protocols consist of a 5-10 day differentiation process with an additional maturation phase that can last up to 60 days before the ECs can be used in a functional assay [23-28]. Additionally, many of these studies don't observe the expression of mature endothelial cell markers such as CD31 and VE-Cadherin until the final day of differentiation (Day 5-7) or after the maturation phase (Day 12-15) [23-28]. Furthermore, current protocols entail the use of more than one media formulation, including MEF conditioned media, from the pluripotency stage to the differentiation and maturation process [18,22-28]. Taking into account the culture and maintenance of the pluripotent stem cells prior to differentiation, the total process can take up to 3 months with 2-3 different media formulations.

This dissertation presents a novel method for obtaining a CD31+ endothelial cell population from hiPSCs that requires the use of a chemically defined basal medium from the pluripotency stage to the final stage of differentiation, and does not require a maturation period. To assess the behavior of these hiPSC-ECs, a growth factor sequestering hyaluronic acid (HyA) matrix was used to promote cell survival and maintenance of lineage-specific function [29-31]. HyA offers many benefits as a matrix to support hiPSC-ECs, since it is a naturally occurring biopolymer that is biocompatible, biodegradable, non-immunogenic, and has been shown to promote cell migration, proliferation, and angiogenesis in wound healing processes [29-33].

hiPSC-ECs were encapsulated within the HyA matrix and their ability to respond to biochemical and biophysical cues was demonstrated with dynamic, and corresponding changes in capillary-like network formation and nitric oxide production similar to physiological angiogenesis. The dependence of network formation on proangiogenic signaling was further demonstrated by treatment with a small-molecule VEGFR2/FGFR inhibitor which eliminated network formation and permitted the calculation of an IC_{50} value that was in agreement with previous reports. An *in vitro* angiogenesis model containing the HyA matrix and hiPSC-ECs was then developed within a tri-chamber microfluidic device that demonstrated perfusion of the hollow capillary tube networks.

Finally, an *in vitro* cardiovascular tissue model was developed by culturing hiPSC-CMs in the HyA hydrogel alone and with the hiPSC-ECs. The hiPSC-CMs demonstrated a limited ability to survive, function, and support angiogenesis within the hydrogel. These results highlight the complexity of recapitulating multi-cellular tissues *in vitro*. They indicate the cells are not interacting in a physiologically relevant manner when co-cultured, since cardiomyocytes and endothelial cells engage in mutually beneficial paracrine signaling in the human myocardium.

1.2 Specific Aims

1 Characterize and validate novel directed differentiation method for obtaining functional endothelial cells (ECs) from human induced pluripotent stem cells (hiPSCs).
2 Develop an *in vitro* angiogenesis model with hiPSC-ECs encapsulated in a bioinspired HyA matrix to study cellular response to biochemical and biophysical stimuli.
3 Develop an *in vitro* cardiovascular tissue model to study cellular interaction of hiPSC-EC and hiPSC-CM co-culture in the HyA matrix.

1.3 Dissertation Outline

- *Chapter 2* provides a review of the fundamental biochemical signaling in vasculogenesis, physiological angiogenesis, pathological angiogenesis, and atherosclerosis that is relevant to understanding the endothelial differentiation process and the development of a physiologically relevant *in vitro* angiogenesis model in this dissertation. Additionally, a literature review and discussion on the current endothelial cell differentiation methods and *in vitro* angiogenesis models dominating the field of vascular tissue engineering are also presented.

- *Chapter 3* addresses Aim 1. A novel endothelial cell differentiation method from human pluripotent stem cells is developed and validated in this study. The phenotype and gene expression of the total differentiated population and the purified CD31+ population was characterized for endothelial lineage with phase contrast microscopy, flow cytometry, fluorescence microscopy, and RT-qPCR analysis. The purified endothelial cell population was further validated with functional assays including Ac-LDL uptake and network formation within a Matrigel angiogenesis assay.

- Chapter 4 addresses Aim 2. This study presents an *in vitro* angiogenesis model that was developed by incorporating the purified hiPSC derived endothelial cells (discussed in chapter 3) in a tunable, growth factor sequestering acrylated hyaluronic acid (HyA) scaffold to promote cell survival and maintenance of lineage-specific function. The system's ability to respond to biochemical and biophysical cues is demonstrated through characterization of changes in tube formation with confocal microscopy and measurement of nitric oxide production using a fluorescence-based Griess assay. The dependence of network formation on proangiogenic signaling was further demonstrated by treatment with a small-molecule VEGFR2/FGFR inhibitor. Additionally, perfusion of the capillary networks is demonstrated by culturing the 3D system in a tri-chamber microfluidic device that mimics vascular flow. A fluid dynamics analysis of the HyA flow through the microfluidic device's capillary burst valve (CBV) system during sample loading is also discussed.

- *Chapter 5* addresses Aim 3. An *in vitro* cardiovascular tissue model is developed by culturing hiPSC-CMs in the HyA hydrogel alone and with the hiPSC-ECs. The hiPSC-

CMs ability to survive, function, and support angiogenesis within the hydrogel was analyzed through live/dead fluorescence staining, beat rate analysis with motion tracking software, and confocal microscopy characterization of the cellular morphology, organization and sarcomere organization.

- *Chapter 6* provides a summary of the conclusions from this dissertation along with providing a discussion of future directions for this work.

CHAPTER 2:
BACKGROUND

2.1 Vascular Disease and Endothelial Dysfunction

2.1.1 Pathology of Atherosclerosis

Endothelial dysfunction initiates atherosclerosis; it is caused by several factors including high levels of oxidized low-density lipoprotein (LDL), reactive oxygen species (ROS), genetic mutations, or endogenous inflammatory signals. [4,34-36] Dysfunctional endothelium is characterized by loss of normal nitric oxide (NO) production, increased permeability, and increased expression of leukocyte adhesion molecules including VCAM-1, ICAM, P-selectin, and E-selectin. [4,34-36] The adhesion of leukocytes to the dysfunctional endothelium initiates atherosclerosis and the permeability allows them, along with lipids, to migrate into the blood vessel wall. Within the intima, dysfunctional endothelial cells along with the leukocytes express chemoattractive cytokines such as CCL-2, CXC-9, CXC-10, CXC-11, TNF-alpha, IL-1, IL-2 which attract more T cells and monocytes, promoting a continued inflammatory response. The growth factors and cytokines, MCSF-1, TNF-alpha, and IFN-gamma, released within the intima cause monocytes to differentiate into macrophages, which take up the surrounding lipids and mature to foam cell macrophages. [3,37-39] The aggregation of these foam cells within the intima of the blood vessel is referred to as a "fatty streak" lesion and is considered the onset of atherosclerosis. Progression of atherosclerosis occurs with the establishment of a necrotic core with the apoptosis of the foam cell macrophages and the development of a fibrous cap. The necrotic core is composed of the released macrophage contents, which cause accumulation of lipids and inflammatory cytokines. The secretion of PDGF, TGFβ-1, FGF-2, MMPs from degranulated platelets, endothelial cells, macrophages, and foam cells promotes migration of vascular smooth muscle cells (VSMCs) into the intima. The fibrous cap is caused by the proliferation and secretion of extracellular matrix (ECM) by vascular smooth muscle cells around the growing lesion. The proliferation of cells and ECM around the lesion leads to the formation of an advanced plaque that protrudes into the blood vessel lumen. The stability of the plaque depends on the size of the necrotic core and the thickness of the fibrous cap. A plaque with large necrotic core, high concentration of leukocytes, and a thin cap is unstable and more prone to rupture. If the plaque ruptures, artery occlusion may occur which could cause a stroke or myocardial infarction.[3,34,36,38]

2.1.2 Pathological Angiogenesis

Pathological angiogenesis shares a very similar mechanism to physiological angiogenesis in that it is driven by proangiogenic signaling molecules. However, these factors are upregulated by activated oncogenes such as RAS or Myc in overly proliferative, cancer cells. They are also upregulated in response to a hypoxic, nutrient deficient microenvironment by tumor associated fibroblasts (TAFs) and macrophages (TAMs). Oncogene expression and hypoxia stimulated cells drive vascularization of growing tumors by the upregulation of the hypoxia inducible factor (HIF) family of transcription factors that upregulate the

secretion of VEGF-A, bFGF (FGF2), SDF-1α, TGFβ-1, and PDGF to attract endothelial cells and facilitate their proliferation.[40] The tumor vasculature is composed of tortuous, disorganized, and leaky capillaries that cannot supply sufficient oxygen and nutrients to the growing tumor. This creates a vicious cycle where tumor cells are not getting enough oxygen from the malfunctioning vasculature then secrete more proangiogenic factors to stimulate further angiogenesis. Thus, unlike physiological angiogenesis where new blood vessels stabilize once they anastomose with existing ones, the tumor vasculature continues to grow.[19,41-43] Finally, while abnormally high levels of VEGF-A and other proangiogenic factors are detected in the tumor microenvironment, nitric oxide, which stabilizes blood vessels, is found at lower concentrations. This is due to endothelial dysfunction and consequently decreased eNOS activity. [35,44]

2.2 Developmental Vasculogenesis and Angiogenesis

The circulatory system is one of the first organs to develop during mammalian embryogenesis. Vasculogenesis is the *de novo* formation of blood vessels from the differentiation of precursor cells to endothelial cells and occurs shortly after gastrulation. The angiogenic precursor cells, hemangioblasts, are formed from the cells in the mesoderm layer. Hemangioblasts are bipotential since they can differentiate into endothelial progenitor cells called angioblasts and hematopoetic stem cells which give rise to blood cells. Vasculogenesis occurs both intra- and extra-embryonically. Within the yolk sac, hemangioblasts form clusters where the cells at the outer edge differentiate into angioblasts while the internal cells differentiate into hematopoetic cells. The highly mobile angioblasts continue to proliferate and associate to form nascent vessels. The angioblasts start to differentiate to endothelial cells with lumen and establish basal lamina. The extra-embryonic nascent vessels form a primitive capillary plexus within the yolk sac and anastomose with the primitive vessels formed within the embryo, which then connect to the developing heart tube. As embryonic remodeling continues, the endothelial cells recruit perivascular cells via TGFβ-1, PDGF-B, and Angiopoietin-1 signaling to form stable, mature vessels.[19,45]

Angiogenesis is the sprouting of endothelial cells from pre-existing blood vessels to form new vessels. Endothelial cells line the inner lumen of blood vessels and are defined by their expression of growth factor receptors that can bind and respond to proangiogenic signals, which cause the cells to proliferate, migrate, and form new vessels. These proangiogenic signals include VEGF, bFGF (FGF2), Ang-1, TGFβ-1, IGF-1, and HGF. However, the process is predominately driven by the vascular endothelial growth factor family, specifically VEGF-A, which binds to the extracellular receptor VEGFR2 that initiates MAPK signaling. The endothelial cells that drive the formation of new blood vessels are called tip cells. Upon binding VEGF-A, these cells loosen cell-cell contacts, secrete enzymes to degrade their basement membrane, extend filopodia, and begin to migrate until they connect with adjacent vessels. The activation of VEGFR2 by binding VEGF-A upregulates the expression of the Notch ligand, DLL4 in the tip cells. This ligand then binds notch receptors, Notch 1 and Notch 4, in the adjacent ECs. This keeps the adjacent ECs in a quiescent state since notch receptors inhibit VEGFR2 expression.[19,43] These quiescent ECs are called stalk cells and they remain bound to the tip cells as they migrate to form new blood vessels. Once

anastomosis with existing blood vessels has occurred, the ECs attract stabilizing perivascular cells via TGFβ-1, PDGF-B, and Angiopoietin-1 signaling. [45-47]

2.3 Current methods for Endothelial Cell Differentiation from Human Pluripotent Stem Cells

Several endothelial cell differentiation methods have been developed within the last decade. These protocols have evolved from spontaneous embryoid body formation to directed differentiation of 2D pluripotent stem cell monolayers with small molecules and growth factors. The latter methods modulate the Wnt, SMAD, and MEK/MAPK pathways to recapitulate developmental vasculogenesis during the differentiation and specification of endothelial cells *in vitro*. [9,7,11,17,21-24,26,28,48-53]

Kusuma and colleagues developed a 12-day monolayer differentiation protocol for hiPSCs to early vascular lineage cells (EVCs) with a 6-day maturation phase to endothelial cell lineage.[23] This consisted of culturing the hiPSCs for 6 days in alpha-MEM medium supplemented with 10% FBS, 0.1 mM beta-mercaptoethanol. On day 6 the cells were re-plated and fed ECGM with 2% FBS, 50 ng/mL VEGF, 10 uM SB431542 for another 6 days. The VE-CAD+ cells were then sorted with MACS, re-plated, and fed ECGM with 50 ng/mL VEGF, 10 uM SB431542 for another 6 days. They also reported a serum-free alternative for EVC differentiation which consisted of feeding the hiPSCs alpha-MEM with 20% Knockout serum replacement, 0.1 mM beta-mercaptoethanol, 1x non essential amino acids, and 1x L-glutamine for 6 days, followed by 6 days ECGM with 50 ng/mL VEGF, 10 uM SB431542, 10% knockout serum replacement, beta-Mercaptoethanol, essential amino acids, and glutamine. Their protocol yielded 8-25% VCAD+ EVCS which continued on to EC maturation. They found that no subpopulation of Day 12 EVCs were mature ECs since they did not detect CD31, lectin, eNOS, VWF, or Ac-LDL uptake via immunofluorescence in the unsorted populations. Because of these findings, they concluded that additional culture was needed to mature the EVCs to endothelial cell lineage. Magnetically sorted VE-Cad+ cells from EVCs matured toward VE-Cad+, CD31+, and CD146+ ECs. They also exhibited typical membrane expression of VE-cad and CD31, lectin binding, cytoplasmic expression of eNOS and vWF, uptake of acetylated low-density lipoprotein (Ac-LDL), up-regulation of intercellular adhesion molecule 1 (ICAM1) in response to TNF-α, and network formation on Matrigel. Next, the researchers tested the EVC's and matured EC's ability to form networks in collagen and in completely synthetic hyaluronic acid (HA)-based hydrogel. They found EVCs could form networks when encapsulated within collagen gels while sorted VE-cad+ or VE-cad negative cells individually could not. The EVC's were also cultured in a hyaluronic acid hydrogel which demonstrated multicellular networks by Day 3. They detected NG2+ pericytes incorporated in the luminal structures and encircling the emerging tubular structures. An *in vivo* Matrigel plug assay also revealed EVCs anastomosed with perfused murine host microvasculature and generated human-only microvascular structures

Orlova and Mummery developed a 10-day SMAD pathway based endothelial differentiation protocol. [27] Mesoderm specification was induced in human pluripotent stem cells by adding bone morphogenetic protein 4 (BMP4), activin A, small-molecule inhibitor of glycogen synthase kinase-3 (CHIR) and vascular endothelial growth factor (VEGF) in BP(E)L medium

composed of IMDM, Ham's F12, PFHMII, 10% BSA, Lipids (100x), ITS-X (insulin-transferrin-selenium-ethanolamine, 100x), 8αMTG (mono thiol glycerol, 13 8l in 1 ml IMDM), AA2P (5mg/mL), GlutaMAX (200 mM), and Pen-strep (5,000 U/mL). After 3 days, the cells were fed vascular specification medium that consisted of BP(E)L supplemented with VEGF and the transforming growth factorβ (TGFβ) pathway small-molecule inhibitor SB431542. The protocol yielded ~20% CD31+/VCAD+ ECs which were isolated on Day 10. The researchers demonstrated the EC's ability to form functional blood vessels through an *in vivo* assay with a zebrafish xenograft. They found that hPSC-derived ECs anastomosed with the host vasculature and performed better than HUVECS.

Prasain and Yoder developed a 21-day differentiation protocol for pluripotent stem cells to endothelial colony forming cells (ECFCs). [28] They cultured human pluripotent stem cells in mTESR1 medium for 2 days, then directed cultures toward the mesodermal lineage with addition of activin A (10 ng/ml) in the presence of FGF-2, VEGF-A_{165} and BMP4 (10 ng/ml) for 24 hours. The next day, the culture was fed Stemline II complete media containing FGF-2, VEGF165, and BMP4 to promote endothelial cell specification and proliferation. On Day 12 the CD31+/NRP1+ cells were sorted and cultured in 50% EGM-2 and 50% complete Stemline II differentiation media to generate ECFCs. After 2 days, the media was replaced with three parts of EGM-2 and one part of differentiation media was added to the cultures for seven days. The hiPSC-ECFCs were encapsulated in collagen gels and implanted subcutaneously in an immunodeficient mouse to test their angiogenic potential. After 14 days, the implanted ECFCs formed durable and functional *in vivo* human vessels in the subcutaneous pouch. The hiPSC-ECFCs were also injected into mouse models of hypoxia-induced pathological preretinal neovascularization where they found the hiPSC-ECFCs decreased the avascular area by 36% and reduced the occurrence of preretinal neovascular tufts compared to endothelial cells differentiated from embryoid bodies (hiPSC-EBT-CD144+). The ECFCs were also implanted in a mouse model of hind-limb ischemia. The limbs injected with hiPSC-ECFCs demonstrated improved blood flow recovery and greater perfusion compared to hiPSC- EBT-CD144+ ECs.

Lian and Pelacek developed a 5-day protocol to produce endothelial progenitor cells (EPCs) from human pluripotent stem cells which could then be further matured to tube-forming ECs (seen at Day 60).[24] The differentiation protocol was initiated by treating the cells for 2 days with 6–10 uM CHIR99021 in LaSR basal medium consisting of Advanced DMEM/F12, 2.5 mM GlutaMAX, and 60 mg/ml ascorbic acid. The cells were then maintained in LaSR basal medium without CHIR99021 for 3-4 more days. At Day 5 the population consisted of 55% CD34+/CD31+ and 57% KDR+ EPCs. To differentiate the EPCs to mature endothelial cells, the Day 5 CD34+ cells were magnetically sorted and replated on collagen-IV-coated dishes in EGM-2 medium (Lonza) and split every 4–5 days with Accutase. At Day 60, 99.2% of the purified population expressed CD31 and 98.9% was VCAD+. Additionally, the purified day 60 endothelial cells demonstrated Ac-LDL uptake and tube-forming ability in a Matrigel angiogenesis assay supplemented with an additional VEGF treatment.

Bao and Pelacek developed a 5-day chemically-defined albumin-free protocol for differentiation of human pluripotent stem cells to endothelial progenitor cells with an additional 10-day endothelial cell differentiation/maturation stage. [25] At day 0, the cells

were fed DMEM supplemented with 3–9 μM CHIR99021 (Selleckchem) and 100 μg/mL ascorbic acid. After 2 days, cells were cultured in DMEM supplemented with ascorbic acid without CHIR99021 for 3 to 4 days. At Day 5, the population expressed 20% to 32% CD34/31+ and 29% CD144+. At Day 5, the differentiated populations were purified based on CD34 expression. For endothelial cell differentiation, the purified CD34+ cells were plated on collagen IV-coated dishes and fed EGM-2 medium or human endothelial- SFM supplemented with 20 ng/mL bFGF and 10 ng/mL EGF (Life Technologies) for 10 additional days. At Day 15, the endothelial cells demonstrated Ac-LDL uptake and tube formation on a 24-hour Matrigel angiogenesis assay consisting of 24-well tissue culture plate pre-coated with 250 μl Matrigel with EGM-2 supplemented with 50 ng/mL VEGF.

Most recently, Harding and colleagues developed a 8-10 day endothelial cell differentiation protocol. [26] In this study, the hiPSC/hESCs were grown on mouse embryonic fibroblast feeder (MEF) layers and small clusters were manually passaged onto Matrigel coated plates in MEF conditioned hESC medium supplemented with 10 ng/mL of FGF2. After 1 day, the culture medium was switched to StemDiff APEL medium with 6 uM CHIR99021 for 2 days. The cells were then cultured in StemDiff APEL medium supplemented with 25ng/mL, BMP4, 10 ng/mL FGF2, and 50 ng/mL VEGF for another 2 days. On day 4, the culture self-assembled into a monolayer of cells with cobblestone morphology, termed “peripheral cells”, with sporadic clusters of smaller cells, termed “central cells”. The entire population was found to be 67.8% CD31+/CD144+, the “peripheral cells” were 84% CD31+/CD144+ and the “central cells” were 55.6% CD31+/CD144+. The “peripheral cells” were released with shorter accutase exposure time and replated with EC Growth Medium MV2 (ECGM-MV2) supplemented with an additional 50 ng/mL VEGF. The medium was changed every 2 days for 4-6 days to generate mature ECs that were 94%-97% CD31+, 73%-81% CD34+, and 78% to 83% CD144+. After one passage the ECs expressed 99.7% CD31+ and 96.i% CD144+. The hiPSC-ECs were subcutaneously injected with a Matrigel plug in the hind limb of an immune deficient NSG mouse. After 2 weeks, immunostaining for human CD31 of the explanted plug revealed vessels and branches. The hiPSC-ECs were then injected into a hind limb ischemia mouse model. A tail vein injection of FITC-Dextran ten weeks after transplantation revealed some tube formation and localization of human ECs but the ischemic area remained visible.

Significant progress has been made in directed differentiation protocols for human pluripotent stem cell monolayers to endothelial cell lineage. However, many issues remain with total differentiation time, the use of several different culture medias, and late stage expression of mature endothelial cell markers. Total differentiation time needs to be decreased since most protocols consist of a 5-10 day differentiation process with an additional maturation phase that can last up to 60 days before the ECs can be used in a functional capacity. Additionally, current protocols entail the use of more than one media formulation, including MEF conditioned media, from the pluripotency stage to the differentiation and maturation process. Taking into account the culture and maintenance of the pluripotent stem cells prior to differentiation, the total process can take up to 3 months with 2-3 different media formulations. Finally, many protocols report the expression of mature endothelial cell markers such as CD31 and VE-Cadherin on the final day of differentiation or after the maturation phase.

2.4 Current *in vitro* models of angiogenesis

Belair, Thomson, Griffith, and Murphy used human iPSC-ECs purchased from Cellular Dynamics International , Inc. (CDI) to model blood vessel development *in vitro* within biomimetic 3D engineered platforms.[17] The iPSC-ECs were characterized for the endothelial cell lineage markers CD31, CD105, CD144, and VEGFR2 (KDR) with flow cytometry and were determined to be approximately 97.10% CD31+/CD105+, 95% CD31+/CD144+, and 94% VEGFR2+. In 2D culture the iPSC-ECs were shown to proliferate in a dose-dependent manner to VEGFA and a reduction in proliferation was seen when SU1498, a VEGFR2 inhibitor, was added to the media. When exposed to thrombin, impedance measurements demonstrated the disruption of the EC's barrier function, which was recoverable at lower doses. The ECs were also exposed to TNFα and the upregulation of ICAM-1 and MCAM was demonstrated through flow cytometry measurements. The iPSC-ECs formed capillary-like structures similar to HUVECS when concurrently subjected to a Matrigel angiogenesis assay. The ECs were plated on (2D) and encapsulated within (3D) Matrigel and cultured in a perfusable bioreactor that permitted applied fluid shear stress. According, to the authors, the ECs aligned in the direction of flow, however, this is not obvious in the image for the 3D flow culture. The ECs were then co-cultured with normal human lung fibroblasts (NHLFs), encapsulated in a fibrin hydrogel, and loaded into a microfluidic device. The ECs formed perfusable networks that were stabilized by the NHLFs. Finally, the authors developed a sprouting assay by culturing them a in a spheroid in a non-adherent round bottom 96-well plate. They were first seeded onto 20% methylcellulose for 24 hours and then covered with a solution of 40% Matrigel to create a 3D encapsulated spheroid. The cells were then fed either growth medium (VascuLife VEGF Medium supplemented with the complete growth factors kit and CDI provided supplement) or starvation medium with VEGF (VascuLife Basal Medium with 4 mM L-glutamine and 0.1 vol.% iPSC-EC supplement). The medias were supplemented with VEGFA, SU1498 (VEGFR2 inhibitor), SU5402 (VEGFR2/FGFR inhibitor), Sunitinib (tyrosine kinase inhibitor), or nocodazole (microtubule polymerization inhibitor). The inhibition studies in VEGF-containing medium demonstrated that sprouting was abolished in the presence of SU1498, Sunitinib and a SU5402. Sprouting behavior in the presence of Growth Medium was unaffected by treatment with SU1498. Dose-response curves were generated for VEGF, SU5402, and nocodazole supplemented medias where EC50 and IC50 values were determined from sigmoidal regression analysis. These results demonstrated that VEGF/VEGFR2 mediated sprouting is dependent on the characteristics of the cell culture medium. In a migration assay VEGF promoted iPSC-EC to migrate in a dose-dependent manner while treatment with SU1498 eliminated iPSC-EC movement.

Sobrino, Hughes, and George developed a microphysiological system to model human tumor angiogenesis *in vitro* that incorporates human cancer cell lines in a fibrin matrix, supported by perfused human microvessels.[16] The vascular tissue consists of human endothelial colony forming cell-derived endothelial cells (ECFC-ECs) isolated from cord blood supported by normal human lung fibroblastes (NHLFs). The microfluidic device consisted of two outer microfluidic channels that mimic high pressure (arteriole) and low pressure (venule) circulatory vessels which are connected by three central, consecutive

microtissue chambers. The encapsulated cells were loaded into the central chamber and ECs and NHLFs self assembled into an interconnected network that anastomoses with the outer channels within 5-7 days. Permeability of the vessels was demonstrated by perfusion of the vascular network with 70 kDa FITC-dextran, which demonstrated the vessels were minimally leaky. The authors noted that "stromal cells are required for proper formation of the vascular networks, and a subset of these consistently envelop the newly-formed vessels". Several cancer cell lines were encapsulated with the ECFCs and stromal cells to study the development of vascular networks and the effects of anti-cancer drugs. Colorectal cancer (CRC) cell line HCT116 formed small spheroids with vessels found within and around them by Day 6. Two other CRC lines (SW620 and SW480), two breast cancer lines (MCF-7 and MDA-MB-231), and a melanoma cell line (MNT-1) were also combined with the fibrin, ECFCs, and NHLFs within the device. Each combination demonstrated the formation of a vascular network that supported growth of the tumors. However, the different cancer cell lines formed tumors with different patterns of growth. SW480 and MCF-7 grew as tight colonies, while MDA-MB-231 and MNT-1 demonstrated more interspersed, invasive growth patterns. The researchers screened several standard, FDA-approved anticancer therapies to test whether CRC vascularized microtumors (VMTs) responded to these drugs. This included FOLFOX (5-FU), Leucovorin and Oxaliplatin which are the standard-of-care chemotherapy for CRC. After 2 days, FOLFOX had significantly reduced tumor growth and by Day 4 the tumors had decreased below their starting size and the vascular network remained unaffected. The response of the breast cancer line MDA-MB-231 to the standard-of-care chemotherapeutic Taxol (a mitotic disrupter) was examined. These tumor cells grew rapidly and were highly invasive when left untreated for four days, however, treatement with Taxol showed greatly reduced migration and growth. In addition to decreasing the growth of MDA-MB-231 cells, the tumor vasculature was also disrupted in response to Taxol. The effect of several anti-angiogenic drugs on stability of the vascular network was also examined. Exposure of vessels to Sorafenib and Vincristine reagents showed distinct modes of disrupting the vascular networks after four days of treatment. Both drugs caused a significant decrease in total vessel length and total number of branch points, however, regression of neo-vessels was observed only with Sorafenib, while complete disruption of the network was seen with Vincristine. Drugs that only target VEGFR2, Apatinib and Vandetanib, were not effective in disrupting the vascular networks like those that inhibit both VEGFR2 and PDGFR, such as Axitinib and Pazopanib. Fluorescence Lifetime Imaging Microscopy (FLIM) was used to detected the ratio of free to bound NADH which correlates with cell glycolysis. In devices with only ECFCs and NHLFs, a higher relative level of free NADH was found in the EC compared to either the perivascular cells stabilizing the vessels or the interstitial stromal cells. In devices with VMTs, much higher NADH free/bound ratios were found for MCF-7 breast cancer cells relative to other cells in the surrounding microenvironment which is consistent with cancer cell's known preference for aerobic glycolysis. However, treatment with 5-FU strongly decreased the ratio of free/bound NADH in the MCF-7 cells, which is consistent with a slowed glycolytic rate. The 5-FU treatment did not change the metabolic profile of the stroma.

Moya and George developed a 3D *in vitro* vascular tissue model that contains a perfused and interconnected human capillary network within a microfluidic platform that mimics venular and arteriolar flow.[15] The microfluidic device consisted of two fluidic channels

separated by a central channel of 12 consecutively connected diamond tissue chambers. The fluidic channels connected on either side of the tissue chamber via a single connecting pore. The central channel was loaded with Human endothelial colony forming cell-derived ECs (ECFC-ECs) isolated from cord blood and normal human lung fibroblast (NHLFs) encapsulated in fibrin at a ratio of 1:2 respectively. The cells were grown in the device for 14 days under interstitial flow and in the absence of VEGF and bFGF since the NHFLFs were assumed to provide angiogenic signals for EC tube formation. The curved boundaries at the pores prevented the gel from leaking into the fluidic channels by mimicking capillary burst valves where the driving pressure difference at the fibrin–air interface equals the hydrostatic pressure difference across the boundary. Two design variations for connecting the fluidic channels and microtissue chambers were investigated to determine their effect on the vascular tissue formation. One design (VP), consisted of connecting the arterial microfluidic line (high pressure side) from the last microtissue chamber directly to the venular side (low pressure side) of the same chamber. This design created a similar mean pressure within the microtissue chambers and a negligible velocity in the x-direction. However, a wide variation in the pressure drop in the y-direction and interstitial velocity across the microtissue chambers was created. The second design (EQ), consisted of connecting the arterial microfluidic line from the last microtissue chamber to the venular side of the first chamber. This design created a larger pressure drop across the microtissue chambers in the y-direction and a large but constant pressure drop in the x-direction. Cells in the devices were cultured and remained viable through 40 days. Between days 14 and 21, the ECFC-EC, supported by cocultured NHLFs, formed an interconnected network of capillaries measuring from 15 to 50 mm in diameter, Networks formed in both designs, VP and EQ, were well connected, with connectedness values of 0.06 – 0.02 and 0.05 – 0.02, respectively. Connectedness values were measured by the ratio of total number of vessel endpoint to the total number of vessel junctions. The study did not find a significant difference for capillary network diameter and connectedness between the two designs. To characterize the flow in the capillaries formed by the ECs and NHLFs, 1-mm- diameter fluorescent microspheres were introduced in the arterial microfluidic channel. In the VP design only the first three chambers with the highest pressure drop (supraphysiological range) in the x-direction (transverse) demonstrated perfusion of the formed capillaries. The microspheres travelled longitudinally and laterally in the vessels which reflected the pressure gradients within the devices. Fluid velocities ranging from near zero to over 1000 mm/s at any particular position were determined from tracking the microspheres. The authors noted that this is within range of normal blood velocities in human capillaries, which vary from 500 to 1500 mm/s. In devices designed to have identical pressure gradients in the x-direction, EQ, microspheres flowed from the arterial microfluidic channel side of the tissue chamber to the venular side. Microspheres tracked in these devices demonstrated a wide range for velocity from almost zero to over 4000 mm/s at any particular position. Fluorescent dextran (70 and 150kDa) was introduced into the arterial microfluidic channel at day 21 to assess vessel permeability. The vessels demonstrated variable degrees of permeability to the 70-kDa dextran but appeared to be impermeable to 150 kDa dextran. Anastomosis of the vessels on both sides of the microtissue chambers was demonstrated by observing the flow of fluorescent dextran (70kDa) from the arterial side through the network and into the venular microfluidic channel.

Zanotelli, Thomson, and Murphy demonstrated that iPSC-ECs could self-assemble into vascular networks through physiologically-relevant mechanisms in PEG hydrogels polymerized in a tri-channel microfluidic device and remain stable for two weeks.[53] Live/dead staining with calcein and ethidium homodimer demonstrated that iPSC-ECs were viable and self- assembled into interconnected vascular networks during the first three days of culture in peptide-functionalized PEG hydrogels. On Day 3, the capillary networks were evident throughout the hydrogel. Immunofluorescence imaging demonstrated that iPSC- EC networks in the PEG hydrogels were CD31+ and VE-Cadherin+ and both genes were highly expressed by RNA-Seq for 2D and 3D culture. RNA-Seq revealed genes that were highly expressed by iPSC-ECs included many regulators of vascular function, cell- matrix and cell-cell adhesion genes, and genes relevant to matrix remodeling such as KDR/VEGFR-2, MCAM, CLDN5/claudin-5, integrins, laminins, collagens, TIMPs, and MMPs. Vascular network formation was investigated within PEG hydrogels with shear moduli ranging from 183 ± 10 to 1612 ± 95 Pa (40%-60% crosslinking with MMP-degradable peptide). Limited tubule formation was seen after eight days when $1x10^7$ iPSC-ECs per mL were encapsulated in 40–60% crosslinked hydrogels, however, it was improved for each PEG formulation when the basal medium was supplemented with 200ng/mL VEGF. The VEGF concentration was further optimized with hydrogels at 50% crosslinking. The amount of VEGF required to improve network formation was dependent on cell density. The highest degree of network formation was reported to occur at higher cell density ($8.5x10^7$ cells/mL) and intermediate levels of VEGF addition. The highest VEGF dose of 1 ug/mL completely disrupted vascular network formation after 9 days in culture. The networks remained stable for at least 14 days in the microfluidic device when $1x10^7$ iPSC-ECs per mL were encapsulated in 50% crosslinked PEG hydrogels and cultured in medium that was supplemented with 100 ng/mL VEGF. The study reports that the iPSC-ECs encapsulated in the optimized hydrogel within the microfluidic device formed lumen approximately 25 um in diameter, however, no perfusion studies were demonstrated.

Current studies on *in vitro* angiogenesis models provide much insight into the angiogenesis process, however, many continue to rely on endothelial cells sourced from primary cell lines. This presents a problem for creating patient-specific angiogenesis models since primary cells have a limited supply and are notoriously difficult to culture and expand, Additionally, many studies include secondary stromal cells from a different source to stabilize the endothelial cell vascular networks. This approach adds a confounding factor since it is unclear if the ECs are directly affected by the treatment in question or if they are reacting to the fibroblast response. Furthermore, current studies use matrices that do not recapitulate the natural extracellular matrix (ECM), which is a complex and dynamic environment. The matrix used in an *in vitro* angiogenesis model should have a well-defined, consistent composition that promotes vascular tube formation by facilitating cellular adhesion, movement, and remodeling in addition to proangiogenic growth factor sequestration. [9,12,31]

2.5 Hyaluronic Acid and common natural biopolymer scaffolds in Vascular tissue engineering

Biomimetic extracellular matrix scaffold material intended for in-vitro studies or implantation into damaged/ischemic tissue must meet several requirements to ensure cell survival and function in addition to being safe and effective. First, materials should be biocompatible so they support normal cellular function and don't elicit an immune response for rejection of the implant. The scaffold should be synthesized and cross-linked using mild and safe reagents. The matrix should also be biodegradable so that it decomposes through inherent biological activities like hydrolysis or enzymatic degradation. To avoid health complications to the host, the biomaterial degradation products need to be resorbable into the body or excreted through the urine. The biomaterial should also have cell adhesion sites to promote cell attachment, migration, and paracrine signaling since the purpose of encapsulating cells in a scaffold is to improve their survival, retention, and engraftment to the host (if it is implanted). [9,12,13,31,54]

Hyaluronic Acid (HyA), offers many benefits as a scaffold to support angiogenesis since it is a naturally occurring biopolymer that is biocompatible, biodegradable, non-immunogenic, and can absorb a large amount of water. It is the most abundantly occurring polysaccharide in the human body and is an essential component of the human extracellular matrix (ECM). *In vivo* it helps regulate cell migration, proliferation, angiogenesis, and wound healing processes by binding to membrane receptors, CD44, RHAMM, LYVE-1, and HARE, which are expressed by endothelial cells, fibroblasts, smooth muscle cells, and immune cells. Additionally, it is hydrolyzed, enzymatically degraded, and recycled by endogenous enzymes including hyaluronidase, glucoronidase, and hexosaminidase. Hyaluronic acid has poor mechanical strength and does not directly bind integrins, however, due to its high molecular weight (up to 10^6 Da) and negative charge density the biological and mechanical properties can be controlled. This is done through relatively easy chemical modification of the carboxylic acid group on the D-glucoronic acid molecule, which is bound to D-N-acetylglucosamine as part of the repeating disaccharide unit that makes up HyA. [32,33,54,55]

Alginate is another naturally occurring polysaccharide that can be chemically modified and used as a semi-synthetic scaffold for cardiovascular tissue engineering. It is an anionic biopolymer extracted from brown algae and is composed of the monomers β-D-mannuronic acid and α-L-guluronic acid. Calcium cations are used to crosslink the alginate polymer chains, which negates the need for chemical modification to form a 3D scaffold. However, alginate is not degradable in the human body and is secreted by time-dependent erosion where the polymer chains are excreted through the kidneys. Additionally, alginate does not have any cell binding motifs and must be chemically modified to provide sites for cell attachment. [12,55,56]

Scaffolds based on ECM proteins, referred to as "natural" matrices, have dominated the field of vascular tissue engineering due to their inherent biocompatibility and integrin binding sites that makes them easier to use in complex *in vitro* or *in vivo* studies. The most commonly used protein biopolymers include collagen, gelatin, Matrigel, and fibrin. Collagen is the most abundant extracellular protein found throughout the human body. Collagen I, is

widely used in cardiovascular tissue engineering applications as a crosslinked hydrogel scaffold since it is commercially available, FDA approved for many existing biomedical applications, and it has inherent binding sites for β1 integrins which are expressed by cardiomyocytes and endothelial cells. In the human body, fibrin forms blood clots at sites of injury by covalently crosslinking with circulating fibrinogen and factor XIIIa, which makes it an attractive scaffold material since it does not require chemical modification to form a 3D structure. Thus, Fibrin based scaffolds are also widely used for vascular tissue engineering since it is an abundantly available biopolymer with RGD domains that are bound by αvβ3 and α5β3 integrins which are important for angiogenesis. Additionally, fibrin has FDA approval for several other medical applications such as a surgical adhesive. Matrigel is a heterogenous mixture of different ECM components including laminin, collagen, and heparan sulfate and is secreted from mouse sarcoma cells. Matrigel plugs are regularly used to support implanted endothelial cells into ischemic tissue animal models. However, due to its source, Matrigel may promote the formation of tumors, thus it is not biocompatible for human hosts and does not have FDA approval for any medical applications. Although protein based polymer hydrogels have several benefits, they suffer from batch-to-batch composition variability that results in inconsistent gelation times. Additionally, it is well known that these scaffolds do not support long term survival of encapsulated cells since they degrade quickly *in vitro* and *in vivo* relative to semi-synthetic hydrogels.[12,55,56]

2.6 References

1 Hanahan, D. & Weinberg, R. A. Hallmarks of cancer: the next generation. *Cell* **144**, 646-674, (2011).

2 WHO. *Cancer*, (2017), http://www.who.int/cancer/enl/.

3 George, S. J., Johnson, Jason. *Atherosclerosis: Molecular and Cellular Mechanisms*. (Wiley-VCH Verlag GmbH & Co., 2010).

4 Gimbrone, M. A., Jr. & Garcia-Cardena, G. Endothelial Cell Dysfunction and the Pathobiology of Atherosclerosis. *Circ Res* **118**, 620-636, (2016).

5 Benjamin, E. J., Blaha, M. J., Chiuve, S. E., Cushman, M., Das, S. R., Deo, R., de Ferranti, S. D., Floyd, J., Fornage, M., Gillespie, C., Isasi, C. R., Jimenez, M. C., Jordan, L. C., Judd, S. E., Lackland, D., Lichtman, J. H., Lisabeth, L., Liu, S., Longenecker, C. T., Mackey, R. H., Matsushita, K., Mozaffarian, D., Mussolino, M. E., Nasir, K., Neumar, R. W., Palaniappan, L., Pandey, D. K., Thiagarajan, R. R., Reeves, M. J., Ritchey, M., Rodriguez, C. J., Roth, G. A., Rosamond, W. D., Sasson, C., Towfighi, A., Tsao, C. W., Turner, M. B., Virani, S. S., Voeks, J. H., Willey, J. Z., Wilkins, J. T., Wu, J. H., Alger, H. M., Wong, S. S., Muntner, P., American Heart Association Statistics, C. & Stroke Statistics, S. Heart Disease and Stroke Statistics-2017 Update: A Report From the American Heart Association. *Circulation* **135**, e146-e603, (2017).

6 WHO. *Global Atlas on cardiovascular disease prevention and control*. (2011).

7 Lalit, P. A., Hei, D. J., Raval, A. N. & Kamp, T. J. Induced pluripotent stem cells for post-myocardial infarction repair: remarkable opportunities and challenges. *Circ Res* **114**, 1328-1345, (2014).

8 Mak, I. W., Evaniew, N. & Ghert, M. Lost in translation: animal models and clinical trials in cancer treatment. *Am J Transl Res* **6**, 114-118, (2014).

9 Sanz-Nogues, C. & O'Brien, T. In vitro models for assessing therapeutic angiogenesis. *Drug Discov Today* **21**, 1495-1503, (2016).

10 Morin, K. T. & Tranquillo, R. T. In vitro models of angiogenesis and vasculogenesis in fibrin gel. *Exp Cell Res* **319**, 2409-2417, (2013).

11 Nsair, A. & MacLellan, W. R. Induced pluripotent stem cells for regenerative cardiovascular therapies and biomedical discovery. *Adv Drug Deliv Rev* **63**, 324-330, (2011).

12 Briquez, P., Clegg, Lindsay, Hubbell, Jeffrey. Design principles for therapeutic angiogenic materials review. *Nature Reviews* **1**, 1-15, (2016).

13 Prestwich, G. D. & Healy, K. E. Why regenerative medicine needs an extracellular matrix. *Expert Opin Biol Ther* **15**, 3-7, (2015).

14 Chwalek, K., Tsurkan, M. V., Freudenberg, U. & Werner, C. Glycosaminoglycan-based hydrogels to modulate heterocellular communication in in vitro angiogenesis models. *Sci Rep* **4**, 4414, (2014).

15 Moya, M. L., Hsu, Y. H., Lee, A. P., Hughes, C. C. & George, S. C. In vitro perfused human capillary networks. *Tissue Eng Part C Methods* **19**, 730-737, (2013).

16 Sobrino, A., Phan, D. T., Datta, R., Wang, X., Hachey, S. J., Romero-Lopez, M., Gratton, E., Lee, A. P., George, S. C. & Hughes, C. C. 3D microtumors in vitro supported by perfused vascular networks. *Sci Rep* **6**, 31589, (2016).

17 Belair, D. G., Whisler, J. A., Valdez, J., Velazquez, J., Molenda, J. A., Vickerman, V., Lewis, R., Daigh, C., Hansen, T. D., Mann, D. A., Thomson, J. A., Griffith, L. G., Kamm, R. D., Schwartz, M. P. & Murphy, W. L. Human vascular tissue models formed from human induced pluripotent stem cell derived endothelial cells. *Stem Cell Rev* **11**, 511-525, (2015).

18 Kurokawa, Y. K., Yin, R. T., Shang, M. R., Shirure, V. S., Moya, M. L. & George, S. C. Human Induced Pluripotent Stem Cell-Derived Endothelial Cells for Three-Dimensional Microphysiological Systems. *Tissue Eng Part C Methods* **23**, 474-484, (2017).

19 Chung, A. S. & Ferrara, N. Developmental and pathological angiogenesis. *Annu Rev Cell Dev Biol* **27**, 563-584, (2011).

20 Coulombe, K. L., Bajpai, V. K., Andreadis, S. T. & Murry, C. E. Heart regeneration with engineered myocardial tissue. *Annu Rev Biomed Eng* **16**, 1-28, (2014).

21 Yoder, M. C. Differentiation of pluripotent stem cells into endothelial cells. *Curr Opin Hematol* **22**, 252-257, (2015).

22 Wilson, H. K., Canfield, S. G., Shusta, E. V. & Palecek, S. P. Concise review: tissue-specific microvascular endothelial cells derived from human pluripotent stem cells. *Stem Cells* **32**, 3037-3045, (2014).

23 Kusuma, S., Shen, Y. I., Hanjaya-Putra, D., Mali, P., Cheng, L. & Gerecht, S. Self-organized vascular networks from human pluripotent stem cells in a synthetic matrix. *Proc Natl Acad Sci U S A* **110**, 12601-12606, (2013).

24 Lian, X., Bao, X., Al-Ahmad, A., Liu, J., Wu, Y., Dong, W., Dunn, K. K., Shusta, E. V. & Palecek, S. P. Efficient differentiation of human pluripotent stem cells to endothelial progenitors via small-molecule activation of WNT signaling. *Stem Cell Reports* **3**, 804-816, (2014).

25 Bao, X., Lian, X., Dunn, K. K., Shi, M., Han, T., Qian, T., Bhute, V. J., Canfield, S. G. & Palecek, S. P. Chemically-defined albumin-free differentiation of human pluripotent stem cells to endothelial progenitor cells. *Stem Cell Res* **15**, 122-129, (2015).

26 Harding, A., Cortez-Toledo, E., Zhou, P. . Highly Efficient Differentiation of Endothelial Cells from Pluripotent Stem Cells Requires the MAPK and the PI3K Pathways. *Stem Cells* **35**, 909-919, (2017).

27 Orlova, V. V., van den Hil, F. E., Petrus-Reurer, S., Drabsch, Y., Ten Dijke, P. & Mummery, C. L. Generation, expansion and functional analysis of endothelial cells and pericytes derived from human pluripotent stem cells. *Nat Protoc* **9**, 1514-1531, (2014).

28 Prasain, N., Lee, M. R., Vemula, S., Meador, J. L., Yoshimoto, M., Ferkowicz, M. J., Fett, A., Gupta, M., Rapp, B. M., Saadatzadeh, M. R., Ginsberg, M., Elemento, O., Lee, Y., Voytik-Harbin, S. L., Chung, H. M., Hong, K. S., Reid, E., O'Neill, C. L., Medina, R. J., Stitt, A. W., Murphy, M. P., Rafii, S., Broxmeyer, H. E. & Yoder, M. C. Differentiation of human pluripotent stem cells to cells similar to cord-blood endothelial colony-forming cells. *Nat Biotechnol* **32**, 1151-1157, (2014).

29 Jha, A. K., Mathur, A., Svedlund, F. L., Ye, J., Yeghiazarians, Y. & Healy, K. E. Molecular weight and concentration of heparin in hyaluronic acid-based matrices modulates growth factor retention kinetics and stem cell fate. *J Control Release* **209**, 308-316, (2015).

30 Jha, A. K., Tharp, K. M., Browne, S., Ye, J., Stahl, A., Yeghiazarians, Y. & Healy, K. E. Matrix metalloproteinase-13 mediated degradation of hyaluronic acid-based matrices orchestrates stem cell engraftment through vascular integration. *Biomaterials* **89**, 136-147, (2016).

31 Jha, A. K., Tharp, K. M., Ye, J., Santiago-Ortiz, J. L., Jackson, W. M., Stahl, A., Schaffer, D. V., Yeghiazarians, Y. & Healy, K. E. Enhanced survival and engraftment of transplanted stem cells using growth factor sequestering hydrogels. *Biomaterials* **47**, 1-12, (2015).

32 Collins, M. N. & Birkinshaw, C. Hyaluronic acid based scaffolds for tissue engineering--a review. *Carbohydr Polym* **92**, 1262-1279, (2013).

33 Xu, X., Jha, A. K., Harrington, D. A., Farach-Carson, M. C. & Jia, X. Hyaluronic Acid-Based Hydrogels: from a Natural Polysaccharide to Complex Networks. *Soft Matter* **8**, 3280-3294, (2012).

34 Frangogiannis, N. G. The inflammatory response in myocardial injury, repair, and remodelling. *Nat Rev Cardiol* **11**, 255-265, (2014).

35 Tousoulis, D., Kampoli, A. M., Tentolouris, C., Papageorgiou, N. & Stefanadis, C. The role of nitric oxide on endothelial function. *Curr Vasc Pharmacol* **10**, 4-18, (2012).

36 Sitia, S., Tomasoni, L., Atzeni, F., Ambrosio, G., Cordiano, C., Catapano, A., Tramontana, S., Perticone, F., Naccarato, P., Camici, P., Picano, E., Cortigiani, L., Bevilacqua, M., Milazzo, L., Cusi, D., Barlassina, C., Sarzi-Puttini, P. & Turiel, M. From endothelial dysfunction to atherosclerosis. *Autoimmun Rev* **9**, 830-834, (2010).

37 Hansson, G. K. & Hermansson, A. The immune system in atherosclerosis. *Nat Immunol* **12**, 204-212, (2011).

38 Pober, J. S. & Sessa, W. C. Evolving functions of endothelial cells in inflammation. *Nat Rev Immunol* **7**, 803-815, (2007).

39 Gistera, A. & Hansson, G. K. The immunology of atherosclerosis. *Nat Rev Nephrol* **13**, 368-380, (2017).

40 Carmeliet, P. & Jain, R. K. Principles and mechanisms of vessel normalization for cancer and other angiogenic diseases. *Nat Rev Drug Discov* **10**, 417-427, (2011).

41 Papageorgis, P. & Stylianopoulos, T. Role of TGFbeta in regulation of the tumor microenvironment and drug delivery (review). *Int J Oncol* **46**, 933-943, (2015).

42 Bierie, B. & Moses, H. L. Tumour microenvironment: TGFbeta: the molecular Jekyll and Hyde of cancer. *Nat Rev Cancer* **6**, 506-520, (2006).

43 Herbert, S. P. & Stainier, D. Y. Molecular control of endothelial cell behaviour during blood vessel morphogenesis. *Nat Rev Mol Cell Biol* **12**, 551-564, (2011).

44 Fukumura, D., Kashiwagi, S. & Jain, R. K. The role of nitric oxide in tumour progression. *Nat Rev Cancer* **6**, 521-534, (2006).

45 Patel-Hett, S. & D'Amore, P. A. Signal transduction in vasculogenesis and developmental angiogenesis. *Int J Dev Biol* **55**, 353-363, (2011).

46 Ferrara, N., Gerber, H. P. & LeCouter, J. The biology of VEGF and its receptors. *Nat Med* **9**, 669-676, (2003).

47 Simons, M., Gordon, E. & Claesson-Welsh, L. Mechanisms and regulation of endothelial VEGF receptor signalling. *Nat Rev Mol Cell Biol* **17**, 611-625, (2016).

48 Adams, W. J., Zhang, Y., Cloutier, J., Kuchimanchi, P., Newton, G., Sehrawat, S., Aird, W. C., Mayadas, T. N., Luscinskas, F. W. & Garcia-Cardena, G. Functional vascular endothelium derived from human induced pluripotent stem cells. *Stem Cell Reports* **1**, 105-113, (2013).

49 Amr Youssef, E. R., Phillip Yang. the promise and challenge of human induced pluripotent stem cells for cardiovascular applications *JACC:Basic to Translational Science* **1**, 510-523, (2016).

50 Lee, S., Valmikinathan, C. M., Byun, J., Kim, S., Lee, G., Mokarram, N., Pai, S. B., Um, E., Bellamkonda, R. V. & Yoon, Y. S. Enhanced therapeutic neovascularization by CD31-expressing cells and embryonic stem cell-derived endothelial cells engineered with chitosan hydrogel containing VEGF-releasing microtubes. *Biomaterials* **63**, 158-167, (2015).

51 Marcelo, K. L., Goldie, L. C. & Hirschi, K. K. Regulation of endothelial cell differentiation and specification. *Circ Res* **112**, 1272-1287, (2013).

52 Sommer, C. A. & Mostoslavsky, G. Experimental approaches for the generation of induced pluripotent stem cells. *Stem Cell Res Ther* **1**, 26, (2010).

53 Zanotelli, M. R., Ardalani, H., Zhang, J., Hou, Z., Nguyen, E. H., Swanson, S., Nguyen, B. K., Bolin, J., Elwell, A., Bischel, L. L., Xie, A. W., Stewart, R., Beebe, D. J., Thomson, J. A., Schwartz, M. P. & Murphy, W. L. Stable engineered vascular networks from human induced pluripotent stem cell-derived endothelial cells cultured in synthetic hydrogels. *Acta Biomater* **35**, 32-41, (2016).

54 Lu, Y. A., A.; Langer, R.; Gu, Z. Bioresponsive materials. *Nat Rev* **2**, 1-17, (2016).

55 Caliari, S. R. & Burdick, J. A. A practical guide to hydrogels for cell culture. *Nat Methods* **13**, 405-414, (2016).

56 Ruvinov, E. S., Y.; Cohen, S. *Cardiac Tissue Engineering: Principles, Materials, and Applications*. (Morgan and Claypool Publishers Inc., 2014).

CHAPTER 3:
CHARACTERIZATION OF NOVEL METHOD FOR ENDOTHELIAL CELL DIFFERENTIATION FROM HUMAN PLURIPOTENT STEM CELLS

3.1 Abstract

Human induced pluripotent stem cell (**hiPSC**) derived endothelial cells (**hiPSC-ECs**) have the potential to provide a limitless supply of patient-specific vascular cells to research pathological angiogenesis, vascular diseases, and regeneration of ischemic tissues. Incorporating hiPSC-ECs into angiogenesis models provides a unique, patient-specific platform to study *in vitro* the complex process of angiogenesis and endothelial cell response to biochemical and biophysical changes in their microenvironments [1-5]. Toward this end, significant progress has been made in directed differentiation protocols for human pluripotent stem cell monolayers to the endothelial cell lineage. However, many issues remain with total differentiation time, late stage expression of mature endothelial cell markers, and the use of several different culture medias for a single differentiation. Taking into account the culture and maintenance of the pluripotent stem cells prior to differentiation, the total process can take up to 3 months with 2-3 different media formulations. This study presents a novel method for obtaining a CD31+ endothelial cell population from hiPSCs that requires the use of a chemically defined basal medium from the pluripotency stage to the final stage of differentiation, and does not require a maturation period.

3.2 Introduction

Pathological angiogenesis and vascular diseases are the underlying problem in many life-threatening illnesses. The pathological growth and proliferation of blood vessels, termed the "activated aniogenic switch", is one of the six hallmarks of tumor growth and cancer progression[6]. The WHO reports the global burden of cancer deaths in 2015 to be 8.8 million people and estimates the total annual economic cost of cancer in the U.S. to be $1.16 billion[7]. Cardiovascular disease refers to damaged, narrowed, or blocked blood vessels composed of dysfunctional endothelial cells that can cause a stroke or myocardial infarction [8,9]. According to the 2017 Heart Disease and Stroke Statistics Update by the American Heart Association, Cardiovascular Diseases (CVD) including atherosclerosis, myocardial infarction, stroke, peripheral artery disease, and venous disease collectively remain the leading causes of death in the United States [10]. Additionally, the World Health Organization cites CVD as the leading cause of death worldwide and expects the death rate to continue rising within the next 15 years regardless of socioeconomic backgrounds [11].

Human induced pluripotent stem cell (**hiPSC**) derived endothelial cells (**hiPSC-ECs**) have the potential to provide a limitless supply of patient-specific vascular cells to research pathological angiogenesis, vascular diseases, and regeneration of ischemic tissues. Several endothelial cell differentiation methods have been developed within the last decade. These protocols have evolved from spontaneous embryoid body formation to directed differentiation of 2D pluripotent stem cell monolayers with small molecules and growth

factors. The latter methods modulate the Wnt, SMAD, and MEK/MAPK pathways to recapitulate the differentiation and specification of endothelial cells during developmental vasculogenesis in vitro.[3,4,12]

Kusuma and colleagues developed an 18-day monolayer differentiation protocol for hiPSCs to early vascular lineage cells (EVCs). This consisted of a three 6-day culture stages with two different differentiation medias. First the hiPSCs were fed alpha-MEM medium supplemented with 10% FBS, 0.1 mM beta-mercaptoethanol and after re-plateing, they were fed ECGM with 2% FBS, 50 ng/mL VEGF, 10 uM SB431542. After 12 days of culture, the cells were magnetically sorted for VE-Cadherin since CD31 expression was not detected. The cells were re-plated and allowed to mature further with ECGM containing 50 ng/mL VEGF, 10 uM SB431542. After the third stage of differentiation, the sorted population expressed 80.8% CD31, 95.5% VE-Cadherin, and 98.5% CD146.[5]

Orlova and Mummery developed a 10-day SMAD pathway based endothelial differentiation protocol where mesoderm specification is induced in human pluripotent stem cells by adding BMP4, activin A, small-molecule inhibitor of glycogen synthase kinase-3 (CHIR) and VEGF in BP(E)L medium composed of IMDM, Ham's F12, PFHMII, 10% BSA, Lipids (100x), ITS-X (insulin-transferrin-selenium-ethanolamine, 100x), 22αMTG (mono thiol glycerol, 13 22l in 1 ml IMDM), AA2P (5mg/mL), GlutaMAX (200 mM), and Pen-strep (5,000 U/mL). After 3 days, the cells are fed vascular specification medium that consisted of BP(E)L medium supplemented with VEGF and the TGFβ/SMAD pathway small-molecule inhibitor SB431542. The protocol yielded ~20% CD31+/VCAD+ ECs which were isolated on Day 10.[13]

Prasain and Yoder developed a 21-day differentiation protocol for pluripotent stem cells to endothelial colony forming cells (ECFCs). They cultured human pluripotent stem cells in mTESR1 medium for 2 days, then directed cultures toward the mesodermal lineage with addition of activin A (10 ng/ml) in the presence of FGF-2, VEGF165 and BMP4 (10 ng/ml) for 24 hours. The next day, the culture was fed Stemline II complete media containing FGF-2, VEGF165, and BMP4 to promote endothelial cell specification and proliferation. On Day 12 the CD31+/NRP1+ cells were sorted and cultured in 50% EGM-2 and 50% complete Stemline II differentiation media to generate ECFCs. After 2 days, the media was replaced with three parts of EGM-2 and one part of differentiation media was added to the cultures for seven days.[14]

Lian and Pelacek developed a 5-day protocol to produce endothelial progenitor cells (EPCs) from human pluripotent stem cells which could then be further matured to tube-forming ECs after 55 days in culture. The differentiation protocol was inititated by treating the cells for 2 days with 6–10 uM CHIR99021 in LaSR basal medium consisting of Advanced DMEM/F12, 2.5 mM GlutaMAX, and 60 mg/ml ascorbic acid. The cells were then maintained in LaSR basal medium without CHIR99021 for 3-4 more days. At Day 5 the population consisted of 55% CD34+/CD31+ and 57% KDR+ EPCs. To differentiate the EPCs to mature endothelial cells, the Day 5 CD34+ cells were magnetically sorted and replated on collagen-IV-coated dishes in EGM2 medium and split every 4–5 days with Accutase. At Day 60, 99.2% of the purified population expressed CD31 and 98.9% was VCAD+.

Additionally, at Day 60 the purified endothelial cells demonstrated Ac-LDL uptake and tube-forming ability in a Matrigel angiogenesis assay upon treatment with VEGF supplemented EGM2.[15]

Bao and Pelacek developed a 5-day chemically-defined albumin-free protocol for differentiation of human pluripotent stem cells to endothelial progenitor cells with an additional 10-day endothelial cell differentiation/maturation stage. At day 0, the cells were fed DMEM supplemented with 3–9 μM CHIR99021 and 100 μg/mL ascorbic acid. After 2 days, cells were cultured in DMEM supplemented with ascorbic acid without CHIR99021 for 3 to 4 days. At Day 5, the population expressed 20-32% CD34/31+ and 29% CD144+. At Day 5, the differentiated populations were purified based on CD34 expression. For endothelial cell differentiation, the purified CD34+ cells were plated on collagen IV-coated dishes and fed EGM-2 medium or human endothelial- SFM supplemented with 20 ng/mL bFGF and 10 ng/mL EGF (Life Technologies) for 10 additional days. At Day 15, the endothelial cells demonstrated Ac-LDL uptake and tube formation on a 24-hour Matrigel angiogenesis assay that was fed EGM2 supplemented with 50 ng/mL VEGF.[16]

Most recently, Harding and colleagues developed a 13-15 day endothelial cell differentiation protocol. In this study, the hiPSC/hESCs were grown on mouse embryonic fibroblast feeder (MEF) layers and small clusters were manually passaged onto Matrigel coated plates in mouse embryonic fibroblast (MEF) conditioned hESC medium supplemented with 10 ng/mL of FGF2. After 1 day, the culture medium was switched to StemDiff APEL basal medium with 6 uM CHIR99021 for 2 days. The cells were then cultured in StemDiff APEL medium supplemented with BMP4, bFGF, and VEGF for another 2 days. On day 4, the culture self-assembled into a monolayer of cells with cobblestone morphology, termed “peripheral cells”, with sporadic clusters of smaller cells, termed “central cells”. The entire population was found to be 67.8% CD31+/CD144+, the “peripheral cells” were 84% CD31+/CD144+ and the “central cells” were 55.6% CD31+/CD144+. Due to their higher CD31 expression, the “peripheral cells” were released with shorter accutase exposure time and replated with EC Growth Medium MV2 (ECGM-MV2) supplemented with additional VEGF. The medium was changed every 2 days for 4-6 days to generate mature ECs that were 94%-97% CD31+, 73%-81% CD34+, and 78% to 83% CD144+. After one passage the ECs expressed 99.7% CD31+ and 96.i% CD144+. [17]

Significant progress has been made in directed differentiation protocols for human pluripotent stem cell monolayers to the endothelial cell lineage. However, many issues remain with total differentiation time, late stage expression of mature endothelial cell markers, and the use of several different culture medias for a single differentiation. Total differentiation time is a significant problem and needs to be decreased, since most protocols consist of a 5-10 day differentiation process with an additional maturation phase that can last up to 60 days before the ECs can be used in a functional assay [5,13-17]. Additionally, many of these studies don’t observe the expression of mature endothelial cell markers such as CD31 and VE-Cadherin until the final day of differentiation (Day 5-7) or after the maturation phase (Day 12-15) [5,13-17]. Furthermore, current protocols entail the use of more than one media formulation, including MEF conditioned media, from the pluripotency stage to the differentiation and maturation process [4,5,13-18]. Taking into

account the culture and maintenance of the pluripotent stem cells prior to differentiation, the total process can take up to 3 months with 2-3 different media formulations. This work presents a novel method for obtaining a CD31+ endothelial cell population from hiPSCs that requires the use of a single basal medium from the pluripotency stage to the final stage of differentiation, and does not require a maturation period.

3.3 Materials and Methods

3.3.1 Human Pluripotent Stem Cell Culture and Maintenance

Human induced pluripotent stem cell (hiPSC) line WTC and human embryonic stem cell (hESC) line H9 were grown on plates coated with growth factor-reduced Matrigel (Corning) at 15,000-20,000 cells/cm2 and were fed Essential 8 Medium (ThermoFisher). The cells were passaged every 3 days and 1 uM rho-associated protein kinase (ROCK) inhibitor (Y-27632, STEMCELL Technologies) was added to the culture medium for the first 24 hours after passaging.

3.3.2 Modified Protocol for hPSC-Endothelial Cell Differentiation

The modified protocol for endothelial cell differentiation developed in this study is summarized in Figure 3.1. First, the human pluripotent stem cells were passaged onto plates coated with growth factor-reduced Matrigel (Corning) at 25,000-30,000 cells/cm^2 and fed Essential 8 Medium supplemented with 10 uM ROCK inhibitor (day -2). The medium was replaced the next day (day -1) with Essential 8 without ROCK inhibitor. The cells were grown to approximately 80% confluency which occurs on day 0 with this initial seeding density. Differentiation was initiated on day 0, by feeding the cells Essential 8 Medium supplemented with 6 uM CHIR 99021 (STEMCELL Technologies). Endothelial lineage specification was started on day 2 by the addition of Essential 8 Medium supplemented with 10 ng/ml BMP4 (R&D systems), 50 ng/ml VEGF-A_{165} (R&D Systems), and 10 uM SB431542 (TOCRIS). The cells were fed this medium (E8BVi) everyday for 3 more days up to the final stage of differentiation on day 5. After day 5, the cells were magnetically sorted for CD31+ expression and expanded in EGM2.

3.3.3 Flow Cytometry Analysis

Cells were dissociated using TrypLE (ThermoFisher) with a 7 minute incubation in 37°C (5% CO_2) and quenched with EGM2 (1:5 enzyme to EGM2). The cells were then centrifuged at 1200 rpm for 5 minutes and the supernatant was removed. The cells were then washed with PBS and fixed with 4% paraformaldehyde for 10 minutes. The sample was centrifuged to remove PFA and then washed twice with PBS. The sample was resuspended in FACSB10 buffer [13] and stained with the fluorescently labeled antibodies listed in Table 3.1. The sample and antibodies were incubated overnight at 4°C. Samples were analyzed with a Beckman Coulter FC500 flow cytometer. The data was analyzed with Kaluza software (Beckman Coulter) and gating was based on corresponding isotype controls.

3.3.4 CD31+ Endothelial Cell Magnetic-Activated Cell Sorting (MACS)

Magnetic-activated cell sorting (MACS) was done on day 5 of differentiation or the following day to avoid over-confluence of cultures, which would decrease purity of the positively isolated population. Endothelial cells were magnetically sorted with Dynabeads M-280 Sheep Anti-Mouse (Invitrogen, Carlsbad, CA) coated with primary mouse anti-human CD31 antibody (Invitrogen) at a ratio of 5:1 beads to cells. Prior to sorting, the dynabeads were washed twice with sterile FACSB10 buffer [13] with a DynaMag-15 magnet (Invitrogen). The beads were resuspended in 200 uL FACSB10 and incubated with mouse anti-human CD31 antibody (1:50) for 30 minutes at room temperature with gentle rocking. Antibody conjugated beads were then washed twice with FACSB10 and resuspended in 500 uL FACSB10. Cells were singularized using TrypLE with a 7 minute incubation period (37°C, 5% CO_2) and quenched with EGM2 (1:5 enzyme to EGM2). The cells were then centrifuged at 1200 rpm for 5 minutes and the supernatant was removed. The antibody-conjugated beads were then mixed with the cells and incubated at room temperature with gentle rocking for 30 minutes. The CD31+ cells were then isolated from the rest of the population with the DynaMag-15 magnet with two washes consisting of FACSB10 and one wash with EGM2. The isolated, bead-bound endothelial cells were then resuspended in EGM2 with 10uM Rock Inhibitor. The cells were seeded at 150,000 cells/cm^2 on 0.2% Gelatin coated TCPS plates. The cells were fed EGM2 the following day and every two days thereafter.

3.3.5 Fluorescence Microscopy

Cells were rinsed with PBS and fixed with 4% PFA for 10 minutes. They were then washed with PBS and stained sequentially with primary and secondary antibodies in 1% BSA buffer for either 2 hours at room temperature or overnight at 4°C (antibodies are listed in Table 3.1). The samples were then washed twice with PBS. Fluorescent and phase contrast images were taken on a Nikon Eclipse TE300 microscope with a Hamamatsu C11440 digital camera and Zen lite software (Carl Zeiss, Thornwood, NY).

3.3.6 Reverse Transcription Quantitative Polymerase Chain Reaction (RT-qPCR)

Total RNA was isolated and purified using the RNeasy Mini Kit (Qiagen, Germantown, MD) according to manufacturer specifications, including the DNase I treatment (RNase-Free DNase Set, Qiagen). A NanoDrop™ 2000/2000c spectrophotometer (ThermoFisher) was used to measure RNA concentration. RNA (1-2 ug) was reverse transcribed to cDNA using the SuperScript III Reverse Transcriptase kit (Invitrogen) with Oligo(dT) primer according to manufacturer specifications. Real-time quantitative PCR was done on 10 ng of cDNA from each sample with RT2 SYBR Green Mastermix (Qiagen) on a StepOnePlus thermocycler (Applied Biosystems). The primers for the tested genes are listed in Table 3.2, GAPDH and HSP90AB1 were used as endogenous housekeeping controls.

3.3.7 Ac-LDL Uptake Assay

Live, CD31+ purified cells were incubated with Dil fluorescent dye-labeled acetylated low density lipoprotein (Dil-ac-LDL) (ThermoFisher) at 10 ug/mL in EGM2 for 4 hours at 37°C, 5% CO_2. The cells were then rinsed with PBS and imaged on a Nikon Eclipse TE300 microscope.

3.3.8 Matrigel Angiogenesis Assay

CD31+ purified endothelial cells were seeded at 62,500 cells per cm^2 on 100 uL growth-factor reduced Matrigel in a 96-well plate in EGM2. Tube formation was observed with Nikon Eclipse TE300 phase contrast microscope after 24 hours, 48 hours, and 72 hours of incubation.

3.3.9 Statistical Analysis

All quantitative measurements were performed at least in triplicate samples and values are expressed as mean ± standard deviation (SD). One-way ANOVA with post-hoc Tukey tests were used to compare treatment groups and $p<0.05$ was used to assess statistical significance.

3.4 Results and Discussion

3.4.1 Changes in cell morphology and organization are observed with phase contrast microscopy

The protocol timeline for hiPSC-EC differentiation developed in this study is summarized in Figure 3.1. The protocol is primarily based on the SMAD and MAPK signaling pathways, which are active during embryonic vasculogenesis and angiogenesis.[1,19-21] The Essential 8 medium (E8), which is used to feed pluripotent stem cells, contains bFGF and TGF-β1 (Table 3.3). Therefore, this basal medium can be supplemented with proangiogenic growth factors and cytokines to promote endothelial cell lineage specification. Differentiation begins on Day 0 by inducing mesoderm formation with supplementation of E8 media with the small molecule, CHIR99021, which inhibits the serine/threonine protein kinase, GSK3.[13,15] This prevents the phosphorylation and downstream proteosomal degradation of beta-catenin. Thus, beta-catenin accumulates in the cytoplasm and enters the nucleus where it acts as a co-activator of transcription for target genes of the canonical Wnt signaling pathway, which include those that lead to mesoderm lineage.[22,23] Figure 3.2 shows a general diagram of the canonical Wnt signaling pathway. On Day 2, E8 is supplemented with BMP4, VEGF-A, and the small molecule SB431542. The inherent TGF-β1 and supplemented BMP4 bind the ALK1/5 and ALK3/6 transmembrane receptors respectively and activate the SMAD1/5 signaling pathway which promotes endothelial cell lineage and proliferation. However, TGF-β1 also activates the SMAD 2/3 pathway via Alk 5 activation, which inhibits endothelial cell proliferation. Therefore, the E8 media was also supplemented with an ALK-5 small-molecule inhibitor, SB431542.[1,13,19-21,24,25] A summary schematic of these signaling pathways is shown in Figure 3.3. Finally, VEGF-A and the

inherent bFGF, which are potent proangionenic growth factors, promote endothelial cell specification and proliferation through the MAPK signaling pathway.[1,19,26-28]

Figure 3.4 demonstrates phase contrast images of the WTC11 human induced pluripotent stem cell line undergoing the endothelial cell differentiation protocol. Figure 3.4(a) shows the WTC hiPSCs at Day -2, the cells are organized into a single monolayer due to the addition of ROCK inhibitor in the E8 culture medium. The cells organize into colonies typical of pluripotent stem cells upon removal of ROCK inhibitor (Day -1, Fig. 3.4(b)). At the initiation of differentiation (Day 0, Fig. 3.4(c)), the cells re-organize and continue to proliferate into a confluent monolayer. The cells then continue to reorganize into separate layers as differentiation progresses (Fig. 3.4(e-g)). CD31+ endothelial cells are sorted after the differentiation process is complete and the ligand-bound magnetic beads can be seen 24 hours after re-plating (Fig. 3.4(h)). Figure 3.4(i) demonstrates that after a week in culture, sorted endothelial cells exhibit the same "cobblestone" morphology that is typically seen in cultured primary and immortalized endothelial cell lines.[29] These changes in cell morphology and organization throughout the differentiation process demonstrate an active transition from pluripotency to endothelial linage cells.

3.4.2 Immunofluorescence microscopy demonstrates distinct organization of mixed cell population

At day 5, immunofluorescent staining of the mixed population of terminally differentiated hiPSCs demonstrated a distinct organization of CD31+, CD90+, VE-Cadherin+, and SM22+ cells (Figure 3.5). Cells expressing CD31 were predominately localized in a top layer but could also be seen dispersed throughout the well. Similarly, CD90+ cells were localized to a separate, bottom layer, however, they were also found to penetrate the top layer, and the VE-Cadherin+ cells appeared to be predominately located on the top layer. Figure 3.18(a) shows the differentiated H9 hESCs on day 5 also organized into layers where the CD31+ cells mostly resided in the top.

3.4.3 Flow Cytometry Characterization of the hiPSCs for endothelial cell lineage

Prior to differentiation, pluripotency of the hiPSCs was characterized with flow cytometry on day -1, demonstrating the expression of pluripotency markers OCT3/4, SOX2, and SSEA4 gated relative to their corresponding isotype control (Fig. 3.6). Figure 3.7 shows representative flow cytometry density plots for hiPSC-ECs for CD31, CD34, VEGFR2 (KDR), CD90, and CD45 on day 5 of the differentiation process. The temporal data is summarized in Figure 3.8-3.11 and Figure 3.12, which shows the expression of endothelial cell markers CD34 and VEGFR2, as early as day 1. Figure 3.12 also demonstrates a steady increase in mature endothelial lineage marker CD31 with an average expression of 27% by day 5. VE-Cadherin was relatively unchanged after day 1 with an average 55% expression. To determine if differentiation was complete by day 5, the cells were fed E8BVi for two more days and analyzed with flow cytometry (Figure 3.12). Interestingly, the VEGFR2+ population significantly decreased at day 7, while CD31, VE-Cadherin, and CD34 expression did not significantly increase, which suggested that continuation of the differentiation process past day 5 was not necessary. Finally, to confirm applicability of the differentiation

process across different pluripotent cells, the H9 human embryonic stem cell line was differentiated and analyzed with flow cytometry on day 5 (Fig. 3.18(b)). Similar results were seen with the H9 hESC, with approximately 31% of the differentiated population expressing CD31.

3.4.4 RT-qPCR analysis Characterization of the hiPSCs for endothelial cell lineage

The hiPSCs were also temporally analyzed for gene expression from the pluripotency stage to the final differentiation stage. Figure 3.13 shows quantitative RT-qPCR results for gene expression of pluripotency (OCT4 and NANOG) along with mesoderm (T) and endothelial cell lineage markers (CD34, PECAM1, CDH5, KDR, FLT1, and ENG). These results demonstrate expression of pluripotency markers OCT4 and NANOG at day -1 and no expression by day 5. Accordingly, the upregulation of early mesoderm marker T (Brachyury) was observed 24 hours after differentiation was initiated and little expression was detected by day 5. This was expected since the addition of the GSK3 inhibitor, CHIR 99021, initiates the canonical Wnt signaling pathway which has been shown to cause pluripotent stem cells to differentiate into a mesoderm lineage. Increased gene expression for endothelial cell lineage markers CD34, PECAM1 (CD31), ENG (CD105), KDR (VEGFR2), FLT1 (VEGFR1), and CDH5 (VE-CAD) on day 3 and 5 corresponds with the results from phenotype analysis with flow cytometry.

3.4.5 Characterization of CD31+ purified population demonstrates endothelial cell-specific phenotype, gene expression, and stable network formation

Flow cytometry analysis demonstrates the purified population was 91% CD31+, 98% CD34+, 98% VE-Cadherin+, 52% VEGFR2 (KDR)+, 11% CD90+, and CD45 expression was not detected (Fig. 3.14). Analysis with RT-qPCR demonstrated the purified endothelial cell population retained similar CD31 (PECAM1) and CD34 gene expression while KDR (VEGFR2) and VE-Cadherin (CDH5) expression increased compared to the unpurified, day 5 population (Fig. 3.15). Figure 3.16(a) shows the purified endothelial cells seven days after magnetic sorting readily took up Ac-LDL within 4 hours of treatment. Additionally, the cells stained positive for CD31 and demonstrated limited CD90 expression (Fig. 3.16(b,c)). Finally, the cells spontaneously formed cord-like networks in a 2D Matrigel angiogenesis assay within 24 hours and were stable for approximately 48 hours in culture (Fig 3.17(a-c)).

3.5 Conclusions

This study validated a 5-day hiPSC-EC differentiation protocol using a defined medium (E8) supplemented with proangiogenic factors. This method incorporated the Wnt, SMAD, and MEK/MAPK pathways that regulate embryonic vasculogenesis and angiogenesis. The differentiation protocol resulted in an endothelial cell population that expressed lineage-specific markers at earlier time points compared to previously reported methods [5,13-17], which was demonstrated by flow cytometry and RT-qPCR analysis. The early expression of EC markers likely occurred since the cells were already supplemented with TGF-β1 and bFGF from the complete E8 maintenance media prior to differentiation. This allowed the

SMAD and MEK/MAPK pathways to be enhanced and directed to promote the endothelial cell lineage with the addition of BMP4, VEGF-A, and SB431542. The decreased expression of VEGFR2/KDR on day 7 could signify a shift to a more quiescent state through contact inhibition by the endothelial cell population as they became more confluent, and demonstrated that continuation of the differentiation process beyond day 5 was not necessary [1,19]. Due to the sustained expression of endothelial lineage markers, the terminally differentiated population could be purified based on CD31+ expression. After a week of expansion, the sorted hiPSC-ECs took up Ac-LDL and formed stable networks in a Matrigel angiogenesis assay for up to three days, unlike HUVECs which typically regress within 12-24 hours [12]. The purified population also maintained CD31/CD34 expression, increased VCAD and KDR expression, and diminished expression of CD45 and CD90. The hiPSC-EC's ability to perform lineage-specific functions and maintain endothelial marker expression shortly after sorting demonstrated a maturation stage after differentiation was not necessary, significantly reducing the duration of the protocol.

3.6 References

1 Chung, A. S. & Ferrara, N. Developmental and pathological angiogenesis. *Annu Rev Cell Dev Biol* **27**, 563-584, (2011).

2 Coulombe, K. L., Bajpai, V. K., Andreadis, S. T. & Murry, C. E. Heart regeneration with engineered myocardial tissue. *Annu Rev Biomed Eng* **16**, 1-28, (2014).

3 Yoder, M. C. Differentiation of pluripotent stem cells into endothelial cells. *Curr Opin Hematol* **22**, 252-257, (2015).

4 Wilson, H. K., Canfield, S. G., Shusta, E. V. & Palecek, S. P. Concise review: tissue-specific microvascular endothelial cells derived from human pluripotent stem cells. *Stem Cells* **32**, 3037-3045, (2014).

5 Kusuma, S., Shen, Y. I., Hanjaya-Putra, D., Mali, P., Cheng, L. & Gerecht, S. Self-organized vascular networks from human pluripotent stem cells in a synthetic matrix. *Proc Natl Acad Sci U S A* **110**, 12601-12606, (2013).

6 Hanahan, D. & Weinberg, R. A. Hallmarks of cancer: the next generation. *Cell* **144**, 646-674, (2011).

7 WHO. *Cancer*, (2017), http://www.who.int/cancer/enl/.

8 George, S. J., Johnson, Jason. *Atherosclerosis: Molecular and Cellular Mechanisms*. (Wiley-VCH Verlag GmbH & Co., 2010).

9 Gimbrone, M. A., Jr. & Garcia-Cardena, G. Endothelial Cell Dysfunction and the Pathobiology of Atherosclerosis. *Circ Res* **118**, 620-636, (2016).

10 Benjamin, E. J., Blaha, M. J., Chiuve, S. E., Cushman, M., Das, S. R., Deo, R., de Ferranti, S. D., Floyd, J., Fornage, M., Gillespie, C., Isasi, C. R., Jimenez, M. C., Jordan, L. C., Judd, S. E., Lackland, D., Lichtman, J. H., Lisabeth, L., Liu, S., Longenecker, C. T., Mackey, R. H., Matsushita, K., Mozaffarian, D., Mussolino, M. E., Nasir, K., Neumar, R. W., Palaniappan, L., Pandey, D. K., Thiagarajan, R. R., Reeves, M. J., Ritchey, M., Rodriguez, C. J., Roth, G. A., Rosamond, W. D., Sasson, C., Towfighi, A., Tsao, C. W., Turner, M. B., Virani, S. S., Voeks, J. H., Willey, J. Z., Wilkins, J. T., Wu, J. H., Alger, H. M., Wong, S. S., Muntner, P., American Heart Association Statistics, C. & Stroke Statistics, S. Heart Disease and Stroke Statistics-2017 Update: A Report From the American Heart Association. *Circulation* **135**, e146-e603, (2017).

11 WHO. *Global Atlas on cardiovascular disease prevention and control*. (2011).

12 Sanz-Nogues, C. & O'Brien, T. In vitro models for assessing therapeutic angiogenesis. *Drug Discov Today* **21**, 1495-1503, (2016).

13 Orlova, V. V., van den Hil, F. E., Petrus-Reurer, S., Drabsch, Y., Ten Dijke, P. & Mummery, C. L. Generation, expansion and functional analysis of endothelial cells and pericytes derived from human pluripotent stem cells. *Nat Protoc* **9**, 1514-1531, (2014).

14 Prasain, N., Lee, M. R., Vemula, S., Meador, J. L., Yoshimoto, M., Ferkowicz, M. J., Fett, A., Gupta, M., Rapp, B. M., Saadatzadeh, M. R., Ginsberg, M., Elemento, O., Lee, Y., Voytik-Harbin, S. L., Chung, H. M., Hong, K. S., Reid, E., O'Neill, C. L., Medina, R. J., Stitt, A. W., Murphy, M. P., Rafii, S., Broxmeyer, H. E. & Yoder, M. C. Differentiation of human pluripotent stem cells to cells similar to cord-blood endothelial colony-forming cells. *Nat Biotechnol* **32**, 1151-1157, (2014).

15 Lian, X., Bao, X., Al-Ahmad, A., Liu, J., Wu, Y., Dong, W., Dunn, K. K., Shusta, E. V. & Palecek, S. P. Efficient differentiation of human pluripotent stem cells to endothelial progenitors via small-molecule activation of WNT signaling. *Stem Cell Reports* **3**, 804-816, (2014).

16 Bao, X., Lian, X., Dunn, K. K., Shi, M., Han, T., Qian, T., Bhute, V. J., Canfield, S. G. & Palecek, S. P. Chemically-defined albumin-free differentiation of human pluripotent stem cells to endothelial progenitor cells. *Stem Cell Res* **15**, 122-129, (2015).

17 Harding, A., Cortez-Toledo, E., Zhou, P. . Highly Efficient Differentiation of Endothelial Cells from Pluripotent Stem Cells Requires the MAPK and the PI3K Pathways. *Stem Cells* **35**, 909-919, (2017).

18 Kurokawa, Y. K., Yin, R. T., Shang, M. R., Shirure, V. S., Moya, M. L. & George, S. C. Human Induced Pluripotent Stem Cell-Derived Endothelial Cells for Three-Dimensional Microphysiological Systems. *Tissue Eng Part C Methods* **23**, 474-484, (2017).

19 Patel-Hett, S. & D'Amore, P. A. Signal transduction in vasculogenesis and developmental angiogenesis. *Int J Dev Biol* **55**, 353-363, (2011).

20 Derynck, R. & Zhang, Y. E. Smad-dependent and Smad-independent pathways in TGF-beta family signalling. *Nature* **425**, 577-584, (2003).

21 Lebrin, F., Deckers, M., Bertolino, P. & Ten Dijke, P. TGF-beta receptor function in the endothelium. *Cardiovasc Res* **65**, 599-608, (2005).

22 Reis, M. & Liebner, S. Wnt signaling in the vasculature. *Exp Cell Res* **319**, 1317-1323, (2013).

23 Sonderegger, S., Pollheimer, J. & Knofler, M. Wnt signalling in implantation, decidualisation and placental differentiation--review. *Placenta* **31**, 839-847, (2010).

24 Inman, G. J., Nicolas, F. J., Callahan, J. F., Harling, J. D., Gaster, L. M., Reith, A. D., Laping, N. J. & Hill, C. S. SB-431542 is a potent and specific inhibitor of transforming

growth factor-beta superfamily type I activin receptor-like kinase (ALK) receptors ALK4, ALK5, and ALK7. *Mol Pharmacol* **62**, 65-74, (2002).

25 Bertolino, P., Deckers, M., Lebrin, F. & ten Dijke, P. Transforming growth factor-beta signal transduction in angiogenesis and vascular disorders. *Chest* **128**, 585S-590S, (2005).

26 Marcelo, K. L., Goldie, L. C. & Hirschi, K. K. Regulation of endothelial cell differentiation and specification. *Circ Res* **112**, 1272-1287, (2013).

27 Zhang, W. & Liu, H. T. MAPK signal pathways in the regulation of cell proliferation in mammalian cells. *Cell Res* **12**, 9-18, (2002).

28 Ferrara, N., Gerber, H. P. & LeCouter, J. The biology of VEGF and its receptors. *Nat Med* **9**, 669-676, (2003).

29 Herbert, S. P. & Stainier, D. Y. Molecular control of endothelial cell behaviour during blood vessel morphogenesis. *Nat Rev Mol Cell Biol* **12**, 551-564, (2011).

3.7 Tables

Table 3.1. Antibodies for immunofluorescence staining (IF) and flow cytometry (FC).

Antibody		Application
CD31	ThermoFisher, Mouse IgG1 Clone: WM59 Cat: MA1-26196	1:100 (IF)
CD31-APC	ThermoFisher, Mouse IgG1 Clone: WM59 Cat: 17-0319-41	5 µL (0.5 µg)/test (FC)
CD31-FITC	ThermoFisher, Mouse IgG1 Clone: WM59 Cat: 11-0319-42	5 µL (0.5 µg)/test (FC)
CD34-FITC	Biolegend, Mouse IgG1 Clone: 581 Cat:343518	5 µL/test (FC)
VEGFR2 (KDR)-FITC	R&D Systems, Mouse IgG1 Clone: Cat: FAB357F	10 µL/test (FC)
VE-Cadherin	Abcam, Rabbit IgG1 Cat: ab33321	5 µL/test (FC)
Ms Isotype Control-FITC	Biolegend, Mouse IgG1 Clone: MOPC21 Cat: 400129	10 µL/test (FC)
Ms Isotype Control-APC	Biolegend, Mouse IgG1 Clone: MOPC21 Cat: 400119	10 µL/test (FC)
CD90	ThermoFisher, Mouse IgG1 Clone: 5E10 Cat: 14-0909-82	1:200 (IF)
CD90-APC	ThermoFisher, Mouse IgG1 Clone: 5E10 Cat: 17-0909-42	5 µL (0.25 µg)/test
CD90-FITC	Biolegend, Mouse IgG1 Clone: 5E10 Cat: 328107	5 µL (0.25 µg)/test
CD45-FITC	Biolegend, Mouse IgG1 Clone: HI30 Cat: 304005	5 µL/test (FC)
CD45-APC	Biolegend, Mouse IgG1 Clone: HI30 Cat: 304011	5 µL/test (FC)

Table 3.2. Primers for RT-QPCR.

Gene Name	Catalog Primer ID	Source
NANOG	CAPH2278	Qiagen
POU5F1	CAPH2278	Qiagen
T	CAPH2278	Qiagen
GAPDH	CAPH2278	Qiagen
CD34	Hs00692830 _CE	ThermoFisher Scientific
PECAM1	Hs00490758 _CE	ThermoFisher Scientific
CDH5	Hs00520270_CE	ThermoFisher Scientific
ENG	Hs00564508_CE	ThermoFisher Scientific
KDR	Hs00517313_CE	ThermoFisher Scientific
FLT1	Hs00566183_CE	ThermoFisher Scientific
GAPDH	Hs00608981_CE	ThermoFisher Scientific
HSP90AB1	Hs00610633_CE	ThermoFisher Scientific

Table 3.3. Commercially Available Media Components.

Name:	Essential 8 (ThermoFisher Scientific)	EGM2 (Lonza)
Basal Medium:	DMEM F-12	EBM
Components:	L-scorbic acid	hEGF
	Selenium	VEGF
	Transferrin	R3-IGF-1
	NaHCO3	Ascorbic Acid
	Insulin	Hydrocortisone
	FGF2 (bFGF)	hFGF-β
	TGFβ1	Heparin
		FBS
		Gentamicin/Amphotericin-B

3.8 Figures

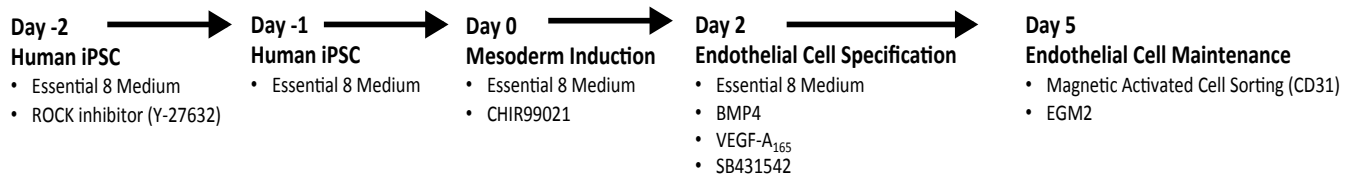

Figure 3.1. Endothelial Cell (EC) Differentiation Protocol for single basal medium from pluripotency to end-stage.

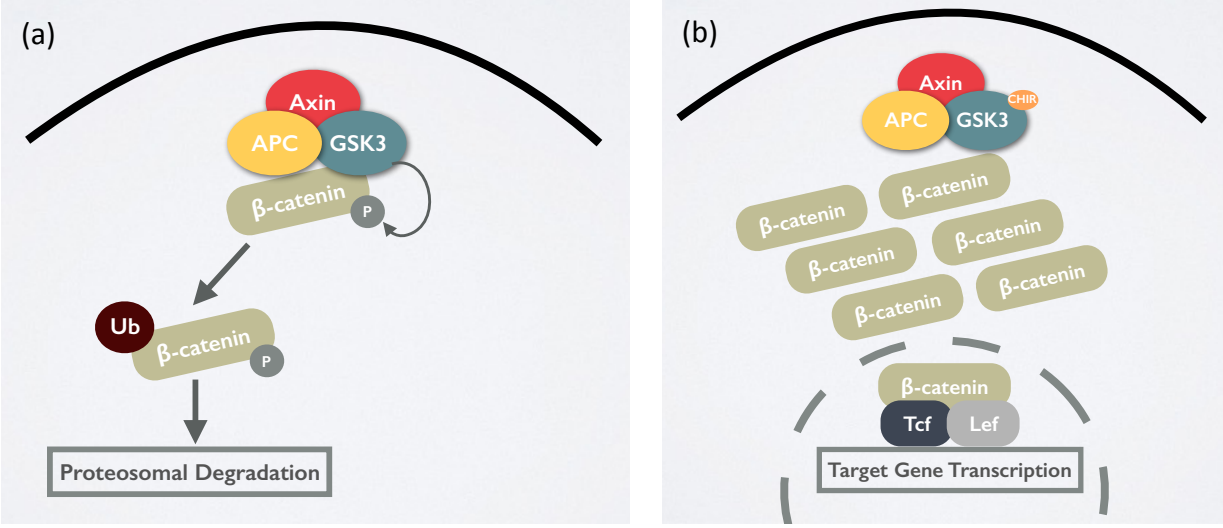

Figure 3.2. Small-molecule inhibition of Canonical Wnt Signaling (a) GSK3 phosphorylation of beta-catenin for proteosomal degradation (b) allosteric inhibition of GSK3 with small-molecule CHIR 99021.

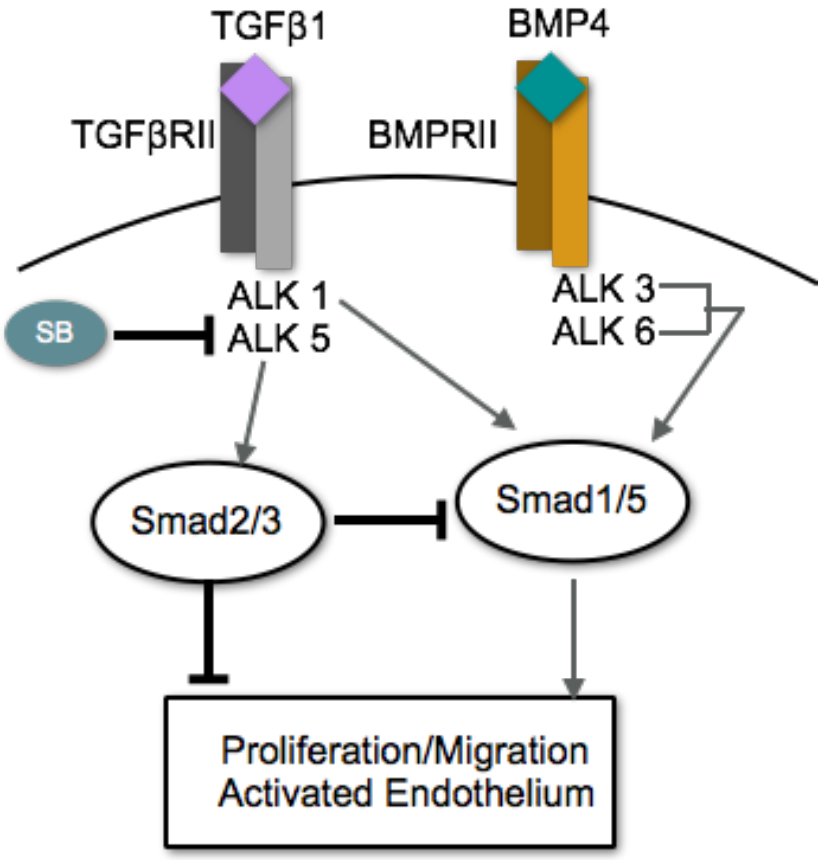

Figure 3.3. Small-molecule inhibition of SMAD Signaling for endothelial cell lineage specification.

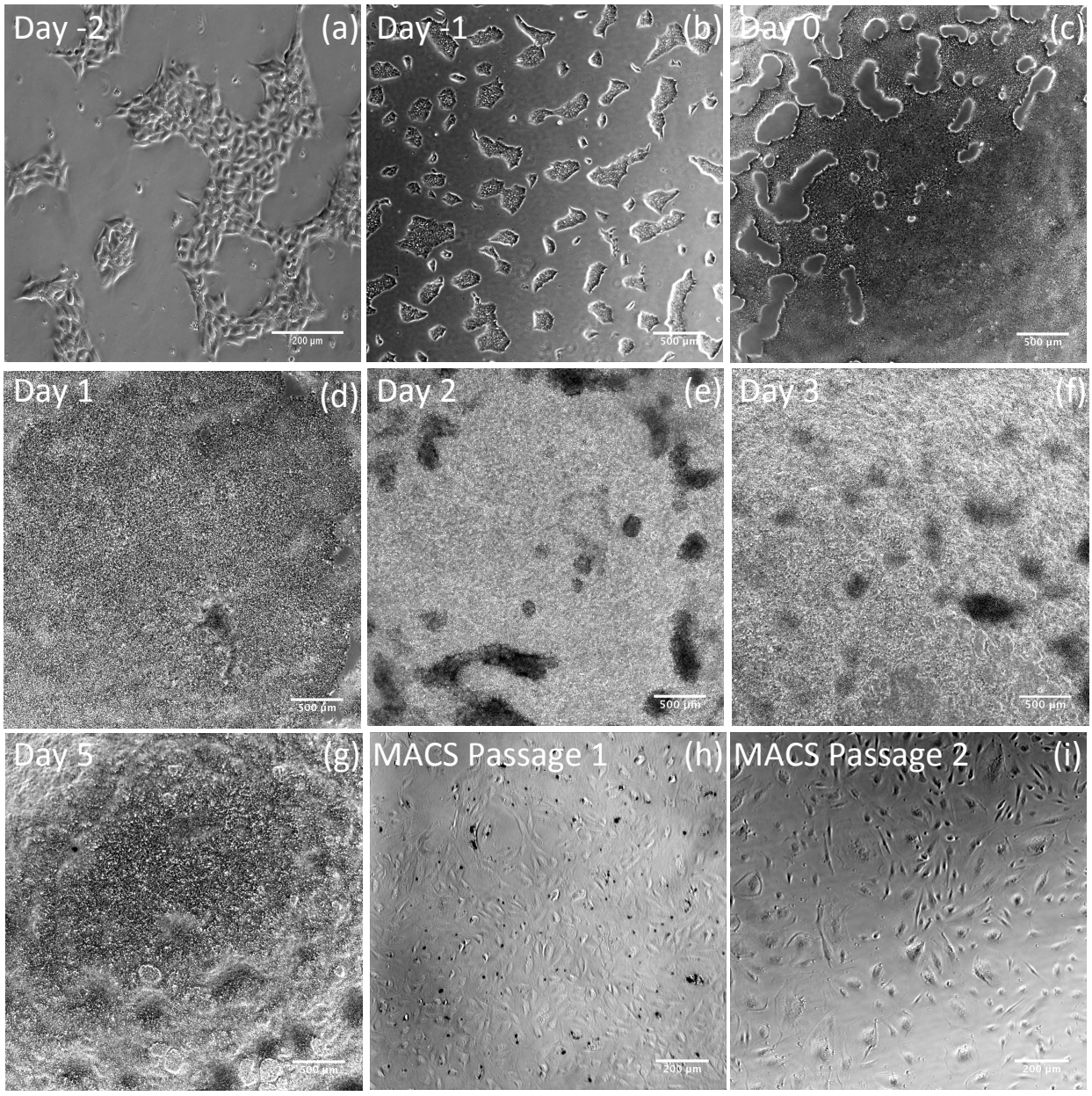

Figure 3.4. Phase contrast images demonstrated temporal changes in organization and morphology of the hiPSCs undergoing endothelial cell differentiation.

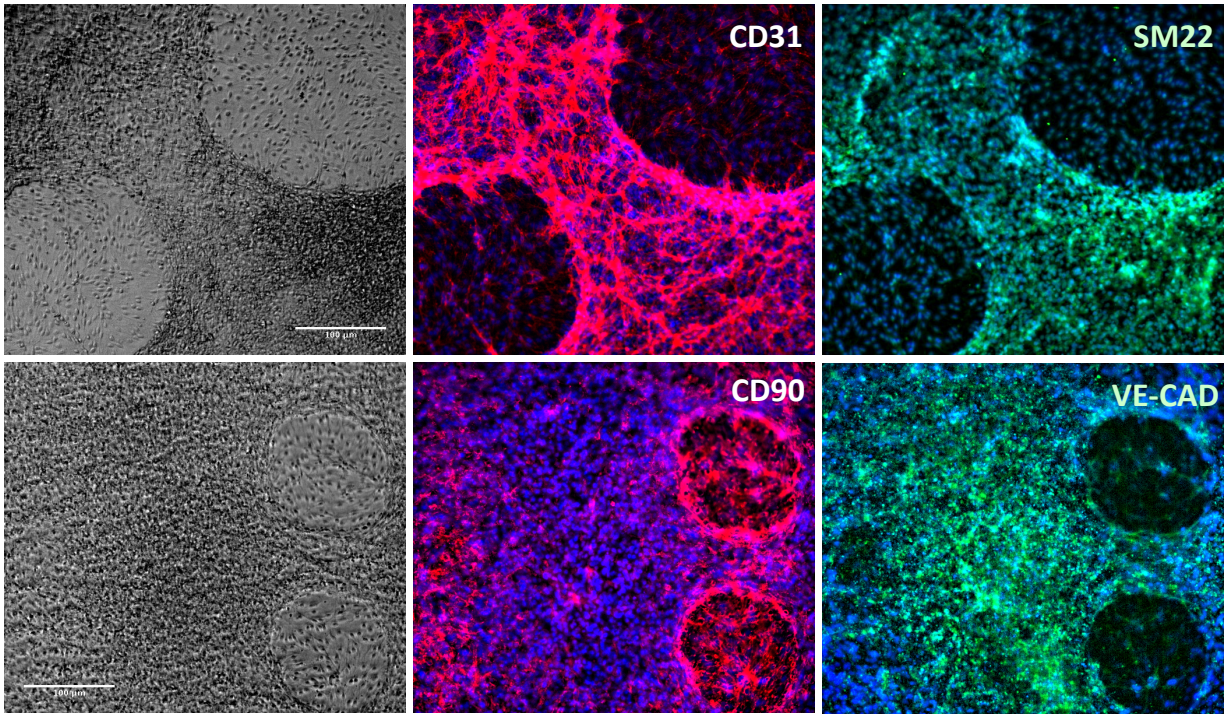

Figure 3.5. immunofluorescence staining at day 5 of differentiation demonstrated a mixed population of endothelial and stromal cell lineages.

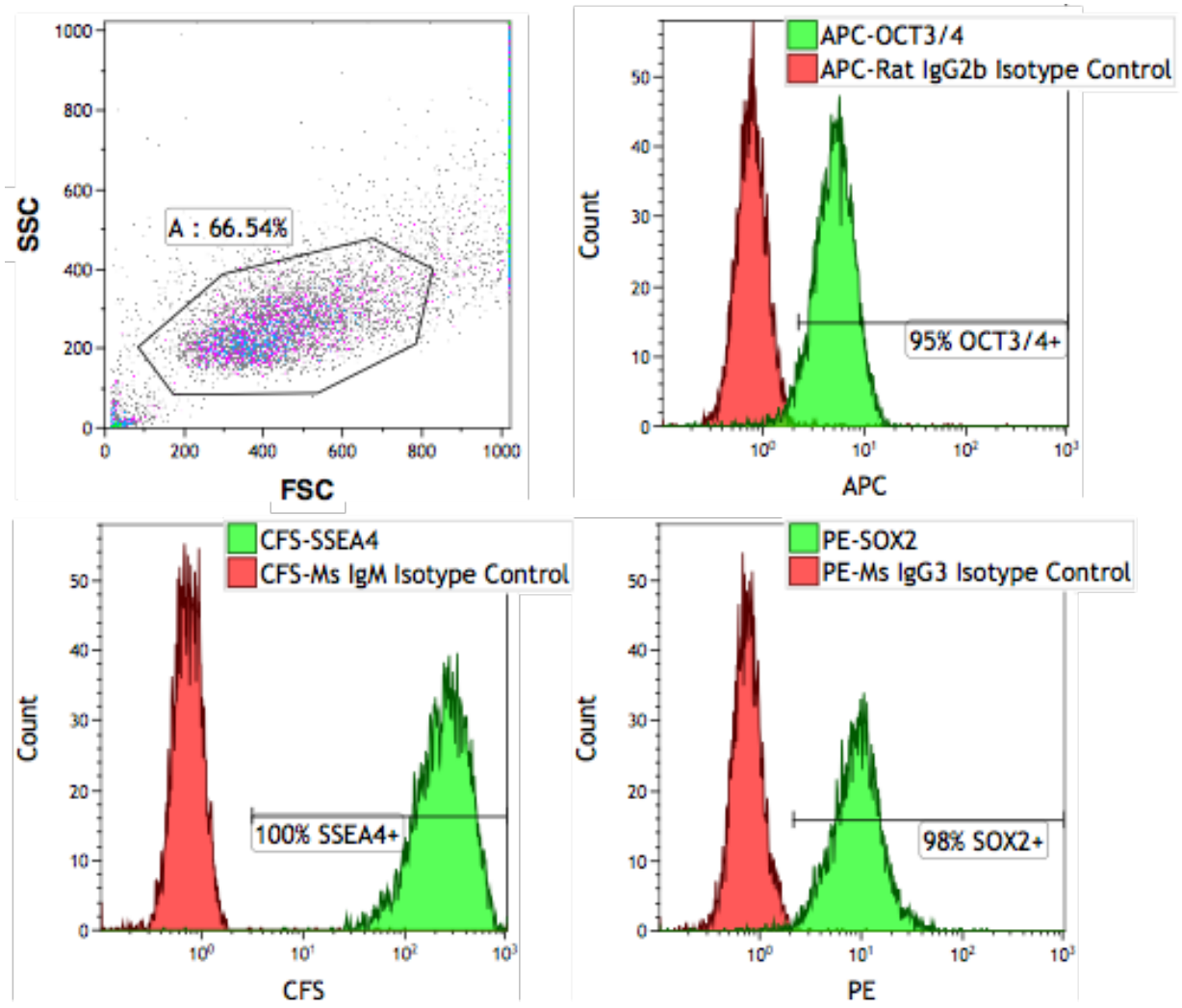

Figure 3.6. Representative flow cytometry analysis of WTC human induced pluripotent stem cell line.

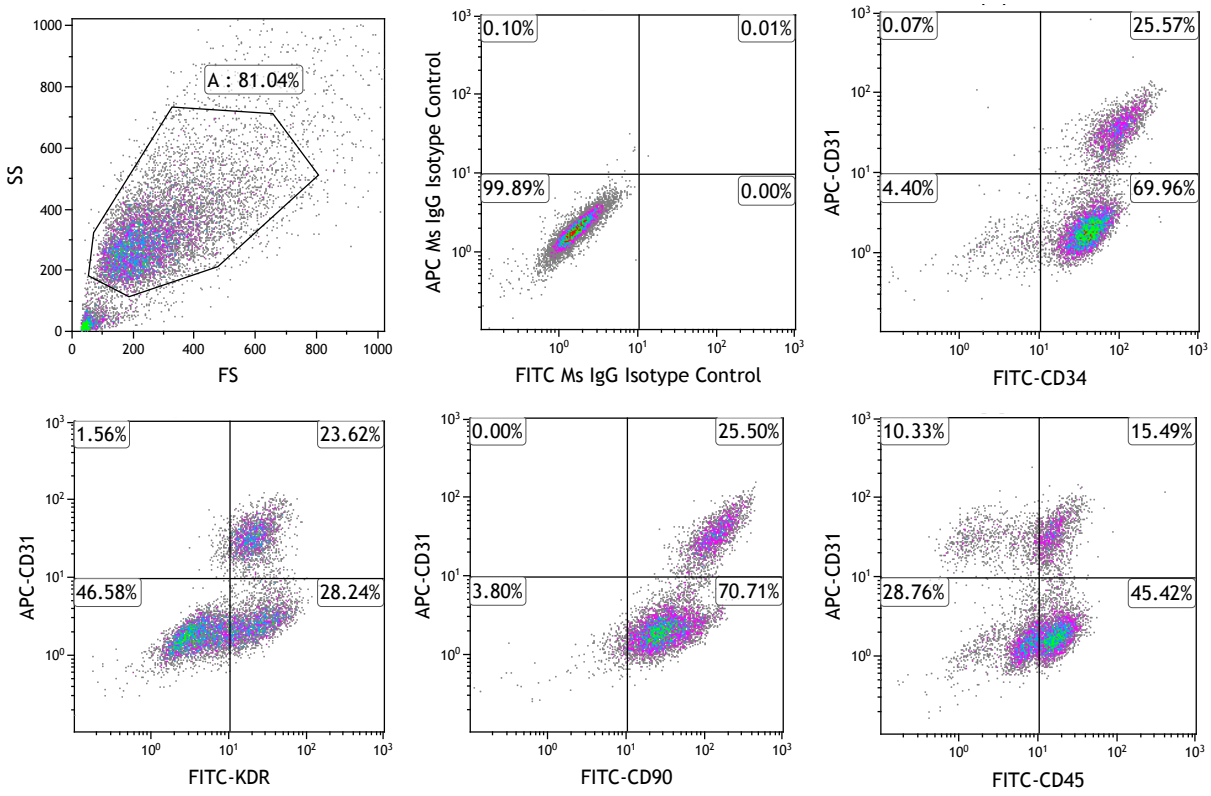

Figure 3.7. Representative flow cytometry density plots of CD31, CD34, VEGFR2 (KDR), CD90, and CD45 expression at day 5 of unpurified population during EC Differentiation.

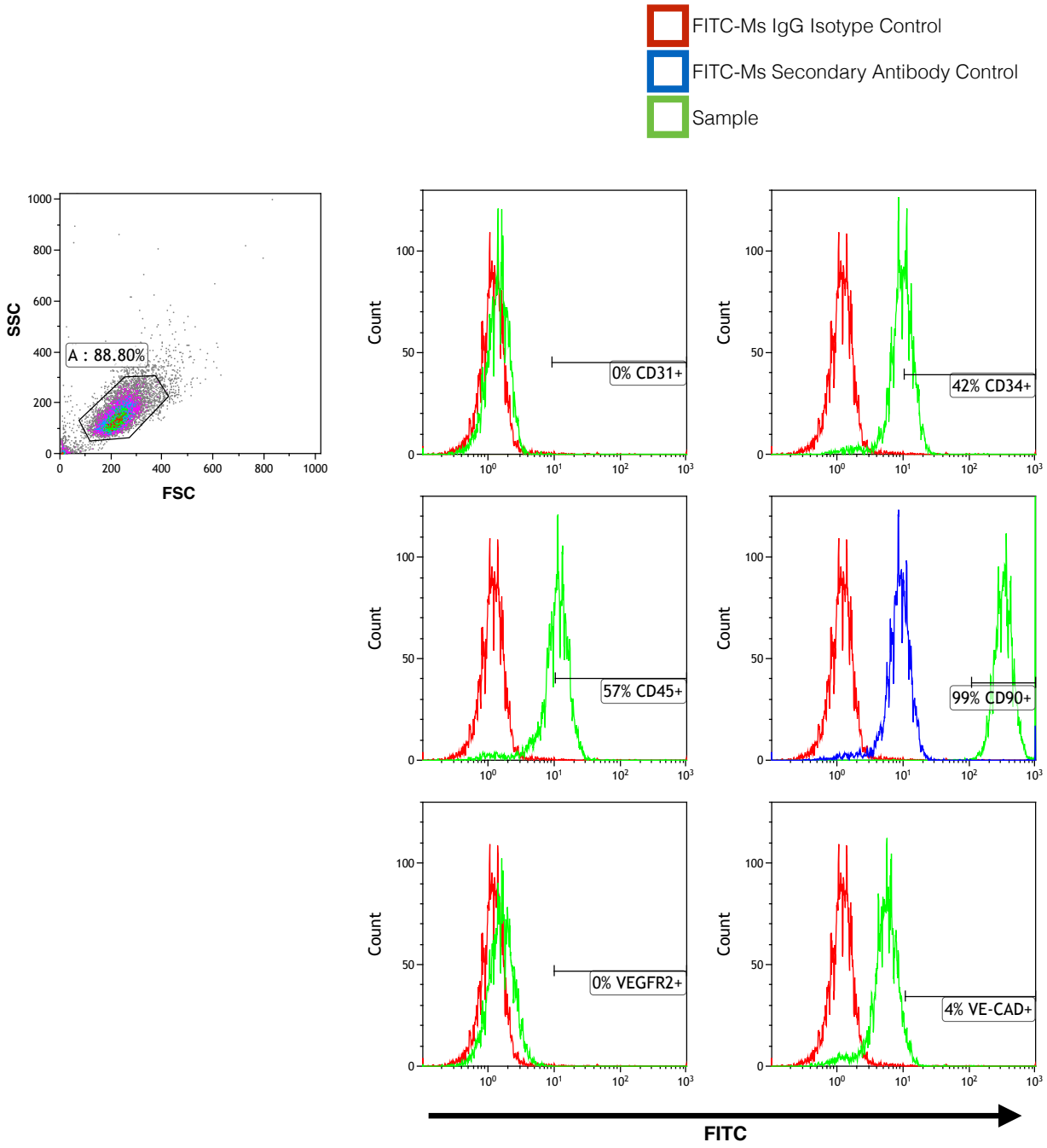

Figure 3.8. Representative histograms for temporal flow cytometry analysis in unpurified hiPSC-EC (Day 1).

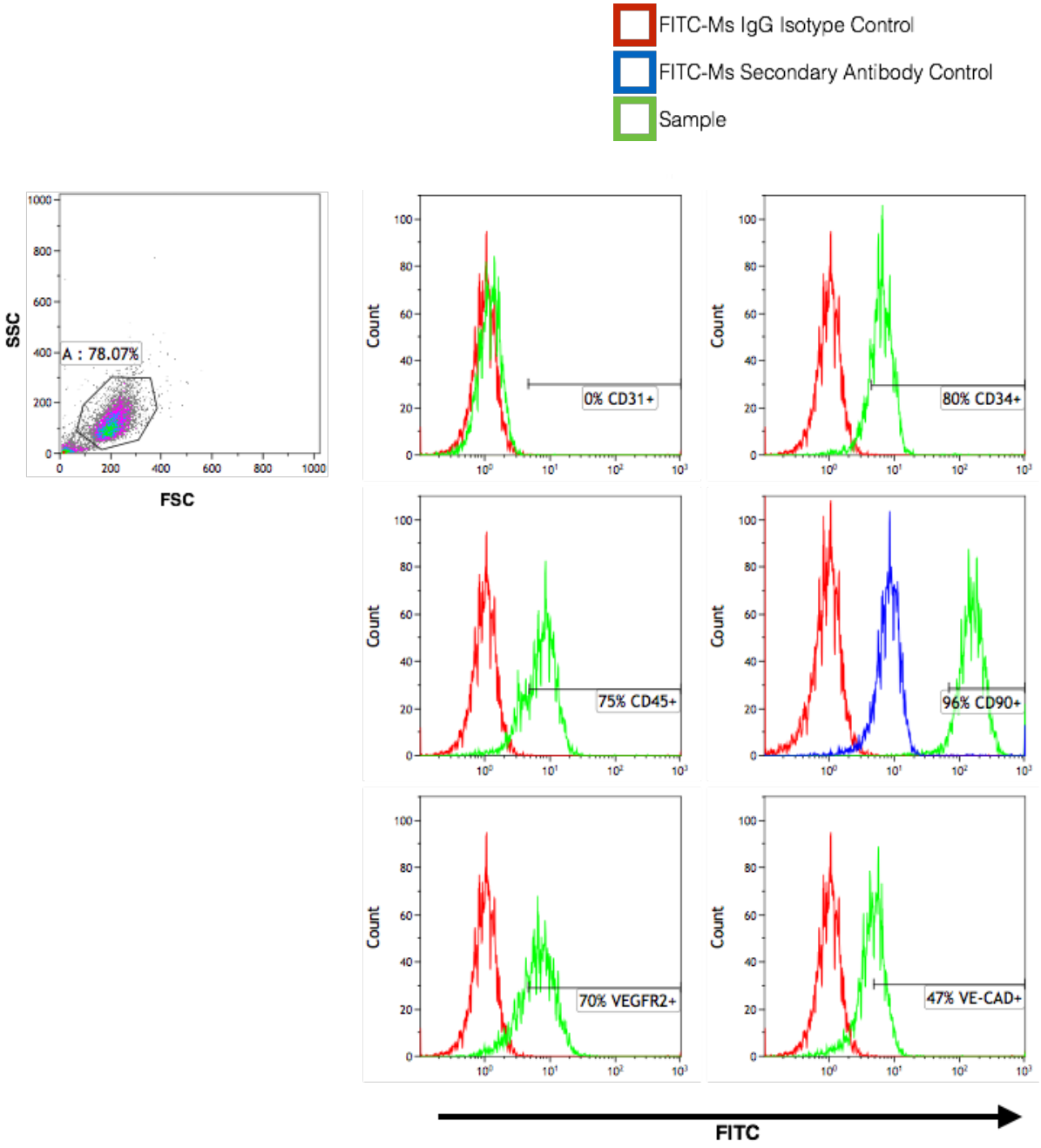

Figure 3.9. Representative histograms for temporal flow cytometry analysis in unpurified hiPSC-EC (Day 3).

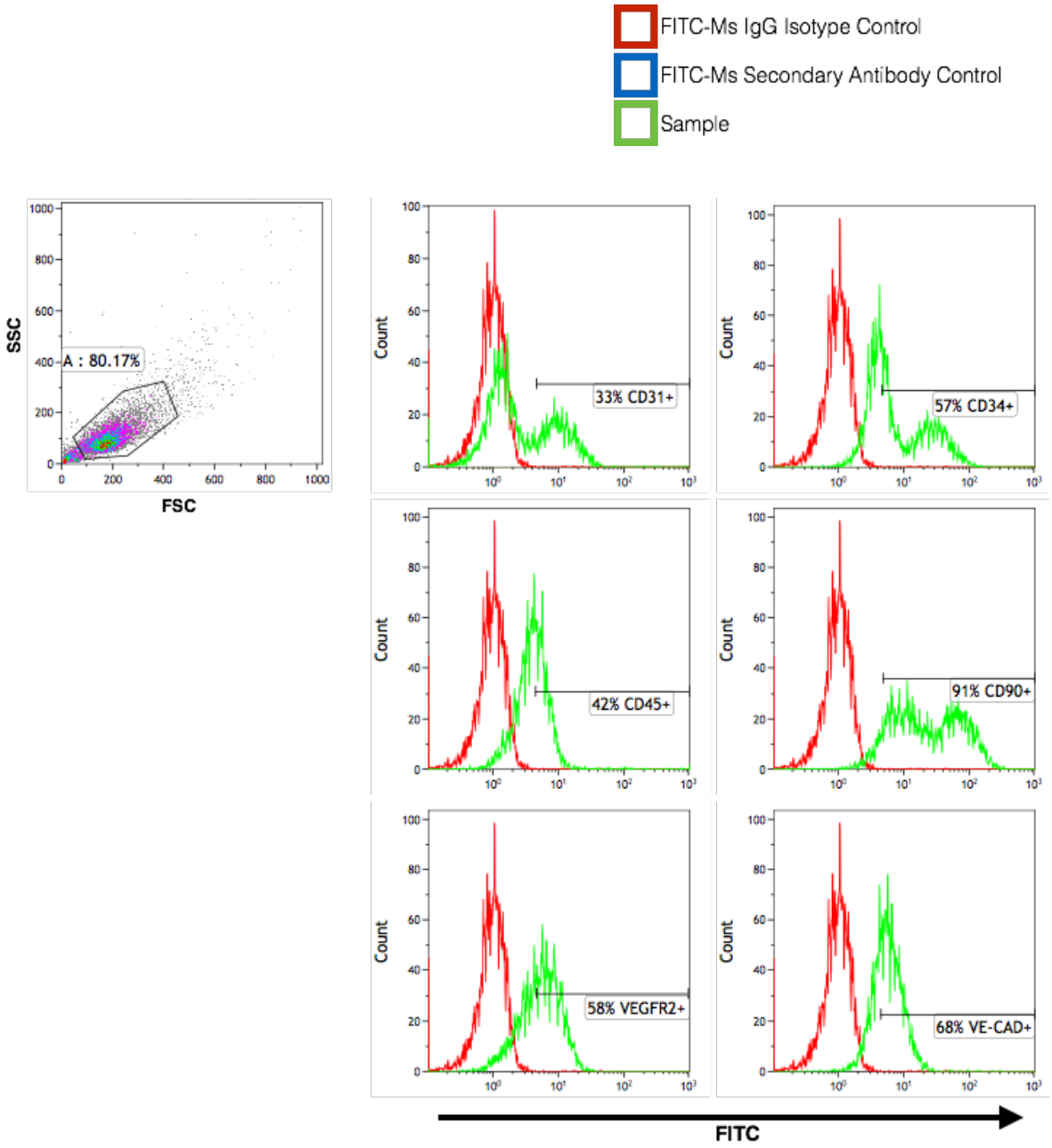

Figure 3.10. Representative histograms for temporal flow cytometry analysis in unpurified hiPSC-EC (Day 5).

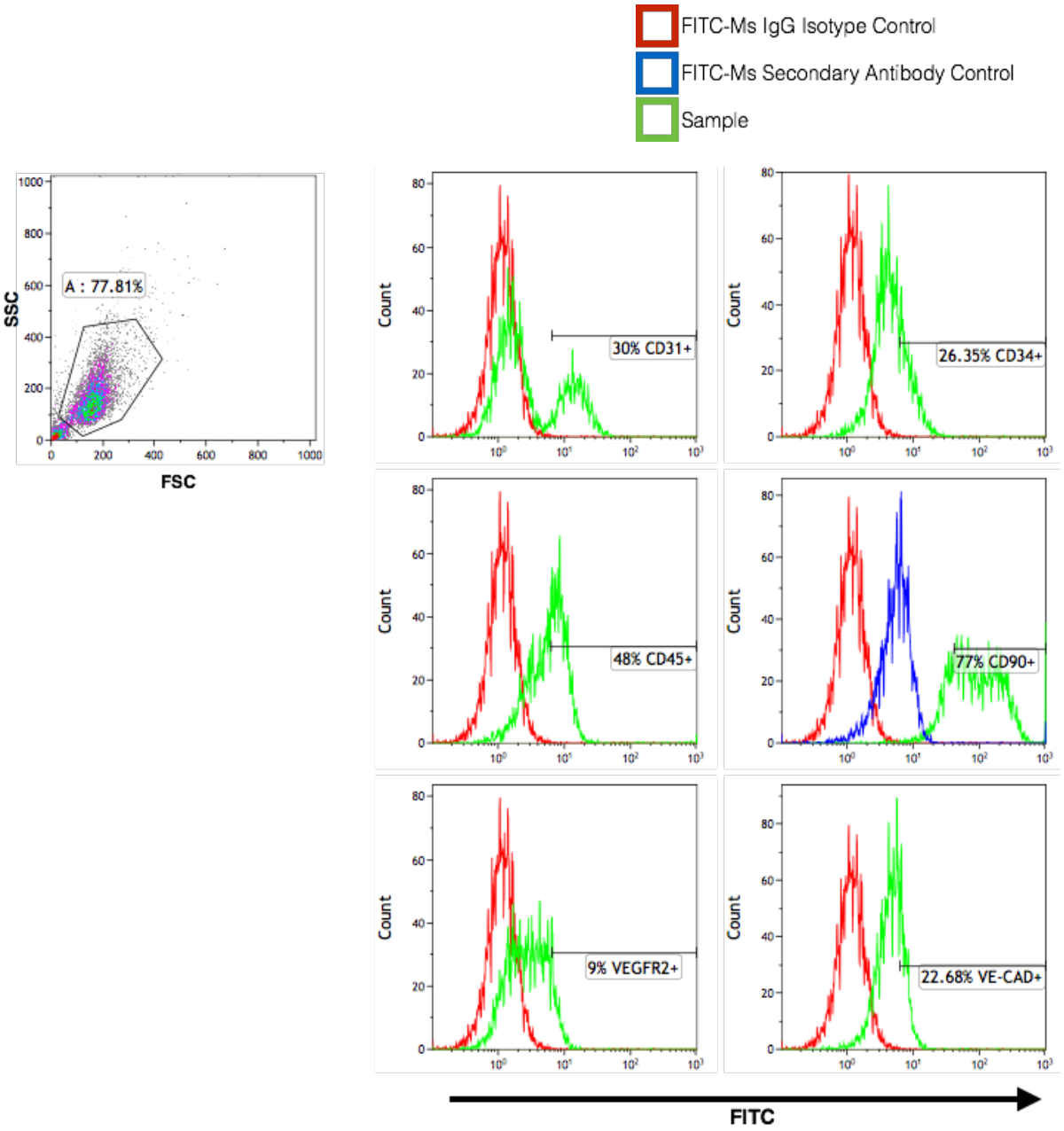

Figure 3.11. Representative histograms for temporal flow cytometry analysis in unpurified hiPSC-EC (Day 7).

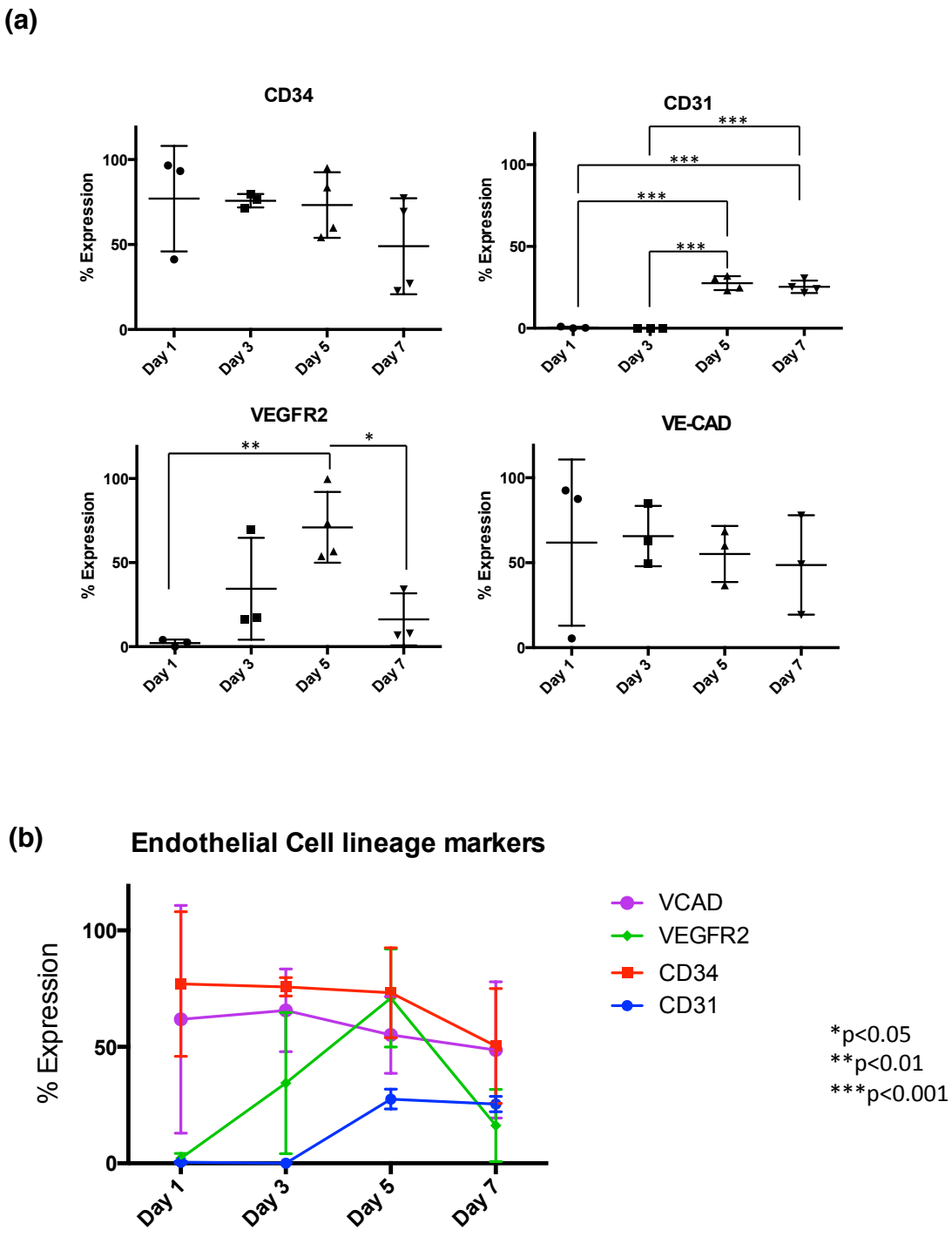

Figure 3.12. Flow cytometry analysis of unpurified population during EC Differentiation. (a) Temporal analysis demonstrated early expression of mature endothelial cell lineage markers CD31, VE-Cadherin, and KDR. (b) Summary of endothelial cell lineage expression demonstrated the protocol does not require extra maturation period after day 5 since KDR expression significantly decreases at day 7.

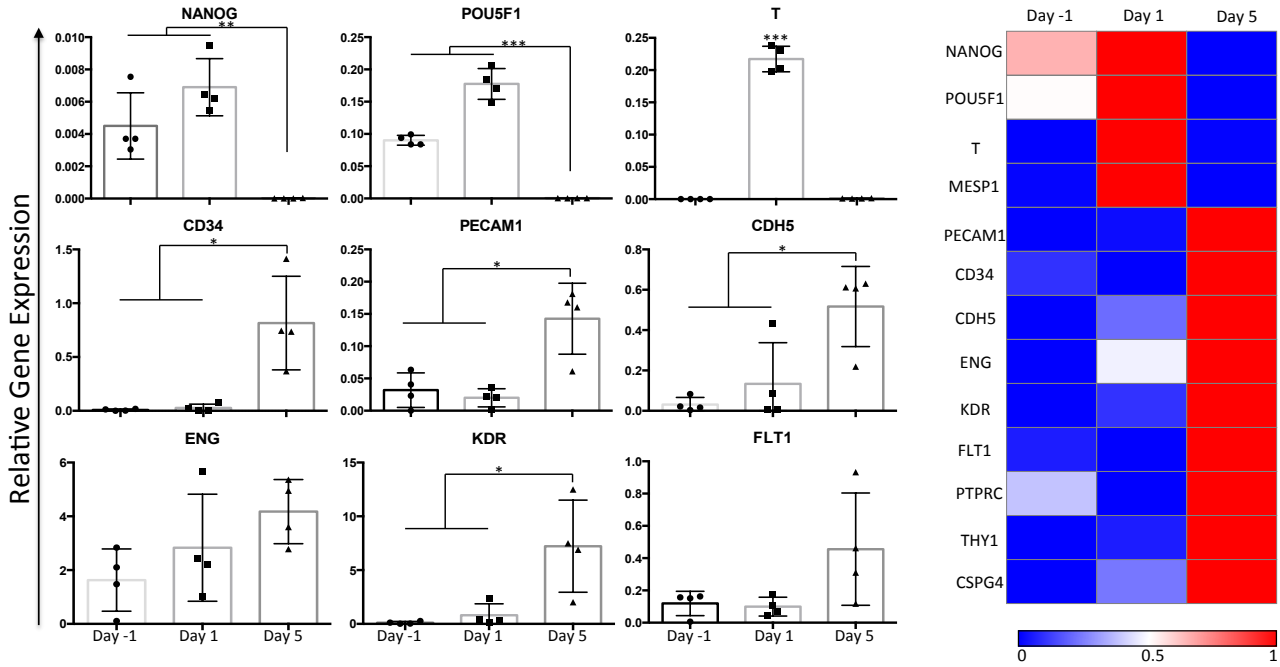

*p<0.05
**p<0.01
***p<0.001

Figure 3.13. Reverse Transcription quantitative PCR (RT-qPCR) analysis of hiPSCs during endothelial cell differentiation. Early expression of endothelial cell lineage markers CD31, VE-Cadherin, FLT1, KDR, and ENG were evident by Day 5. Pluripotency and mesoderm gene expression was upregulated during early stages of differentiation, but were downregulated by day 5.

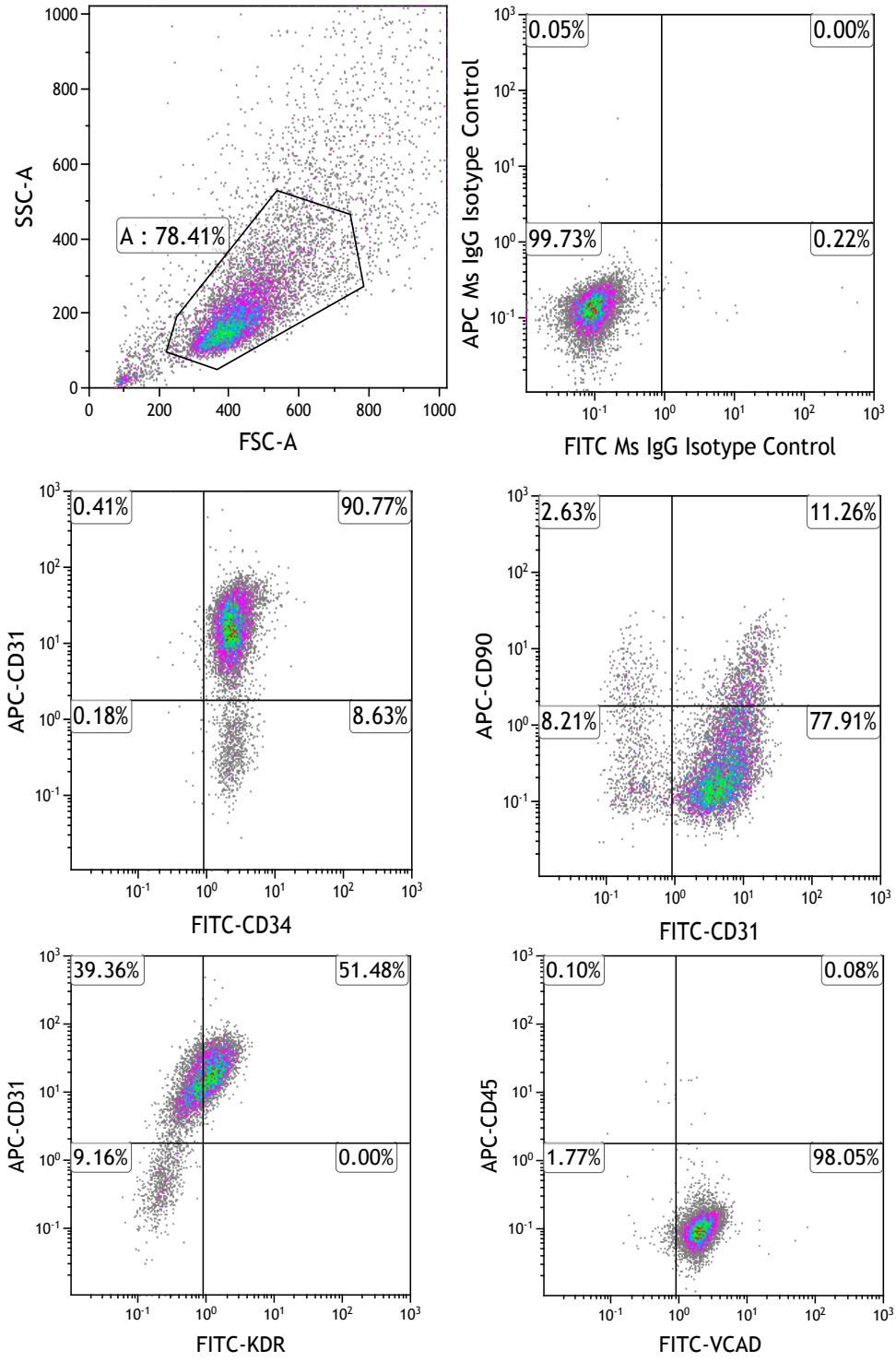

Figure 3.14. Characterization of CD31+ MACS purified endothelial cells. - Representative flow cytometry density plots of CD31, CD34, and CD90 expression.

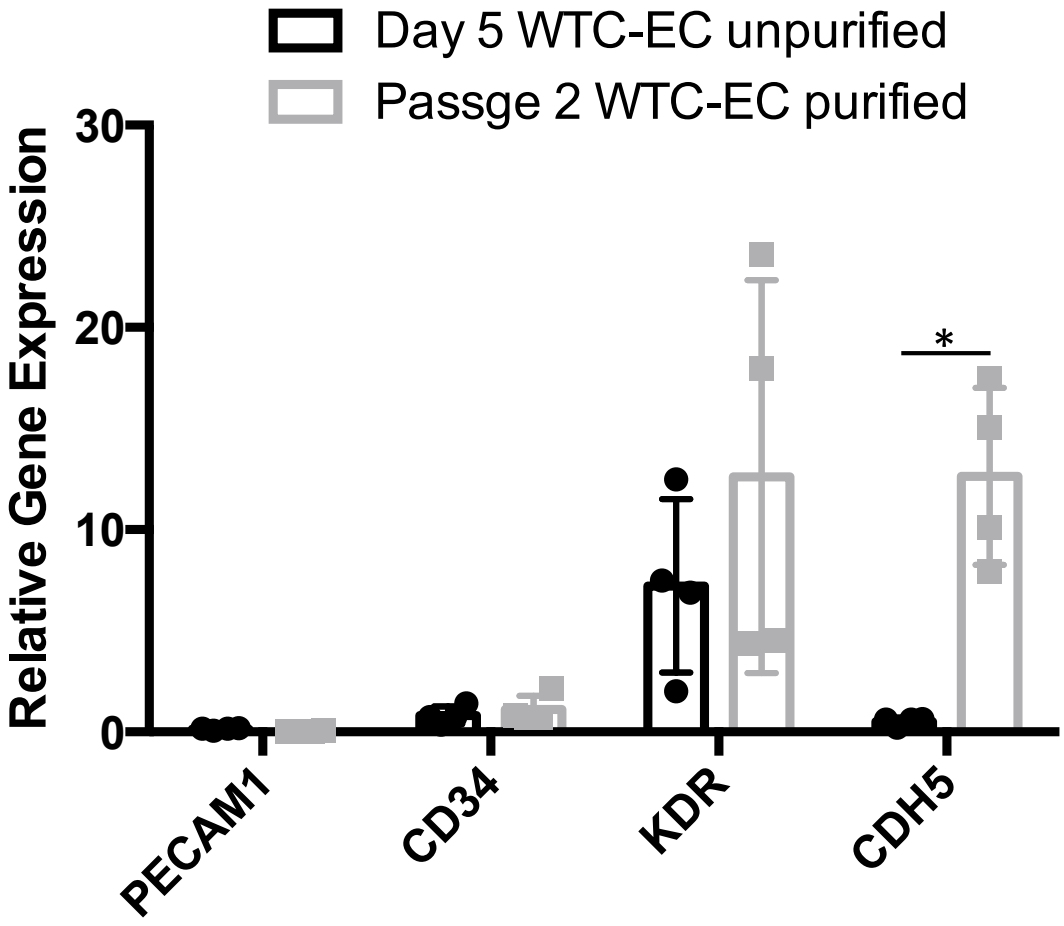

Figure 3.15. Characterization of CD31+ MACS purified endothelial cells - Gene expression of EC-specific markers increased compared to day 5 mixed population.

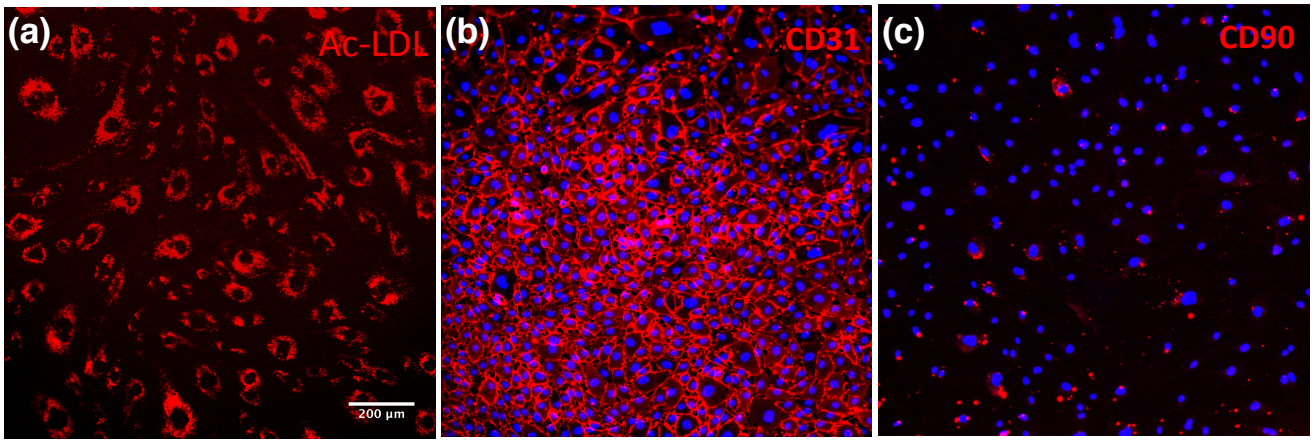

Figure 3.16. Characterization of CD31+ MACS purified endothelial cells - Immunofluorescence staining of CD31+ MACS purified endothelial cells revealed cobblestone morphology.

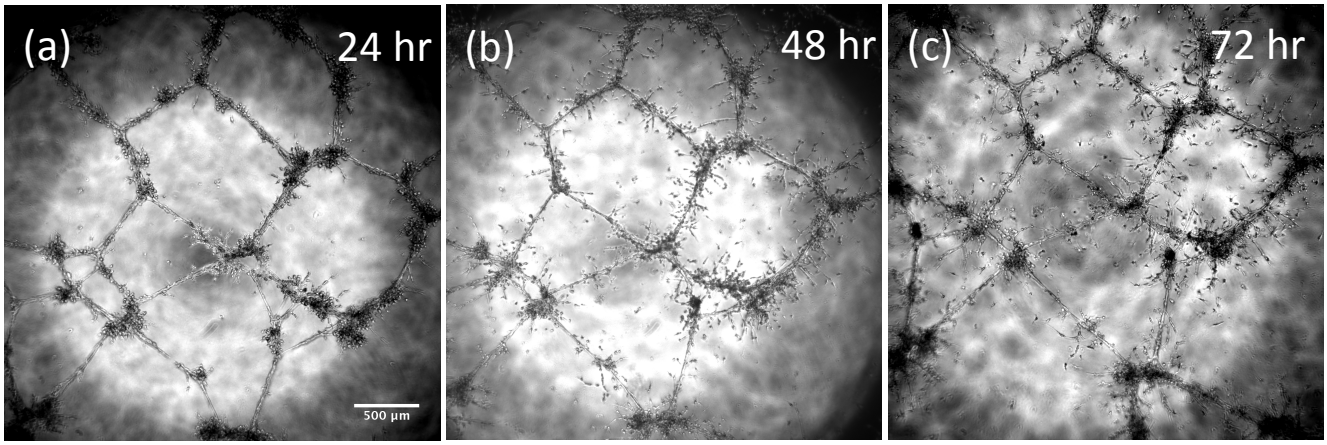

Figure 3.17. Characterization of CD31+ MACS purified endothelial cells. - Matrigel angiogenesis assay demonstrated stable network formation for 3 days.

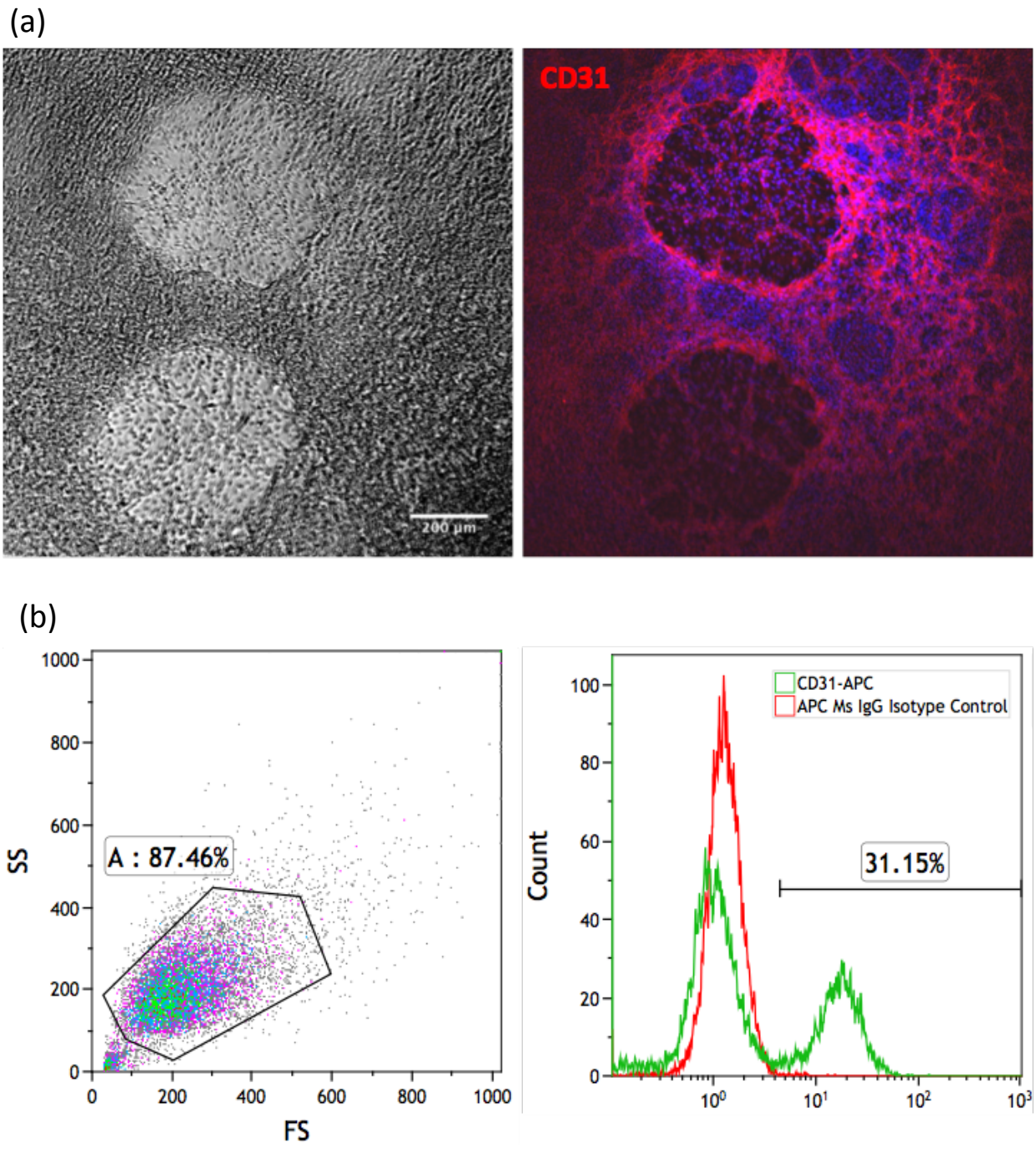

Figure 3.18. Analysis of unpurified H9 human embryonic stem cell line at Day 5 of endothelial Cell Differentiation (a) phase contrast and fluorescence microscopy (b) flow cytometry.

CHAPTER 4:
DEVELOPMENT OF A PHYSIOLOGICALLY RELEVANT 3D *IN VITRO* ANGIOGENESIS MODEL

4.1 Abstract

Stem cell derived angiogenesis models present a unique, patient-specific platform to study the complex process of angiogenesis and endothelial cell response to biochemical and biophysical changes in their microenvironments. Current *in vitro* angiogenesis models have provided insight into this process; however, many continue to rely on primary endothelial cells or immortalized cell lines (HUVEC, HMEC, HAEC, etc) [1-4]. This limits the genetic diversity of the test samples so that patients from different backgrounds (gender, age, race/ethnicity, etc) are not represented in the studies. Furthermore, primary cell lines are limited in supply and are notoriously difficult to culture and expand, so they are not a sustainable source for *in vitro* studies. Additionally, HUVECs have a tendency to form unstable capillary structures *in vitro* that quickly and spontaneously regress. Many studies include secondary stromal cells, often from a different source, to stabilize these capillary-like networks [2,4-6]. However, this approach adds a confounding factor since it is unclear if the ECs are directly affected by the treatment in question or if they are reacting to the fibroblast response. Furthermore, many current studies use matrices that do not recapitulate the natural extracellular matrix which is a complex and dynamic environment.[2,4,5,7] In this study, the hiPSC-EC's were encapsulated within the HyA matrix and their ability to respond to biochemical and biophysical cues was demonstrated with dynamic, and corresponding changes in capillary-like network formation and nitric oxide production similar to physiological angiogenesis. The dependence of network formation on proangiogenic signaling was further demonstrated by treatment with a small-molecule VEGFR2/FGFR inhibitor which eliminated network formation and permitted the calculation of an IC_{50} value that was in agreement with previous reports. An *in vitro* angiogenesis model containing the HyA matrix and hiPSC-ECs was then developed within a tri-chamber microfluidic device that mimicked vascular flow and demonstrated perfusion of the hollow capillary tube networks.

4.2 Introduction

Angiogenesis is a complex process that is involved in disease progression and tissue repair, yet it is not fully understood. The multifaceted mechanisms of angiogenesis along with the relatively high cost and technical skill level associated with *in vivo* studies make it difficult to efficiently evaluate the efficacy of therapies intended to promote angiogenesis [3,8,9]. *In vitro* models provide a less expensive, more controlled, and reproducible platform for better quantification of isolated angiogenic processes in response to a biochemical or biophysical stimulus [3,7,10-12].

Belair and Thomson used human iPSC derived endothelial cells purchased from Cellular Dynamics International , Inc. (CDI) to model blood vessel development in vitro within

biomimetic 3D engineered platforms.[5] The iPSC-ECs were characterized for the endothelial cell lineage markers CD31, CD105, CD144, and VEGFR2 (KDR) with flow cytometry. The iPSC-ECs formed capillary-like structures similar to HUVECS when subjected to a Matrigel angiogenesis assay. The ECs were plated on (2D) and encapsulated within (3D) Matrigel and cultured in a perfusable bioreactor that permitted applied fluid shear stress. According, to the authors, the ECs aligned in the direction of flow, however, this is not obvious in the image for the 3D flow culture. The ECs were then co-cultured in with normal human lung fibroblasts (NHLFs), encapsulated in a fibrin hydrogel, and loaded into a microfluidic device. The ECs formed perfusable networks that were stabilized by the NHLFs. Finally, the authors developed a sprouting assay by culturing them a in a spheroid in a non-adherent round bottom 96-well plate. The medias were supplemented with VEGFA, SU5402 (VEGFR2/FGFR inhibitor), or nocodazole (microtubule polymerization inhibitor). Dose-response curves were generated for VEGF, SU5402, and nocodazole supplemented medias where EC50 and IC50 values could be determined from sigmoidal regression analysis.

Sobrino, Hughes, and George developed a microphysiological system to model human tumor angiogenesis in vitro that incorporates human cancer cell lines in a fibrin matrix, supported by perfused human microvessels.[4] The vascular tissue consists of human endothelial colony forming cell-derived endothelial cells (ECFC-ECs) isolated from cord blood and supported by normal human lung fibroblastes (NHLFs). The microfluidic device consisted of two outer microfluidic channels that mimic high pressure (arteriole) and low pressure (venule) circulatory vessels that were connected by three central, consecutive microtissue chambers.. Permeability of the vessels was demonstrated by perfusion of the vascular network with 70 kDa FITC-dextran, which demonstrates the vessels are minimally leaky. The authors noted that “stromal cells were required for proper formation of the vascular networks, and a subset of these consistently enveloped the newly-formed vessels”. Several cancer cell lines were encapsulated with the ECFCs and stromal cells to study the development of vascular networks and the effects of anti-cancer drugs.

Moya and George developed a 3D in vitro vascular tissue model that contains a perfused and interconnected human capillary network within a microfluidic platform that mimics venular and arteriolar flow.[2] The microfluidic device consisted of two fluidic channels separated by a central channel of 12 consecutively connected diamond tissue chambers. The fluidic channels connected on either side of the tissue chamber via a single connecting pore. The central channel was loaded with Human endothelial colony forming cell-derived ECs (ECFC-ECs) isolated from cord blood and normal human lung fibroblast (NHLFs) encapsulated in fibrin at a ratio of 1:2 respectively. The cells were grown in the device for 14 days under interstitial flow and in the absence of VEGF and bFGF since were assumed to provide angiogenic signals for EC tube formation. Two design variations for connecting the fluidic channels and microtissue chambers were investigated to determine their effect on the vascular tissue formation. One design (VP), consisted of connecting the arterial microfluidic line (high pressure side) from the last microtissue chamber directly to the venular side (low pressure side) of the same chamber. The second design (EQ), consisted of connecting the arterial microfluidic line from the last microtissue chamber to the venular side of the first chamber. Cells in the devices were cultured and remained viable through 40 days. Between days 14 and 21, the ECFC-EC, supported by cocultured NHLFs, formed an

interconnected network of capillaries. Networks formed in both designs, VP and EQ, and were well connected. The study did not find a significant difference for capillary network diameter and connectedness between the two designs. To characterize the flow in the capillaries formed by the ECs and NHLFs, 1-mm- diameter fluorescent microspheres were introduced in the arterial microfluidic channel. Microspheres tracked in these devices demonstrated a wide range for velocity from almost zero to over 4000 mm/s at any particular position. Fluorescent dextran (70 and 150kDa) was introduced into the arterial microfluidic channel at day 21 to assess vessel permeability. The vessels demonstrated variable degrees of permeability to the 70-kDa dextran but appeared to be impermeable to 150 kDa dextran.

Zanotelli, Thomson, and Murphy demonstrated that iPSC-ECs could self-assemble into vascular networks through physiologically-relevant mechanisms in PEG hydrogels polymerized in a tri-channel microfluidic device and remain stable for two weeks.[13] Live/dead staining with calcein and ethidium homodimer demonstrated that iPSC-ECs were viable and self- assembled into interconnected vascular networks during the first three days of culture in peptide-functionalized PEG hydrogels. On Day 3, the capillary networks were evident throughout the hydrogel. Immunofluorescence imaging demonstrated that iPSC- EC networks in the PEG hydrogels were CD31+ and VE-Cadherin+. Vascular network formation was investigated within PEG hydrogels with shear moduli ranging from 183 ± 10 to 1612 ± 95 Pa (40%-60% crosslinking with MMP-degradable peptide). Limited tubule formation was seen after eight days when $1x10^7$ iPSC-ECs per mL were encapsulated in 40–60% crosslinked hydrogels, The highest degree of network formation was reported to occur at higher cell density ($8.5x10^7$ cells/mL) and intermediate levels of VEGF addition. The networks remained stable for at least 14 days in the microfluidic device when $1x10^7$ iPSC-ECs per mL were encapsulated in 50% crosslinked PEG hydrogels and cultured in medium that was supplemented with 100 ng/mL VEGF. The study reports that the iPSC-ECs encapsulated in the optimized hydrogel within the microfluidic device formed lumen approximately 25 um in diameter, however, no perfusion studies were demonstrated.

Current *in vitro* angiogenesis models have provided insight into this process; however, many continue to rely on primary endothelial cells or immortalized cell lines (HUVEC, HMEC, HAEC, etc) [1-4]. This limits the genetic diversity of the test samples so that patients from different backgrounds (gender, age, race/ethnicity, etc) are not represented in the studies. Furthermore, primary cell lines are limited in supply and are notoriously difficult to culture and expand, so they are not a sustainable source for *in vitro* studies. Additionally, HUVECs have a tendency to form unstable capillary structures *in vitro* that quickly and spontaneously regress. Many studies include secondary stromal cells, often from a different source, to stabilize these capillary-like networks [2,4-6]. However, this approach adds a confounding factor since it is unclear if the ECs are directly affected by the treatment in question or if they are reacting to the fibroblast response.

In contrast to primary endothelial cells, human induced pluripotent stem cell (**hiPSC**) derived endothelial cells (**hiPSC-ECs**) have the potential to provide a limitless supply of patient-specific vascular cells to research pathological angiogenesis, vascular diseases, and

regeneration of ischemic tissues. Incorporating hiPSC-ECs into angiogenesis models provides a unique, patient-specific platform to study *in vitro* the complex process of angiogenesis and endothelial cell response to biochemical and biophysical changes in their microenvironments [14-18].

To assess the behavior of the hiPSC-ECs (discussed in Chapter 3), a growth factor sequestering hyaluronic acid (HyA) matrix was used to promote cell survival and maintenance of lineage-specific function [19-21]. HyA offers many benefits as a matrix to support hiPSC-ECs, since it is a naturally occurring biopolymer that is biocompatible, biodegradable, non-immunogenic, and has been shown to promote cell migration, proliferation, and angiogenesis in wound healing processes [19-23].

hiPSC-ECs were encapsulated within the HyA matrix and their ability to respond to biochemical and biophysical cues was demonstrated with dynamic, and corresponding changes in capillary-like network formation and nitric oxide production similar to physiological angiogenesis. The dependence of network formation on proangiogenic signaling was further demonstrated by treatment with a small-molecule VEGFR2/FGFR inhibitor which eliminated network formation and permitted the calculation of an IC_{50} value that was in agreement with previous reports. An *in vitro* angiogenesis model containing the HyA matrix and hiPSC-ECs was then developed within a tri-chamber microfluidic device that mimicked vascular flow and demonstrated perfusion of the hollow capillary tube networks.

4.3 Materials and Methods

4.3.1 Acrylation of Hyaluronic Acid (HyA)

Hyaluronic Acid (HyA) was purchased from LifeCore Biomedical with a reported molecular weight of 500kDa, which was determined through viscosity measurements by the manufacturer. The HyA was first modified to carry hydrazide groups using a previously reported method [21]. Briefly, the hyaluronic acid was dissolved in deionized water overnight to to form a 3 mg/mL solution. A 30 molar excess of adipic acid dihydrazide (ADH) was added to the solution and the pH was adjusted to 6.8 using 0.1 M NaOH and 0.1 M HCl. Next, 1-Ethyl-(3-dimethylaminopropyl)carbodiimide hydrochloride (EDC) (Fisher Scientific) and 1-Hydroxybenzotriazole hydrate (HOBt) (Sigma-Aldrich) were dissolved separately at 3 mmol in DMSO/DI water (1:1 volume ratio, 3 mL) and sequentially added to the reaction solution. The solution pH was then adjusted to 6.8 and maintained for 4 hours before letting the reaction proceed overnight. The solution was exhaustively dialyzed for 3 days in 10 kDa molecular weight cut-off (MWCO) dialysis tubes (Spectrum Labs) against 1 g/L NaCL in DI water for the first two days and pure DI water the third day. Following dialysis, NaCl was added to form a 5 mg/mL solution which was then precipitated in 100% ethanol. The precipitated HyA-ADH was pelleted by centrifugation and re-dissolved in DI water. The solution was again dialyzed using the same method. To generate acrylate groups on the HyA, 700 mg of N-Acryloxysuccinimide (NAS) (Acros Organics) was reacted overnight with the HyA-ADH solution (300 mg, 100 mL DI water). The solution was dialyzed following the same method and then lyophilized for at least 3 days to remove all water and stored at -

20°C. Previous reports confirmed with proton (^{1}H) NMR that ~30% of the available carboxyl groups were conjugated with acrylated groups [21].

4.3.2 Synthesis of Thiolated Heparin

Thiolated Heparin was synthesized using a previously reported method [21]. Briefly, heparin (50 mg) (Sigma Aldrich) was dissolved in DI water to form a 5 mg/mL solution which was reacted with an excess amount of cysteamine (76 mg) and the solution pH was adjusted to 6.8. Next, 1-Ethyl-(3-dimethylaminopropyl) carbodiimide hydrochloride (EDC) (Fisher Scientific) and 1-Hydroxybenzotriazole hydrate (HOBt) (Sigma-Aldrich) were dissolved separately at 3 mmol in DMSO/DI water (1:1 volume ratio, 0.5 mL) and sequentially added to the reaction solution. The solution pH was then adjusted to 6.8 and maintained for 5 hours before letting the reaction proceed overnight. A 10-fold molar excess of tris (2-carboxyethyl) phosphine (TCEP) was added to reduce any disulfide bonds that may have formed between thiol groups. The solution pH was adjusted to 5.0 and then dialyzed following the same method as described for the synthesis of acrylated HyA. Next, the thiolated heparin was lyophilized for at least 3 days and stored at -20°C.

4.3.3 Gelation of HyA for Encapsulation of hiPSC-EC

The gelation procedure for the HyA was previously reported [19-21,24]. To promote cellular adhesion, HyA was conjugated with an integrin binding peptide, bsp-RGD(15) with the amino acid sequence CGGNGEPRGDTYRAY. HyA-RGD was synthesized by reacting 10 mg of bsp-RGD(15) to 25 mg AcHyA in 10 mL of DI water at room temperature. To make a 3 wt% hydrogel HyA (13.3 mg/mL), HyA-RGD (20 mg/mL mg), and heparin-SH (0.03 wt%) were dissolved in 0.3 mL of triethanolamine buffer (TEA; 0.3M, pH 8) and incubated at 37°C for 30 minutes. For gels with exogenous growth factor addition, VEGF-A_{165} (5 ug/mL) or TGF-β1 (1 ug/mL) was reacted with the solution for 30 minutes at 4°C. Sorted CD31+ WTC hiPSC-ECs were then gently mixed into the solution at a concentration of $3x10^6$ cells/mL. Hydrogels were generated by in situ crosslinking with an MMP-13 cleavable peptide sequence CQPQGLAKC (3 mg, 50 μL TEA buffer). The reported shear modulus (G') of the 3 wt% HyA hydrogel was 850 Pa and a 2 wt% hydrogel was reported to have a shear modulus (G') of 170 Pa [21]. Therefore, the 3wt% HyA hydrogel was referred to as **HyA-850** and the 2 wt% hydrogel was **HyA-170**.

4.3.4 Hydrogel Immunofluorescence and confocal microscopy

Cells encapsulated within the hydrogel were rinsed with PBS and fixed with 4% PFA for 30 minutes and permeabilized for 5 minutes with 0.1% Triton. The samples were then rinsed three times with PBS and blocked with 3% BSA for 30 minutest. They were then stained with 1:200 primary anti-human CD31 (Supplemental Table 3.1) and 1:200 Actin-stain 555 phalloidin (Cytoskeleton, Inc.) in PBS overnight at 4°C. Next, the samples were washed in triplicate with PBS and stained with Alexa Fluor 488 goat anti-mouse secondary antibody (1:200 in PBS) and incubated overnight at 4°C. The samples were then washed three times with PBS. Prior to imaging, cell nuclei were stained with DAPI (Invitrogen) for 5 minutes

and washed once with PBS. Fluorescent images were taken with a Prairie Technologies Swept Field Confocal (SFC) microscope (Prairie Technologies, Middleton, WI).

4.3.5 Angiogenesis Analysis

Tube formation in the hiPSC-EC hydrogel samples was quantified with the ImageJ Angiogenesis Analyzer plugin [25] by measuring total branching and segment lengths (termed total network length) in confocal images. To help the software distinguish between tube structures and background, the images were converted to binary images. The Angiogenesis Analysis software was then used to convert the binary image to a "branching skeleton", or binary tree, and the total length was measured using the "Analyze Binary Tree" function.

4.3.6 Nitric Oxide Assay

The presence of nitric oxide released into the culture medium by the encapsulated hiPSC-ECs was detected using the Griess Reagent System (Promega) according to manufacturer specifications. This assay measures the concentration of nitrite, a stable degradation product of nitric oxide, present in the sample culture medium. Hydrogel samples were fed every other day with EGM2, which was collected and tested at days 3, 7, and 14.

4.3.7 Angiogenesis Inhibition Assay

The VEGFA inhibition assay was performed with a ten-fold dilution series of the small molecule VEGFR2/FGFR inhibitor SU5402 (Sigma) in EGM2 and feeding it to hiPSC-ECs encapsulated in 3 wt% HyA hydrogel on day 1 to day 7. The samples were fixed with 4% PFA and stained for F-actin and DAPI, as described above. Fluorescent images were taken with a Prairie two photon/confocal microscope and analyzed with the ImageJ Angiogenesis Analyzer plugin. Nonlinear regression analysis of dose-response curve to calculate IC_{50} was performed with Graphpad Prism 6.

4.3.8 Perfusion Analysis

The 3wt% HyA hydrogel with $3x10^6$ cells/mL (WTC hiPSC-ECs) was loaded with a P200 positive pressure pipette into a 3-chamber microfluidic device shown in **Figure 4.7(a)** and described previously [2,26]. The microfluidic platform was designed to mimic vascular flow and originally consisted of two fluidic channels separated by a central channel of 12 consecutively connected diamond tissue chambers. The central channel containing the tissue chambers had ports at each end where the cell-hydrogel solution was loaded. The fluidic channels connected on either side of the tissue chamber via a single connecting pore designed to act as a capillary burst microvalve to keep liquid from leaking out.

The samples were fed EGM2 every other day through gravity-fed flow from filterless P200 pipette tips. To test perfusion, the samples were fixed on day 14 and the device was loaded with 2 um diameter fluorescent microbeads (Fluospheres, Invitrogen). Fluorescent images

and videos were taken at a 100 fps on the Prairie Technologies Swept Field Confocal (SFC) microscope (Prairie Technologies, Middleton, WI).

4.3.9 Statistical Analysis

All quantitative measurements were performed at least in triplicate samples and values are expressed as mean ± standard deviation (SD). One-way ANOVA with post-hoc Tukey tests were used to compare treatment groups and $p<0.05$ was used to assess statistical significance.

4.4 Results and Discussion

4.4.1 hiPSC-ECs form capillary-like networks that are responsive to biochemical stimuli

To validate the ability of the hiPSC-ECs to respond to proangiogenic signals, the system was cultured in EGM2 only (E) or in EMG2 with exogenous growth factors VEGF-A (EV) or TGF-β1 (ET) loaded within the HyA matrix (HyA-850). Figure 4.1 shows a schematic of the HyA hydrogel synthesis for hiPSC-EC encapsulation which included an integrin binding peptide (bsp-RGD) [24], heparin as a growth-factor presenting agent, and a bis-cysteine MMP-degradable peptide crosslinker. Additionally, to further establish the necessity of biochemical signals for endothelial cell network formation, the system was cultured in RPMI B27 complete medium (R), which lacks proangiogenic growth factors. Figure 4.2 shows confocal images of hiPSC-EC networks with the different culture conditions at day 3, 7, and 14 after cell encapsulation. The corresponding measurements for total length of the vessel network are shown in Figure 4.3. The cells in HyA-850 R remained rounded and exhibited limited CD31 expression at day 3 and day 7. They appeared to aggregate and slightly elongate by day 14 and recovered some CD31 expression, however, no tube formation was observed. The images demonstrate the endothelial cell's limited ability to form networks within the matrix in the complete absence of proangiogenic signals. For HyA-850 E, cell elongation appeared to begin on day 3. Sprouting was observed on day 7, and a stable capillary-like network of vessels was established by day 14. The HyA-850 EV models pathological angiogenesis when exogenous VEGF-A was loaded within the hydrogel during cell encapsulation. By day 7 HyA-850 EV demonstrated a high-density network of small tubes relative to HyA-850 E. This capillary-like network was unstable, and deteriorated by day 14. The HyA-850 ET demonstrated cell elongation and sprouting as early as day 3. The hiPSC-ECs continued to sprout and form nodes by day 7 and a complex capillary-like network was observed by day 14 (Fig. 4.2).

4.4.2 Matrix rigidity affects hiPSC-EC network formation and function

The ability of the system to respond to changes in matrix stiffness was evaluated by comparing hiPSC-EC within HyA-850 E and HyA-170 E matrices. The right column on Figure 4.2 shows early sprouting and tube formation at day 3 in HyA-170 E. However, this was significantly reduced by day 7, where only elongated cells were seen and no tube formation was detected. Some elongated cells remained at day 14, but no further tube formation occurred in the softer HyA-170 E compared to the HyA-850 E with a higher

shear modulus that showed stable tube formation. Figure 4.3 shows the quantitative analysis of the network and demonstrates a significantly higher total network length in HyA-850 E and ET on day 14. Despite being fed EGM2, which contains several proangiogenic factors, HyA-170 E could not support long-term, stable tube formation (Fig. 4.3).

4.4.3 hiPSC-ECs produce nitric oxide in response to microenvironment

Nitric oxide is synthesized by endothelial cells and plays an important role in maintaining vascular homeostasis.[27,28] It's detection in angiogenesis models can serve as an indicator of cellular health, since a decrease in nitric oxide (NO) production is associated with impaired, dysfunctional endothelial cells.[27-31] The presence of NO produced by the hiPSC-ECs in the HyA-850 matrix was similar among the different media conditions on day 3 and 7 (Fig. 4.4). A significant increase in nitric oxide production was found at day 14 in HyA-850 E matrix, compared to those loaded with exogenous VEGF-A and TGF-β1. This finding correlates with the stable tube formation found in HyA-850 E at day 14. Cells in HyA-850 E also demonstrated an overall increase in nitrite concentration from day 7 to day 14.

4.4.4 hiPSC-EC sprouting is eliminated by treatment with an angiogenesis inhibitor

A dose response study was performed with HyA-850 E by treating the culture media with the VEGFR2/FGFR small-molecule inhibitor SU5402 for 7 days. Figure 4.5 shows the untreated samples exhibited normal sprouting behavior by day 7. In contrast, the treated groups demonstrated a pronounced decrease in cell elongation at the lowest dose, while angiogenic sprouting was eliminated and only rounded cells remained in the highest dose of 10 μM. The IC_{50} value was determined to be 0.017 μM (Fig 4.6), which is in agreement with previously published data that reports an IC_{50} value of 0.02 μM [32].

4.4.5 hiPSC-ECs loaded within HyA matrix in a microfluidic device demonstrates perfusion of capillary-like network

The patency of the tube networks was demonstrated by loading the HyA-850 E into a previously designed tri-chamber microfluidic device intended to allow vascular-like fluid flow (Fig 4.7(a-b)) [2,26]. The hiPSC-ECs formed interconnected tubes with visibly hollow lumen that remained stable throughout the experiment. Prior to fixation, the system was treated with fluorescently conjugated Ac-LDL to demonstrate the cells remained functional and viable when loaded into the device (Fig. 4.7(c)). The device with the fixed HyA-850 E was then loaded with 2 μm diameter fluorescent microbeads to demonstrate the perfusability of the tube networks. Figure 4.8 shows a time-lapse montage of the beads flowing into an open-ended tube (*see*, Suppl. Movie 1).

4.4.6 Evaluation of capillary burst valve (CBV) for loading hydrogel samples into tri-chamber microfluidic device

Although tube formation was possible within the microfluidic device, the acrylated hyaluronic acid hydrogel (HyA-850) consistently flowed into and clogged the media channels connected to the main tri-chamber channel during sample loading (Fig. 4.9). Despite several variations in loading techniques, the issue could not be resolved. Further investigation into the device design, specifically the capillary burst valves (CBV) that connect the main chamber to the media channels demonstrated that the optimal viscosity for fluid flow and retention within the main chamber was approximately equivalent to the viscosity of water (0.001 Pa*s). The Young-Laplace equation (Eqn. 4.1) describes the maximum pressure difference across a liquid/gas interface to maintain a pinned, static liquid meniscus within a rectangular channel at an abruptly diverging section (Fig. 4.10).[33]

$$P_A - P_B = -2\sigma\left[\frac{\cos\dot{\theta}_I}{w} + \frac{\cos\theta_A}{h}\right] = \Delta P_m$$

Equation 4.1[33]

$$\dot{\theta}_I = \min\{\theta_A + \beta, 180^\cdot\}$$

w=channel width , h=channel height , θ=contact angle , σ=surface tension,
β=channel divergence angle

According to Cho et al, "The meniscus is kept pinned until the driving pressure becomes large enough to overcome the maximum pressure difference that the bulging interface can withstand".[33] Therefore, when the liquid is moving through a channel with a pressure difference at the liquid/air interface that exceeds the maximum static pressure difference at the section with the abrupt increase in width, the liquid will not pin and will continue to flow, or "burst", into the larger section of the channel. The Hagen-Poisuelle equation, Equation 4.2, describes the driving pressure difference and velocity for a pressure-driven fluid flowing through a pipe with a rectangular cross-section.[34]

$$\Delta P_D = \frac{2\eta L v (h+w)^2}{(hw)^2}$$

Equation 4.2[34]

w=channel width , h=channel height L=channel length, v=loading velocity,
η=dynamic viscosity

This equation can be used to approximate the driving pressure of a liquid moving through a microfluidic channel, it assumes laminar flow and the length of the channel is greater than the width.[34,35]

To calculate the maximum hydrostatic pressure (ΔP_m) at the capillary burst valve (CBV) (diverging channel section) for a static fluid meniscus in the tri-chamber microfluidic device developed in Dr. Steven George's lab[2], the dynamic contact angles for water and the 3 wt% HyA (HyA-850) on PDMS were measured using a Rame-Hart goniometer and Drop Image software. Table 4.2 shows the average dynamic contact angle measurements from three different experimental replicates for water and 3 wt% HyA. The reported surface tension values for water and 3 wt% hyaluronic acid with a molecular weight ranging from 6 to 2000 kDa, were used in this calculation.[36] The maximum hydrostatic pressure difference, ΔP_m, was determined to be 0.7 kPa for water and 1.2 kPa for HyA. This value was then used in Equation 4.2 to determine the equilibrium loading velocity ($v_{e,H2O}$ and $v_{e,AcHyA}$) for water and HyA that would allow the liquid meniscus to remain pinned at the CBV (Fig. 4.11). The equilibrium loading velocity for water (210 cm/s) was determined to be four orders of magnitude higher than that of the HyA (204 μm/s). These results indicate the HyA needs to be loaded 10^4 times slower than water to keep it from bursting through the CBV.

The driving pressure difference for HyA was determined for different loading velocities, including the equilibrium loading velocity for water (Table 4.3). This analysis and resulting COMSOL model (Fig. 4.12) demonstrate that when the HyA is loaded at the equilibrium loading velocity for water (2.1 m/s) to remain pinned at the CBV, the driving pressure difference is 11.9 MPa. Since the driving pressure difference for HyA exceeds ΔP_m at the interface when it is loaded at this velocity, it will burst the CBV and flow into the media channels. Within the current device design, the hydrogel would have to be loaded at a rate of 0.000021 m/s (loading time = 4.75 minutes) to avoid exceeding the maximum hydrostatic pressure difference (ΔP_m) at the CBV. This is problematic since the AcHyA gel begins to solidify within 1-2 minutes after crosslinker addition.[21]

Finally, Figure 4.13 and Table 4.4 demonstrate that changing the dimensions of the capillary burst valve (length, width, diverging angle) to reduce the driving pressure difference (ΔP_D) during loading correspondingly decreases the maximum hydrostatic pressure difference (ΔP_m) at the CBV. The analysis shows the 3 wt% HyA hydrogel will continue to burst through the CBV regardless of the dimensional changes. This design does not appear to be suitable for high viscosity liquids since it seems the only workaround is to decrease the HyA viscosity so that it is approximately equal to water. Figure 4.14 demonstrates how changes in hydrogel viscosity affect the driving pressure difference during loading. In order to decrease the viscosity of the HyA, the concentration would have to be reduced to less than 3 wt%. This study and previous reports have demonstrated that HyA hydrogels with lower weight percentage could not support stable endothelial cell tube formation *in vitro*.

4.5 Conclusions

This study verified the endothelial cells derived from the novel differentiation method (discussed in Chapter 3) could be used in a physiologically relevant *in vitro* angiogenesis model. The hiPSC-ECs ability to respond to biochemical and biophysical cues within a bioinspired matrix was demonstrated with dynamic, and corresponding changes in tube

formation and nitric oxide production. First, I confirmed that without proangiogenic signals, the encapsulated hiPSC-ECs did not sprout or self-assemble into capillary-like networks (HyA-850 R). The EC's ability to form stable networks once the system was cultured in the growth factor-rich endothelial growth medium, EGM2, (HyA-850 E) showed that like physiological angiogenesis, the encapsulated hiPSC-ECs were dependent on proangiogenic signaling. Pathological angiogenesis could also be modeled with this system by loading the HyA hydrogel with excessively high concentrations of VEGF-A and TGF-β1 similar to a tumor microenvironment. During tumor angiogenesis, the upregulation of VEGF-A causes the formation of an unstable, high-density vasculature, which occurred in the HyA-850 EV [37]. The HyA-850 ET system demonstrated stable capillary-like network formation, which modeled late-stage tumor progression where TGF-β1 promotes high-density angiogenesis [29,38]. These results are in agreement with a previous study that demonstrated TGF-β1 loaded in the HyA hydrogel promoted capillary-like network formation of mouse cardiac progenitor cells [21]. Next, I demonstrated the encapsulated ECs responded to changes in matrix rigidity in a physiologically relevant manner that is in congruence with several published studies where slower, but more stable tube formation was seen in the stiffer matrix (HyA-850 E) compared to the softer matrix (HyA-170 E) [13,21,39,40].

Nitric oxide is synthesized by endothelial cells and plays an important role in maintaining vascular homeostasis [27,28]. Its detection in angiogenesis models can serve as an indicator of cellular health, since a decrease in nitric oxide (NO) production is associated with impaired, dysfunctional endothelial cells [27-31]. This is apparent in the tumor microenvironment where nitric oxide is found at lower concentrations despite the abnormally high levels of VEGF-A, TGF-β1, and other proangiogenic factors [28,30]. The Griess assay further validated the system's physiologically relevant behavior, since higher NO production was detected in the HyA-850 E compared to the hydrogels loaded with high concentrations of proangiogenic growth factors (HyA-850 EV and HyA-850 ET), suggesting similarities with a tumor microenvironment for the latter.

The dependence of tube formation on proangiogenic signaling and the potential for this angiogenesis model to be used in preclinical toxicology testing was further demonstrated by treating the HyA-850 E system with a small-molecule inhibitor of VEGFR2/FGFR (SU5402). As expected, the tube formation was responsive to inhibitor dosage and provided the calculation of an IC_{50} value that is in agreement with previous reports. Finally, tube patency and perfusion was demonstrated by loading the HyA-850 E in a microfluidic device that allowed fluid flow within the vascular network, consistent with a recent report using a modified differentiation protocol and fibrin as the matrix [6]. The demonstrated sensitivity to microenvironmental changes and 3D capillary-like structure makes this system a physiologically relevant *in vitro* angiogenesis model for pre-clinical development and screening of anti-angiogenic or cardiovascular drugs.

Analysis of the capillary burst valve that connects the media channels and main chambers in the microfluidic device provided insight on why the 3 wt% AcHyA hydrogel (HyA-850) consistently "burst" through the CBV during loading. It was shown that because the AcHyA is more viscous than water, it has a greater driving pressure difference at its leading edge

during loading which exceed the maximum pressure difference at the CBV to maintain a pinned meniscus. Furthermore, in order to keep the HyA from bursting the CBV, it needs to be loaded 10^4 times slower than water. Additionally, the analysis demonstrates that reducing the driving pressure difference during loading by changing the dimensions of the capillary burst valve also decreases the maximum hydrostatic pressure difference at the CBV. This indicates the 3 wt% AcHyA hydrogel will continue to burst through the CBV regardless of the dimensional changes. Based on this study, and previous publications which use gels with viscosities similar to water, it can be concluded that this microfluidic device design is not suitable for highly viscous liquids.[2,4]

4.6 References

1 Chwalek, K., Tsurkan, M. V., Freudenberg, U. & Werner, C. Glycosaminoglycan-based hydrogels to modulate heterocellular communication in in vitro angiogenesis models. *Sci Rep* **4**, 4414, (2014).

2 Moya, M. L., Hsu, Y. H., Lee, A. P., Hughes, C. C. & George, S. C. In vitro perfused human capillary networks. *Tissue Eng Part C Methods* **19**, 730-737, (2013).

3 Sanz-Nogues, C. & O'Brien, T. In vitro models for assessing therapeutic angiogenesis. *Drug Discov Today* **21**, 1495-1503, (2016).

4 Sobrino, A., Phan, D. T., Datta, R., Wang, X., Hachey, S. J., Romero-Lopez, M., Gratton, E., Lee, A. P., George, S. C. & Hughes, C. C. 3D microtumors in vitro supported by perfused vascular networks. *Sci Rep* **6**, 31589, (2016).

5 Belair, D. G., Whisler, J. A., Valdez, J., Velazquez, J., Molenda, J. A., Vickerman, V., Lewis, R., Daigh, C., Hansen, T. D., Mann, D. A., Thomson, J. A., Griffith, L. G., Kamm, R. D., Schwartz, M. P. & Murphy, W. L. Human vascular tissue models formed from human induced pluripotent stem cell derived endothelial cells. *Stem Cell Rev* **11**, 511-525, (2015).

6 Kurokawa, Y. K., Yin, R. T., Shang, M. R., Shirure, V. S., Moya, M. L. & George, S. C. Human Induced Pluripotent Stem Cell-Derived Endothelial Cells for Three-Dimensional Microphysiological Systems. *Tissue Eng Part C Methods* **23**, 474-484, (2017).

7 Morin, K. T. & Tranquillo, R. T. In vitro models of angiogenesis and vasculogenesis in fibrin gel. *Exp Cell Res* **319**, 2409-2417, (2013).

8 Lalit, P. A., Hei, D. J., Raval, A. N. & Kamp, T. J. Induced pluripotent stem cells for post-myocardial infarction repair: remarkable opportunities and challenges. *Circ Res* **114**, 1328-1345, (2014).

9 Mak, I. W., Evaniew, N. & Ghert, M. Lost in translation: animal models and clinical trials in cancer treatment. *Am J Transl Res* **6**, 114-118, (2014).

10 Nsair, A. & MacLellan, W. R. Induced pluripotent stem cells for regenerative cardiovascular therapies and biomedical discovery. *Adv Drug Deliv Rev* **63**, 324-330, (2011).

11 Briquez, P., Clegg, Lindsay, Hubbell, Jeffrey. Design principles for therapeutic angiogenic materials review. *Nature Reviews* **1**, 1-15, (2016).

12 Prestwich, G. D. & Healy, K. E. Why regenerative medicine needs an extracellular matrix. *Expert Opin Biol Ther* **15**, 3-7, (2015).

13 Zanotelli, M. R., Ardalani, H., Zhang, J., Hou, Z., Nguyen, E. H., Swanson, S., Nguyen, B. K., Bolin, J., Elwell, A., Bischel, L. L., Xie, A. W., Stewart, R., Beebe, D. J., Thomson, J. A., Schwartz, M. P. & Murphy, W. L. Stable engineered vascular networks from human induced pluripotent stem cell-derived endothelial cells cultured in synthetic hydrogels. *Acta Biomater* **35**, 32-41, (2016).

14 Chung, A. S. & Ferrara, N. Developmental and pathological angiogenesis. *Annu Rev Cell Dev Biol* **27**, 563-584, (2011).

15 Coulombe, K. L., Bajpai, V. K., Andreadis, S. T. & Murry, C. E. Heart regeneration with engineered myocardial tissue. *Annu Rev Biomed Eng* **16**, 1-28, (2014).

16 Yoder, M. C. Differentiation of pluripotent stem cells into endothelial cells. *Curr Opin Hematol* **22**, 252-257, (2015).

17 Wilson, H. K., Canfield, S. G., Shusta, E. V. & Palecek, S. P. Concise review: tissue-specific microvascular endothelial cells derived from human pluripotent stem cells. *Stem Cells* **32**, 3037-3045, (2014).

18 Kusuma, S., Shen, Y. I., Hanjaya-Putra, D., Mali, P., Cheng, L. & Gerecht, S. Self-organized vascular networks from human pluripotent stem cells in a synthetic matrix. *Proc Natl Acad Sci U S A* **110**, 12601-12606, (2013).

19 Jha, A. K., Mathur, A., Svedlund, F. L., Ye, J., Yeghiazarians, Y. & Healy, K. E. Molecular weight and concentration of heparin in hyaluronic acid-based matrices modulates growth factor retention kinetics and stem cell fate. *J Control Release* **209**, 308-316, (2015).

20 Jha, A. K., Tharp, K. M., Browne, S., Ye, J., Stahl, A., Yeghiazarians, Y. & Healy, K. E. Matrix metalloproteinase-13 mediated degradation of hyaluronic acid-based matrices orchestrates stem cell engraftment through vascular integration. *Biomaterials* **89**, 136-147, (2016).

21 Jha, A. K., Tharp, K. M., Ye, J., Santiago-Ortiz, J. L., Jackson, W. M., Stahl, A., Schaffer, D. V., Yeghiazarians, Y. & Healy, K. E. Enhanced survival and engraftment of transplanted stem cells using growth factor sequestering hydrogels. *Biomaterials* **47**, 1-12, (2015).

22 Collins, M. N. & Birkinshaw, C. Hyaluronic acid based scaffolds for tissue engineering--a review. *Carbohydr Polym* **92**, 1262-1279, (2013).

23 Xu, X., Jha, A. K., Harrington, D. A., Farach-Carson, M. C. & Jia, X. Hyaluronic Acid-Based Hydrogels: from a Natural Polysaccharide to Complex Networks. *Soft Matter* **8**, 3280-3294, (2012).

24 Rezania, A. & Healy, K. E. Integrin subunits responsible for adhesion of human osteoblast-like cells to biomimetic peptide surfaces. *J Orthop Res* **17**, 615-623, (1999).

25 Chevalier, F., Lavergne, M., Negroni, E., Ferratge, S., Carpentier, G., Gilbert-Sirieix, M., Sineriz, F., Uzan, G. & Albanese, P. Glycosaminoglycan mimetic improves enrichment and cell functions of human endothelial progenitor cell colonies. *Stem Cell Res* **12**, 703-715, (2014).

26 Hsu, Y. H. M., M.L.; Hughes, C.C.; George, S.C.; Lee, A.P. A microfluidic platform for generating large-scale nearly identical human microphysiological vascularized tissue arrays. *Lab Chip* **13**, 2990-2998, (2013).

27 Kelm, M. Nitric oxide metabolism and breakdown. *Biochim Biophys Acta* **1411**, 273-289, (1999).

28 Tousoulis, D., Kampoli, A. M., Tentolouris, C., Papageorgiou, N. & Stefanadis, C. The role of nitric oxide on endothelial function. *Curr Vasc Pharmacol* **10**, 4-18, (2012).

29 Carmeliet, P. & Jain, R. K. Principles and mechanisms of vessel normalization for cancer and other angiogenic diseases. *Nat Rev Drug Discov* **10**, 417-427, (2011).

30 Fukumura, D., Kashiwagi, S. & Jain, R. K. The role of nitric oxide in tumour progression. *Nat Rev Cancer* **6**, 521-534, (2006).

31 Gimbrone, M. A., Jr. & Garcia-Cardena, G. Endothelial Cell Dysfunction and the Pathobiology of Atherosclerosis. *Circ Res* **118**, 620-636, (2016).

32 Sun, L., Tran, N., Liang, C., Tang, F., Rice, A., Schreck, R., Waltz, K., Shawver, L. K., McMahon, G. & Tang, C. Design, synthesis, and evaluations of substituted 3-[(3- or 4-carboxyethylpyrrol-2-yl)methylidenyl]indolin-2-ones as inhibitors of VEGF, FGF, and PDGF receptor tyrosine kinases. *J Med Chem* **42**, 5120-5130, (1999).

33 Cho, H., Kim, H. Y., Kang, J. Y. & Kim, T. S. How the capillary burst microvalve works. *J Colloid Interface Sci* **306**, 379-385, (2007).

34 Bruus, H. Acoustofluidics 1: Governing equations in microfluidics. *Lab Chip* **11**, 3742-3751, (2011).

35 Geankoplis, C. *Transport Processes and Separation Process Principles*. 4 edn, (Prentice Hall, 2003).

36 Vorvolakos, K., Coburn, J. C. & Saylor, D. M. Dynamic interfacial behavior of viscoelastic aqueous hyaluronic acid: effects of molecular weight, concentration and interfacial velocity. *Soft Matter* **10**, 2304-2312, (2014).

37 Farnsworth, R. H., Lackmann, M., Achen, M. G. & Stacker, S. A. Vascular remodeling in cancer. *Oncogene* **33**, 3496-3505, (2014).

38 Lebrin, F., Deckers, M., Bertolino, P. & Ten Dijke, P. TGF-beta receptor function in the endothelium. *Cardiovasc Res* **65**, 599-608, (2005).

39 Bordeleau, F., Mason, B. N., Lollis, E. M., Mazzola, M., Zanotelli, M. R., Somasegar, S., Califano, J. P., Montague, C., LaValley, D. J., Huynh, J., Mencia-Trinchant, N., Negron Abril, Y. L., Hassane, D. C., Bonassar, L. J., Butcher, J. T., Weiss, R. S. & Reinhart-King, C. A. Matrix stiffening promotes a tumor vasculature phenotype. *Proc Natl Acad Sci U S A* **114**, 492-497, (2017).

40 LaValley, D. R.-K., C. Matrix stiffening in the formation of blood vessels. *Advances in Regenerative Biology* **1**, 1-4, (2014).

4.7 Tables

Table 4.1. Commercially Available medias used to culture hydrogel samples.

Name:	EGM2 (Lonza)	RPMI + B27 serum-free supplement (ThermoFisher Scientific)
Basal Medium:	EBM	RPMI 1640
Components:	hEGF	Biotin
	VEGF	DL Alpha Tocopherol Acetate
	R3-IGF-1	DL Alpha-Tocopherol
	Ascorbic Acid	Proteins
	Hydrocortisone	BSA, fatty acid free Fraction V
	hFGF-β	Catalase
	Heparin	Human Recombinant Insulin
	FBS	Human Transferrin
	Gentamicin/Amphotericin-B	Superoxide Dismutase
		Corticosterone
		D-Galactose
		Ethanolamine HCl
		Glutathione (reduced)
		L-Carnitine HCl
		Linoleic Acid
		Linolenic Acid
		Progesterone
		Putrescine 2HCl
		Sodium Selenite
		T3 (triodo-I-thyronine)
		Linolenic Acid

Table 4.2. Average Dynamic Contact Angle on PDMS (m=100).

N	Water	3 wt% AcHyA
1	116.46	112.5
2	90.2	123.4
3	134.69	100.59
Average	113.78	112.16

Table 4.3. Hagen-Poisuelle Driving pressure difference (ΔP_d) for 3 wt% HyA at different loading velocities (v).

velocity (m/s)	*Loading time (s)	ΔP_d (kPa)
2.1	0.03	11972.39124
0.21	0.29	1197.239124
0.021	2.86	119.7239124
0.0021	28.57	11.97239124
0.00021	285.71	1.197239124
0.000021	2857.14	0.119723912
0.0000021	28571.43	0.011972391
0.00000021	285714.29	0.001197239

*loading time = device length (~6 cm)/velocity

Table 4.4. Effect of changes in CBV width (w) and diverging channel angle (β) on Young-Laplace maximum pressure difference (ΔP_m, kPa).

ΔP_m (kPa)															
w (μm)	β° 5	10	15	20	25	30	35	40	45	50	55	60	65	70	75
1	89.2	106.9	-29.4	-124.9	-42.0	99.2	97.3	-45.6	-124.7	-26.7	108.0	86.4	-60.5	-122.3	-10.4
2	44.3	53.2	-15.0	-63.0	-21.3	49.1	48.1	-23.3	-62.9	-13.9	53.5	-35.7	32.4	-26.5	-10.8
3	29.4	35.3	-10.2	-42.3	-14.4	32.4	31.7	-15.9	-42.3	-9.6	35.3	-32.3	39.7	20.5	34.5
4	21.9	26.3	-7.8	-32.0	-10.9	24.0	23.5	-12.2	-32.0	-7.5	26.2	10.3	-29.8	-23.2	28.3
5	17.4	20.9	-6.3	-25.8	-8.9	19.0	18.6	-10.0	-25.8	-6.2	20.7	-7.5	-13.8	19.6	-19.2
6	14.4	17.3	-5.4	-21.7	-7.5	15.7	15.3	-8.5	-21.7	-5.3	17.1	15.2	-21.7	17.0	18.8
7	12.3	14.8	-4.7	-18.8	-6.5	13.3	13.0	-7.4	-18.7	-4.7	14.5	10.5	14.6	3.5	-18.8
8	10.7	12.9	-4.2	-16.5	-5.7	11.5	11.2	-6.6	-16.5	-4.3	12.6	14.0	-5.0	-14.9	13.5
9	9.4	11.4	-3.8	-14.8	-5.2	10.1	9.9	-6.0	-14.8	-3.9	11.1	-14.8	8.8	12.4	-11.7
10	8.4	10.2	-3.4	-13.5	-4.7	9.0	8.8	-5.5	-13.4	-3.6	9.8	1.6	-12.8	-10.9	-3.0
20	3.9	4.8	-2.0	-7.3	-2.6	3.9	3.8	-3.3	-7.3	-2.3	4.4	-1.3	0.1	-5.5	-3.6
30	2.4	3.0	-1.5	-5.2	-1.9	2.3	2.2	-2.6	-5.2	-1.9	2.6	-5.2	-3.7	-0.8	-1.5
40	1.7	2.1	-1.3	-4.2	-1.6	1.4	1.4	-2.2	-4.2	-1.7	1.7	1.8	-3.6	0.9	-4.2
50	1.2	1.6	-1.1	-3.5	-1.4	0.9	0.9	-2.0	-3.5	-1.6	1.1	-1.6	-0.3	-3.5	-1.9
100	0.3	0.5	-0.9	-2.3	-1.0	-0.1	-0.1	-1.5	-2.3	-1.3	0.0	-0.1	-2.2	-1.2	-1.9
150	0.0	#DIV/0!	-0.6	#DIV/0!	-0.6	#DIV/0!	-0.6	#DIV/0!	-0.6	#DIV/0!	-0.6	#DIV/0!	-0.6	#DIV/0!	-0.6

4.8 Figures

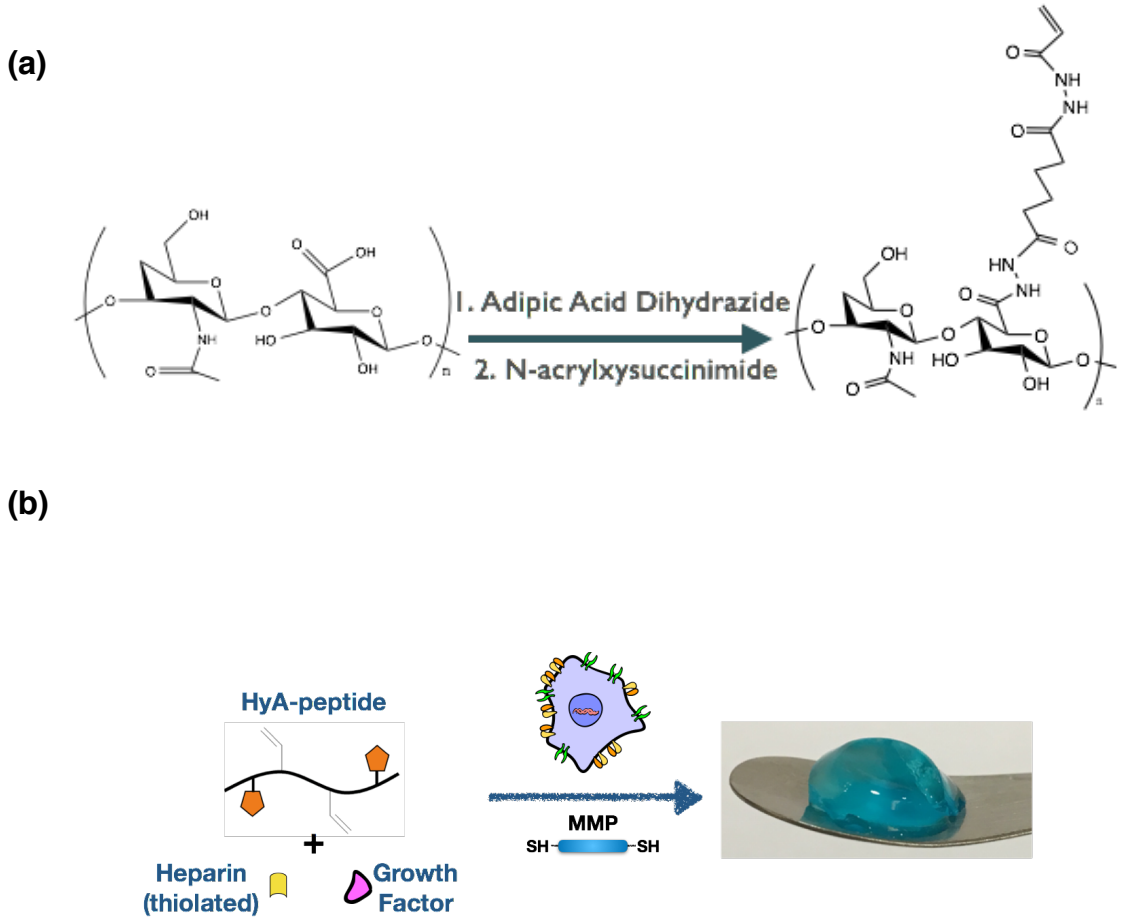

Figure 4.1. (a) Synthesis of acrylated hyaluronic acid by sequential conjugation of adipic acid dihydrazide and N-acryloxysuccinimide.[21] (b) Schematic for acrylated hyaluronic acid (AcHyA) hydrogel synthesis for hiPSC-EC encapsulation. Hydrogel contained integrin binding bsp-RGD peptide, heparin as a growth-factor (GF) presenting agent, bis-cysteine MMP-degradable peptide crosslinkers that reacted via a Michael-type addition to acryl groups functionalized on HyA precursors.[21]

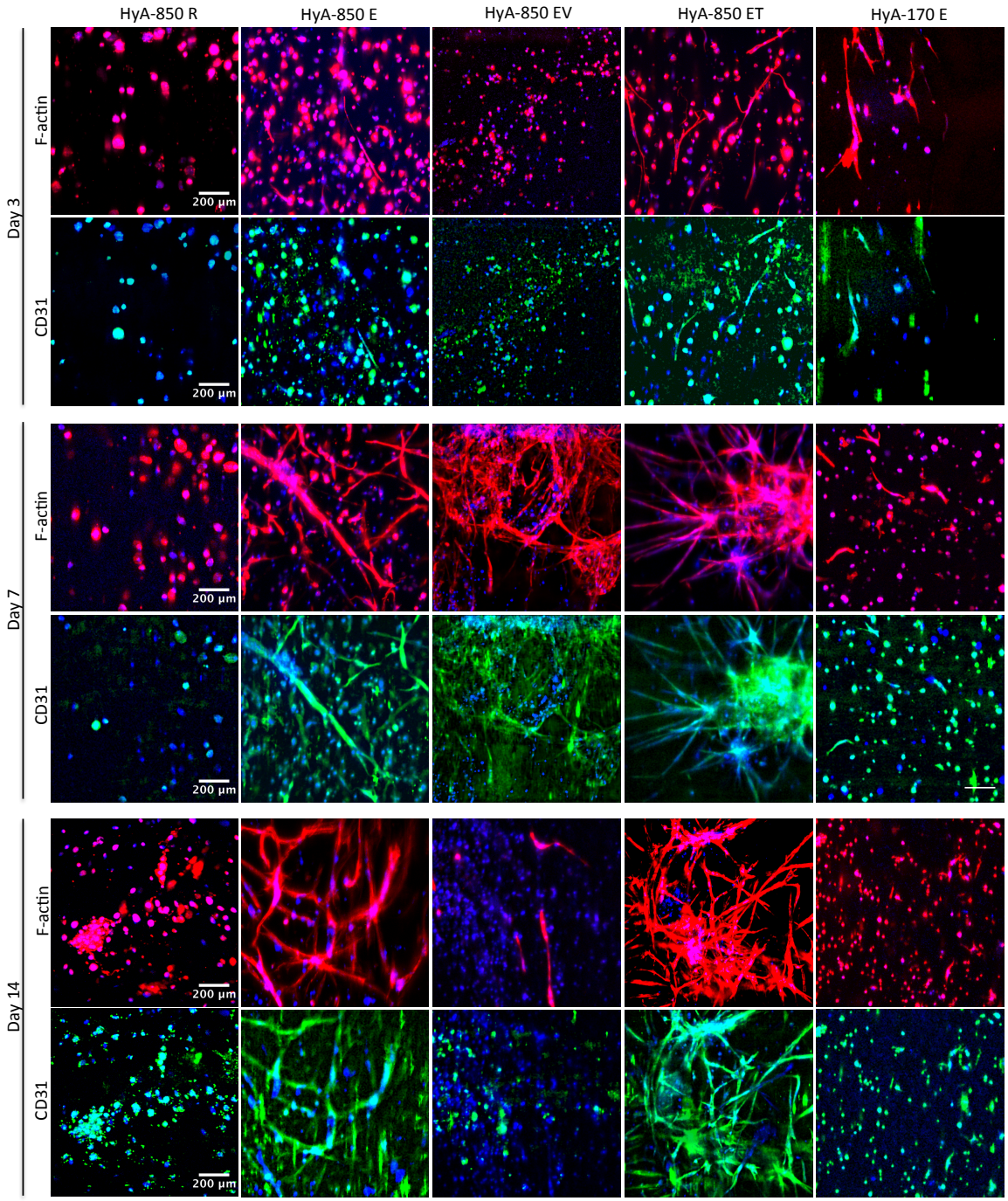

Figure 4.2. hiPSC-ECs encapsulated in acrylated HyA hydrogel formed capillary-like networks responsive to biochemical and biophysical changes in microenvironment. -Representative confocal images of hydrogel samples stained for F-actin and CD31 at day 3, 7, 14 demonstrated tube formation and stability dependent on biochemical signals and matrix rigidity.

HyA-850 R = 3wt% HyA +WTC hiPSC-EC+RPMI B27 complete media
HyA-850 E = 3wt% HyA +WTC hiPSC-EC+EGM2 media
HyA-850 ET = 3wt% HyA +WTC hiPSC-EC+EGM2 media + TGF-β1 (gel)
HyA-850 EV= 3wt% HyA +WTC hiPSC-EC+EGM2 media + VEGF-A_{165} (gel)
HyA-170 E = 2wt% HyA +WTC hiPSC-EC+EGM2 media

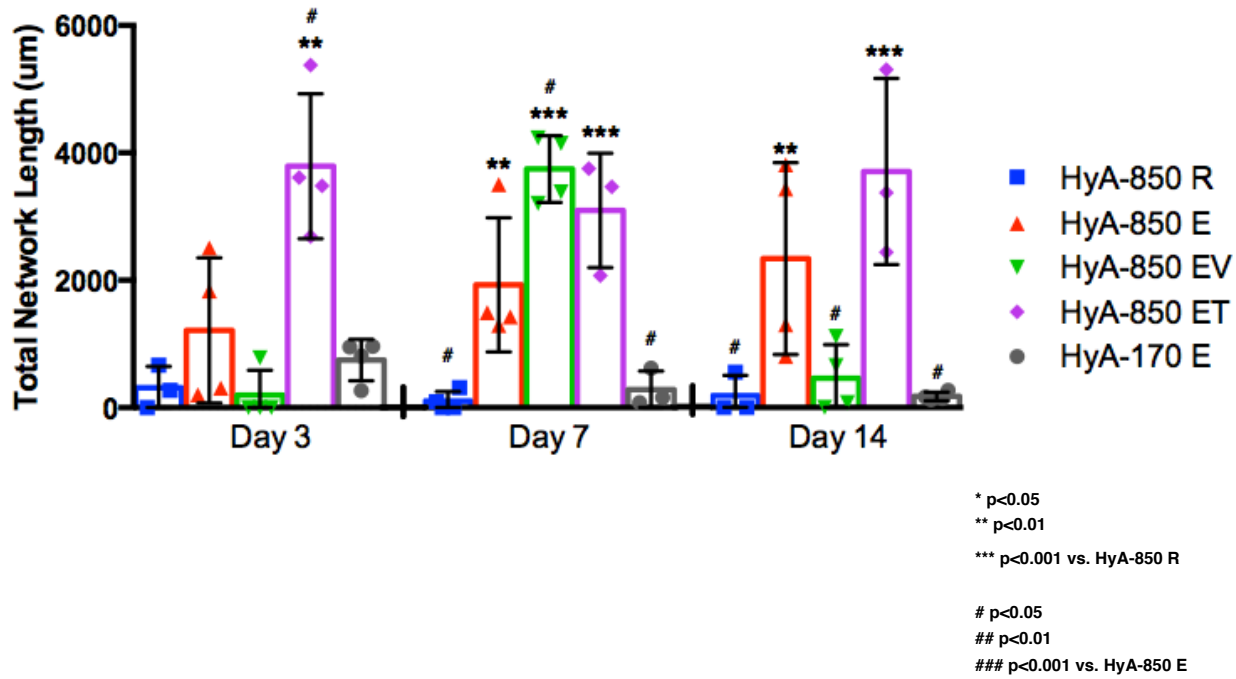

Figure 4.3. hiPSC-ECs encapsulated in acrylated HyA hydrogel formed capillary-like networks responsive to biochemical and biophysical changes in microenvironment. - Analysis of total network length in confocal images demonstrated proangiogenic signals are required for tube formation and stability; analysis of total network length relative to matrix stiffness demonstrated matrix with higher shear modulus formed significantly more tubes that are stable at 2 weeks compared to the softer matrix.

HyA-850 R = 3wt% HyA +WTC hiPSC-EC+RPMI B27 complete media
HyA-850 E = 3wt% HyA +WTC hiPSC-EC+EGM2 media
HyA-850 ET = 3wt% HyA +WTC hiPSC-EC+EGM2 media + TGF-β1 (gel)
HyA-850 EV= 3wt% HyA +WTC hiPSC-EC+EGM2 media + VEGF-A_{165} (gel)
HyA-170 E = 2wt% HyA +WTC hiPSC-EC+EGM2 media

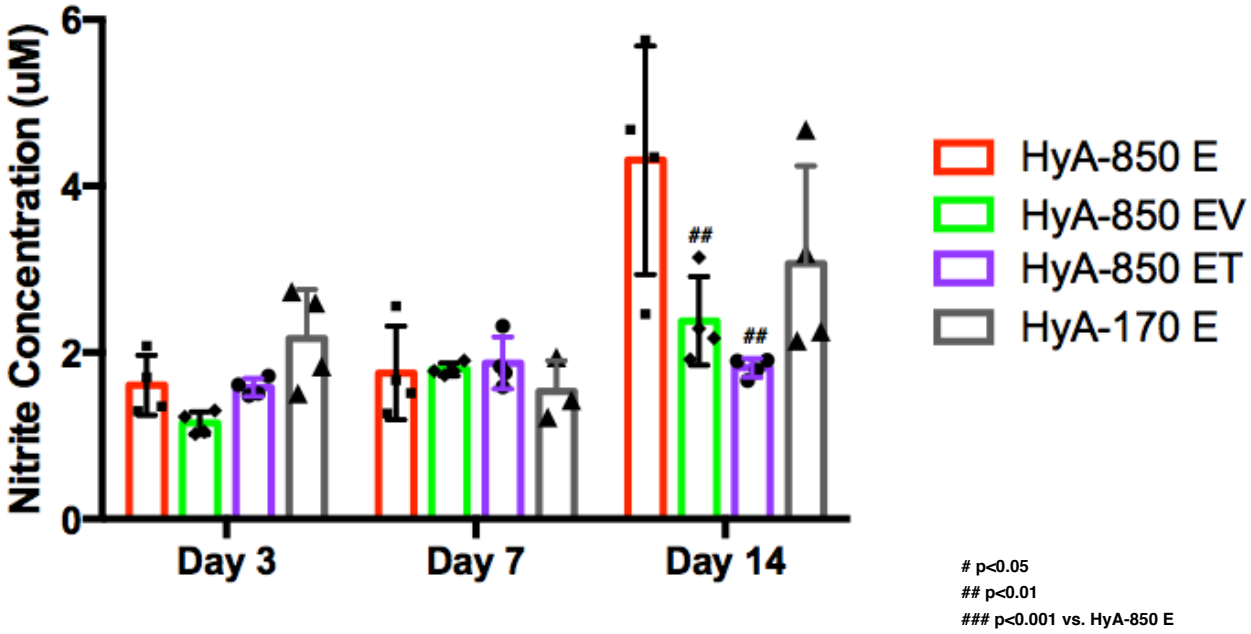

Figure 4.4. hiPSC-ECs encapsulated in acrylated HyA hydrogel formed capillary-like networks responsive to biochemical and biophysical changes in microenvironment. - Highest nitric oxide production, an indicator of endothelial cell function, corresponded with HyA-850 E which demonstrated most tube formation with long-term stability.

HyA-850 R = 3wt% HyA +WTC hiPSC-EC+RPMI B27 complete media
HyA-850 E = 3wt% HyA +WTC hiPSC-EC+EGM2 media
HyA-850 ET = 3wt% HyA +WTC hiPSC-EC+EGM2 media + TGF-β1 (gel)
HyA-850 EV= 3wt% HyA +WTC hiPSC-EC+EGM2 media + VEGF-A_{165} (gel)
HyA-170 E = 2wt% HyA +WTC hiPSC-EC+EGM2 media

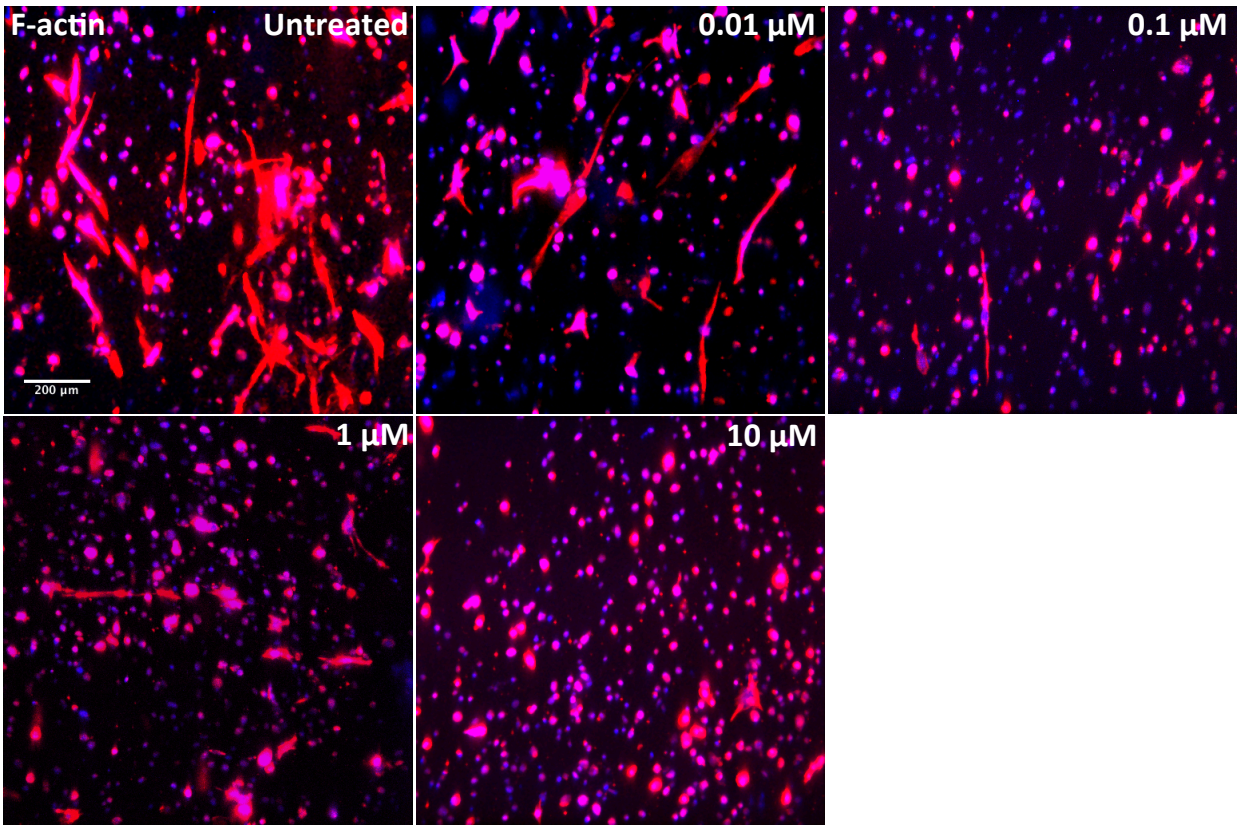

Figure 4.5. hiPSC-EC sprouting was eliminated by treatment with small-molecule angiogenesis inhibitor for 7 day's after hydrogel encapsulation. (Representative confocal images).

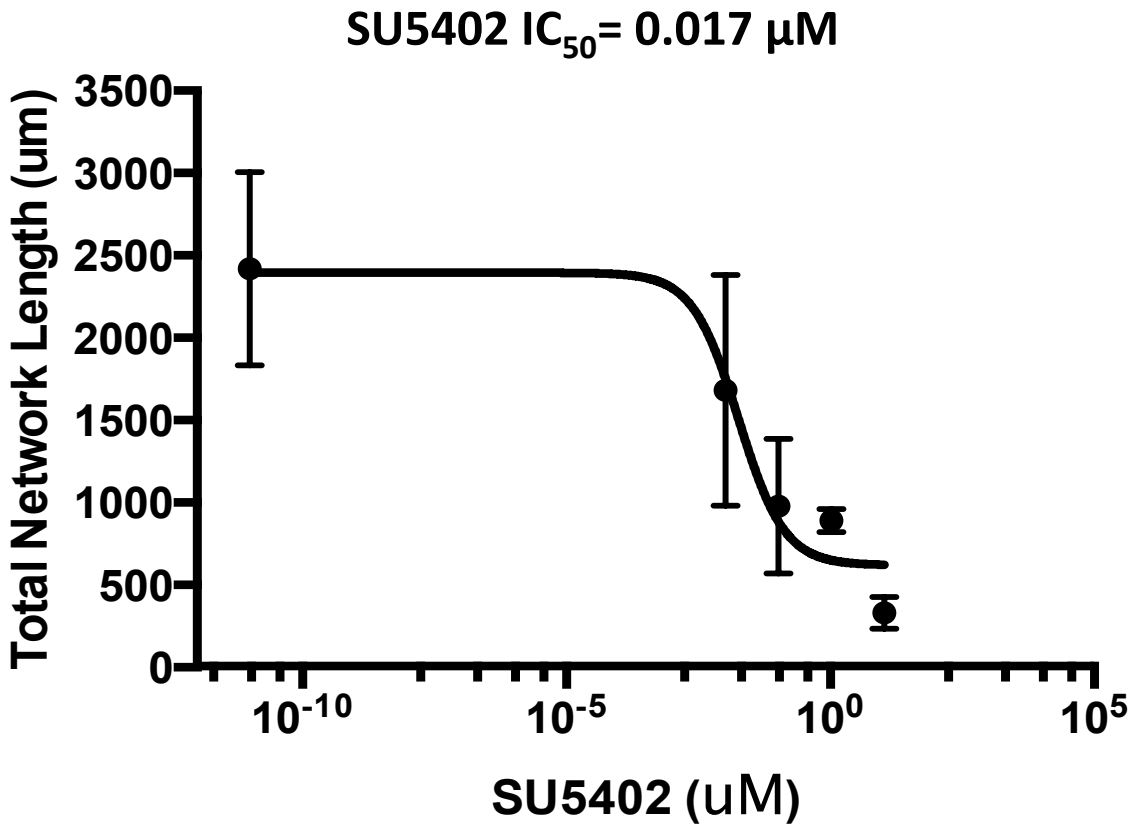

Figure 4.6. hiPSC-EC sprouting was eliminated by treatment with small-molecule angiogenesis inhibitor for 7 day's after hydrogel encapsulation. IC_{50} value determined from dose-response curve was in agreement with previously published data.

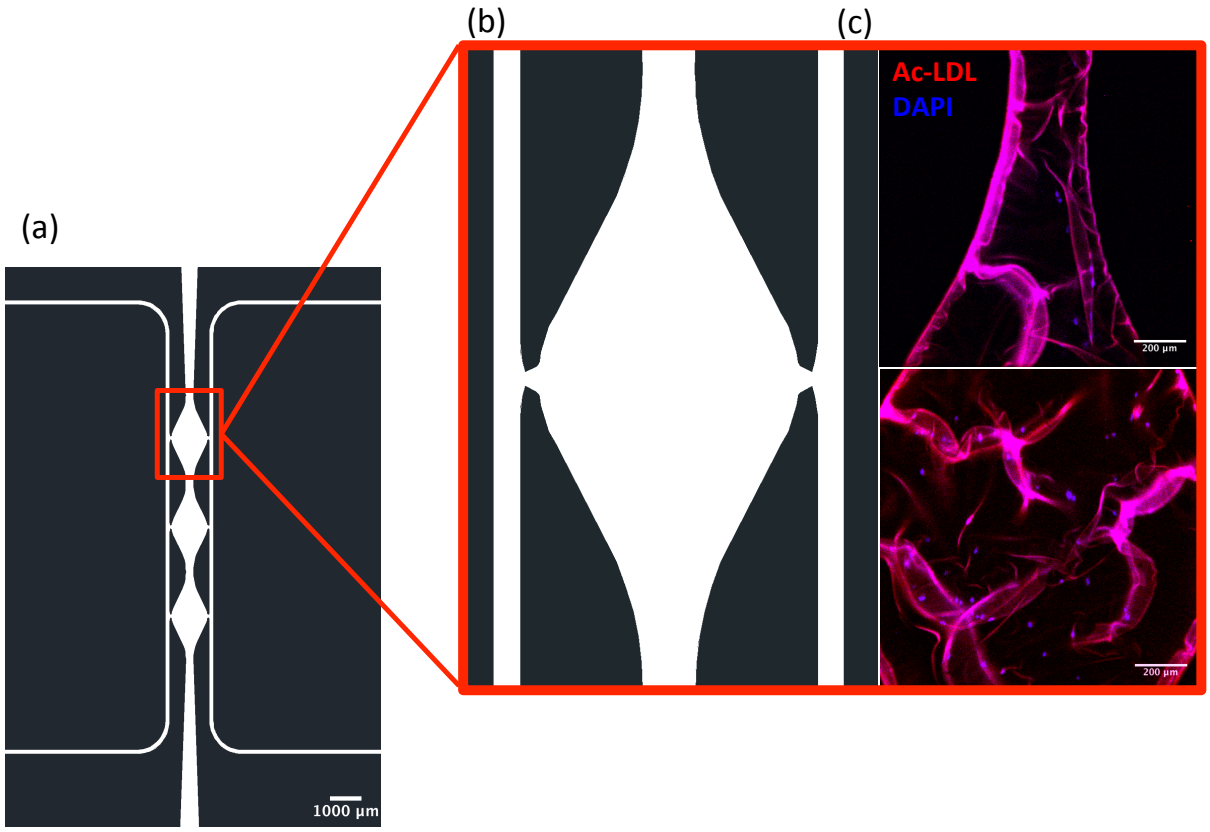

Figure 4.7. Cultured HyA-850 E in tri-chamber microfliudic device. (a) Schematic of device design.[2,26] (b) Magnified image of diamond-shaped sample chamber with flanking media channels, and (c) confocal image of fixed HyA-850 E loaded into device demonstrated functional capillary-like networks.

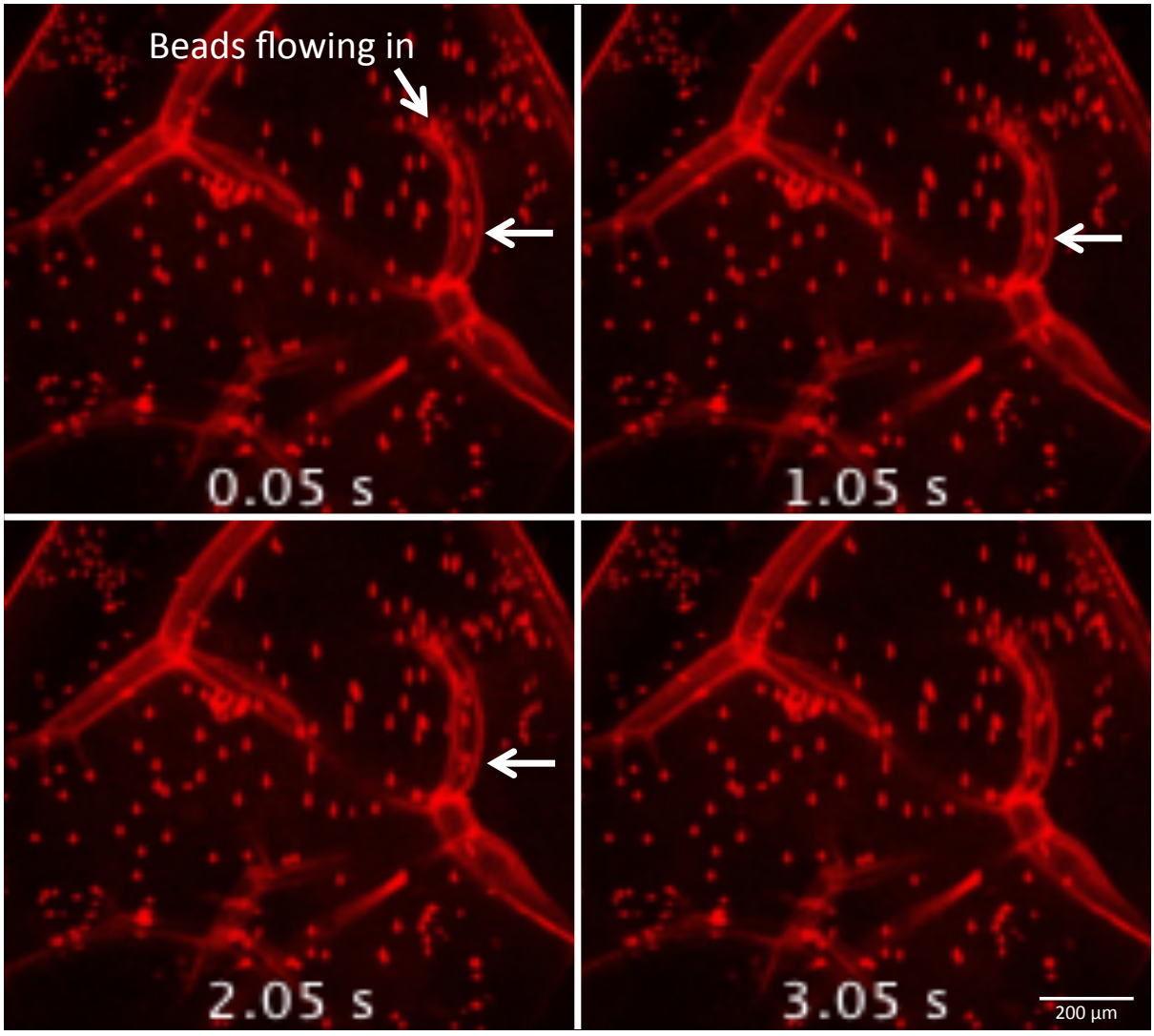

Figure 4.8. Cultured HyA-850 E in tri-chamber microfliudic device. Time-lapse montage of 2 µm diameter fluorescent microbeads flowing into fixed sample stained for F-actin demonstrated networks are hollow and perfusable.

(a)

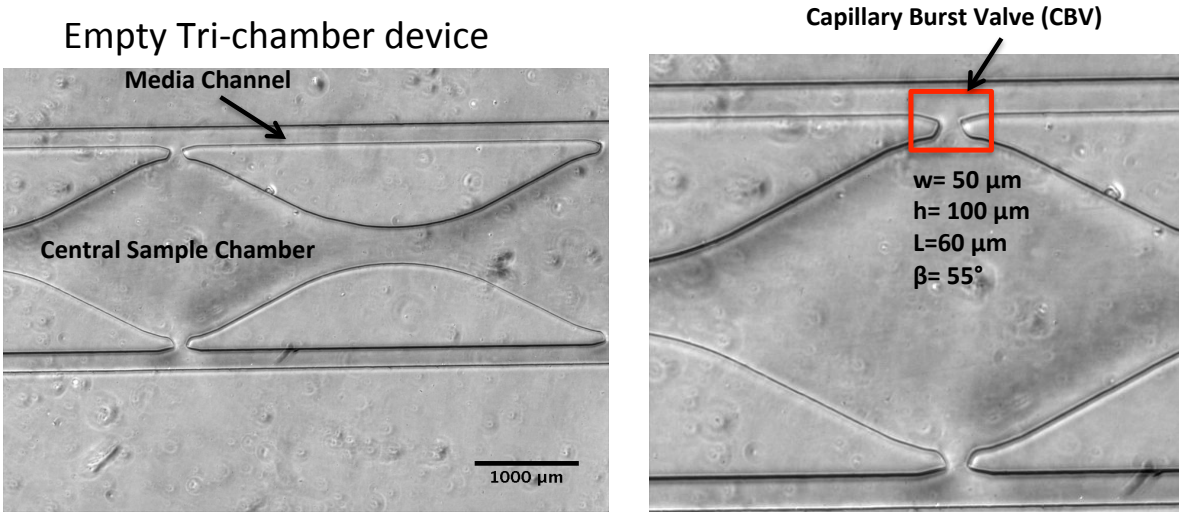

(b)

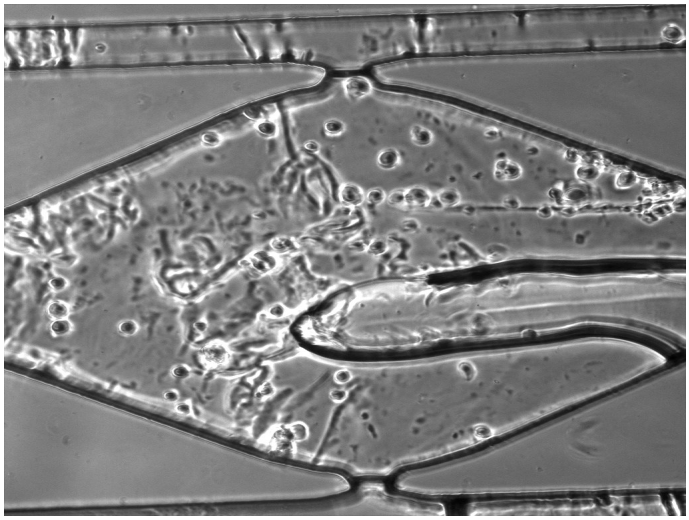

Figure 4.9. Representative phase contrast images of tri-chamber microfluidic device[2,26] (a) empty device (b) magnified image of empty device highlighting capillary burst valve (CBV) location (c) hiPSC-ECs encapsulated in AcHyA gel that burst through CBV into media channel.

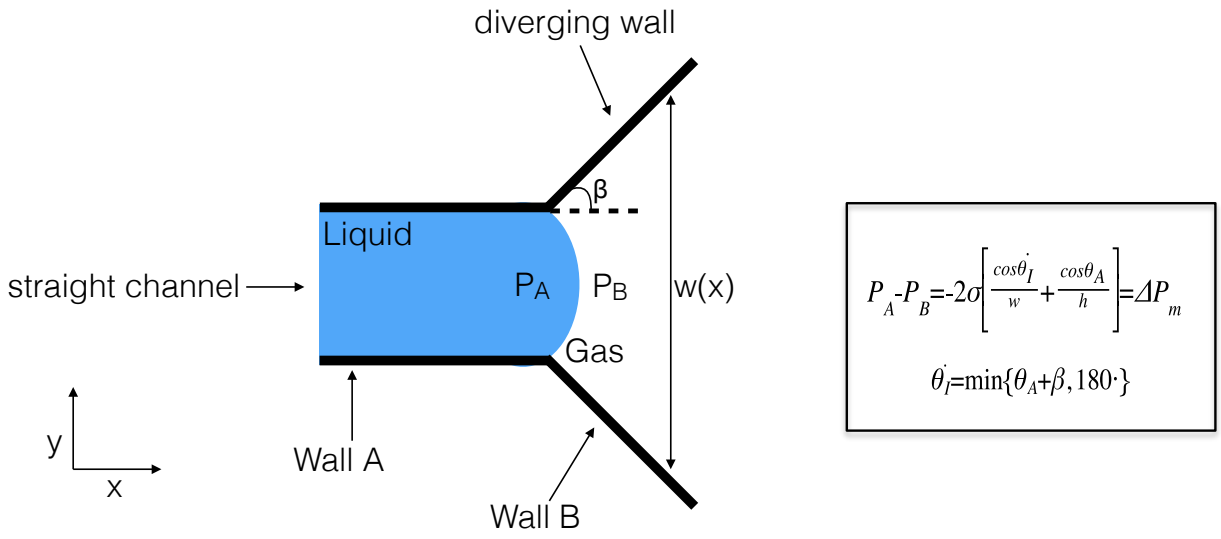

Figure 4.10. Schematic of rectangular channel with a sudden diverging wall and corresponding Young-Laplace equation that describes maximum pressure difference of static (pinned) liquid meniscus at this position.[33]

$$\Delta P_D = \frac{2\eta L v (h+w)^2}{(hw)^2}$$

$$v = \frac{\Delta P_D (hw)^2}{2\eta L (h+w)^2}$$

$$v_e = \frac{\Delta P_{max} (hw)^2}{2\eta L (h+w)^2}$$

w=50 um, h=100 um, L=60 um, η_{ACHA}=13.56 $Pa{\cdot}s$, η_{H2O}= 0.001 $Pa{\cdot}s$

$$v_{e,H2O} = 210 \ \frac{cm}{s}$$

$$v_{e,AcHyA} = 204 \ \frac{\mu m}{s}$$

if $v_{AcHyA} = v_{e,H20}$

then ΔP_{AcHyA}=11.9 MPa >> $\Delta P_{max,AcHyA}$=1.1 kPa

Figure 4.11. Hagen-Pouieselle calculation of equilibrium loading velocity ($v_{e,AcHyA}$) of hydrogel to maintain prevent bursting CBV and its corresponding driving pressure ($\Delta P_{d,AcHyA}$).

CBV when AcHA flowing at equilibrium velocity (204 um/s)

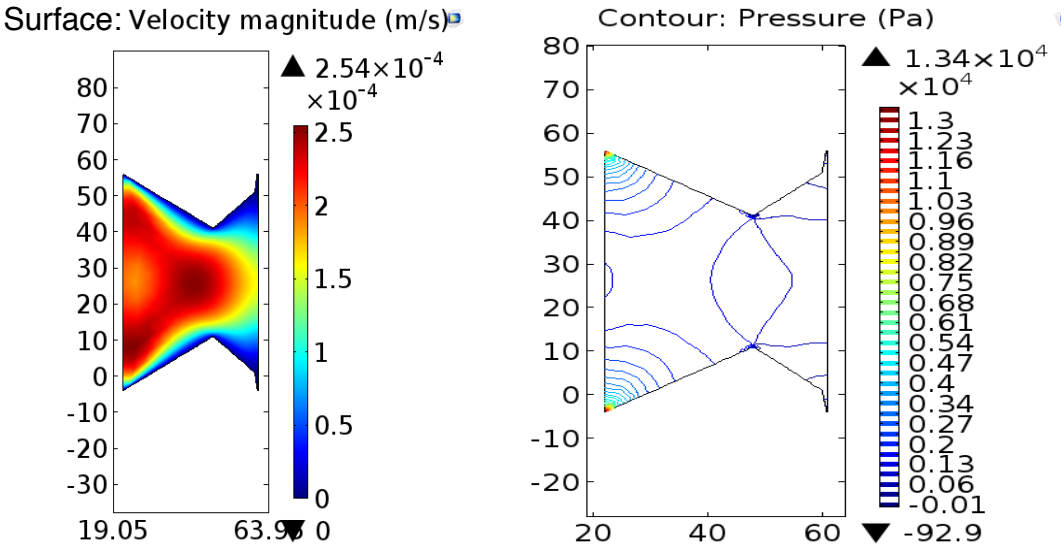

CBV when AcHA flowing at water equilibrium velocity (210 cm/s)

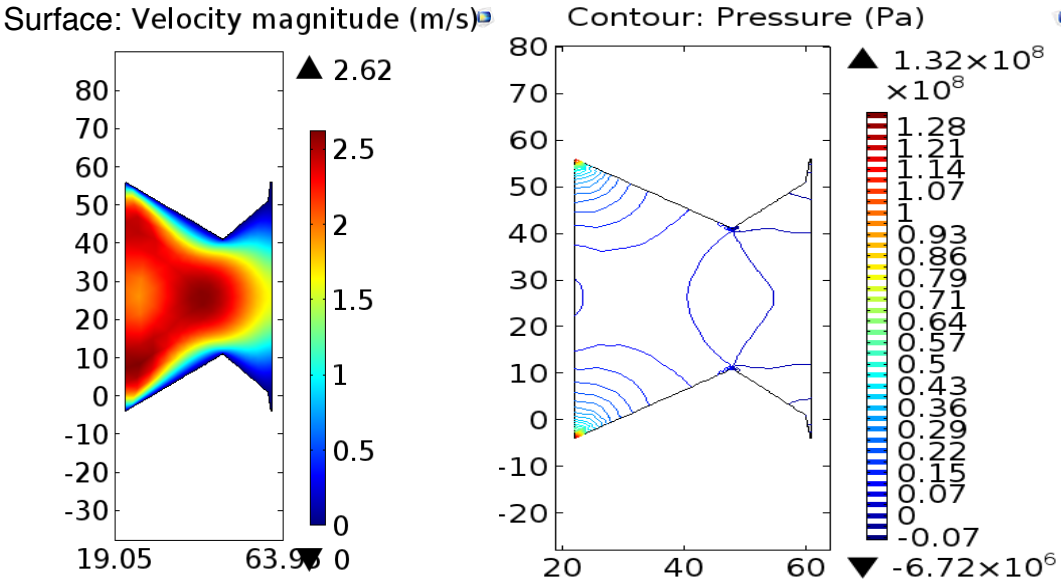

Figure 4.12. COMSOL model of CBV for AcHyA hydrogel flowing at equilibrium velocity ($v_{e,AcHyA}$) and at water equilibrium velocity ($v_{e,water}$).

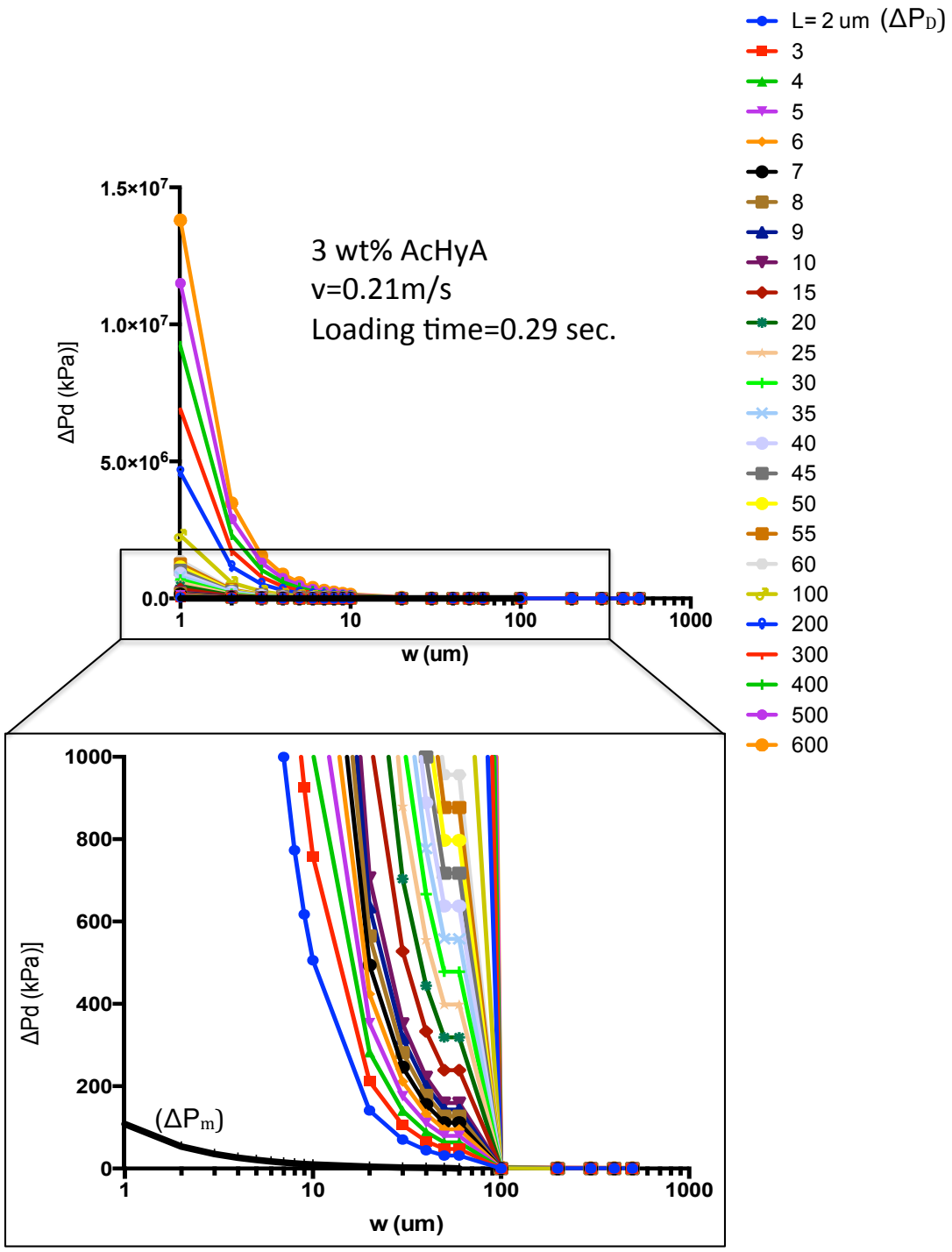

Figure 4.13. Effect of changing the length and width of the CBV on the driving pressure difference ($\Delta P_{d,AcHyA}$) during loading and the maximum pressure difference (ΔP_{max}) of the pinned liquid meniscus.

Material	η (Pa*s)	ΔPd (kPa)
3 wt% AcHyA	13.56	1197.23
2 wt% AcHyA	2.72	191.92
	1	70.56
1 wt% AcHyA	0.25	17.64
	0.01	0.70
H2O	0.001	0.070

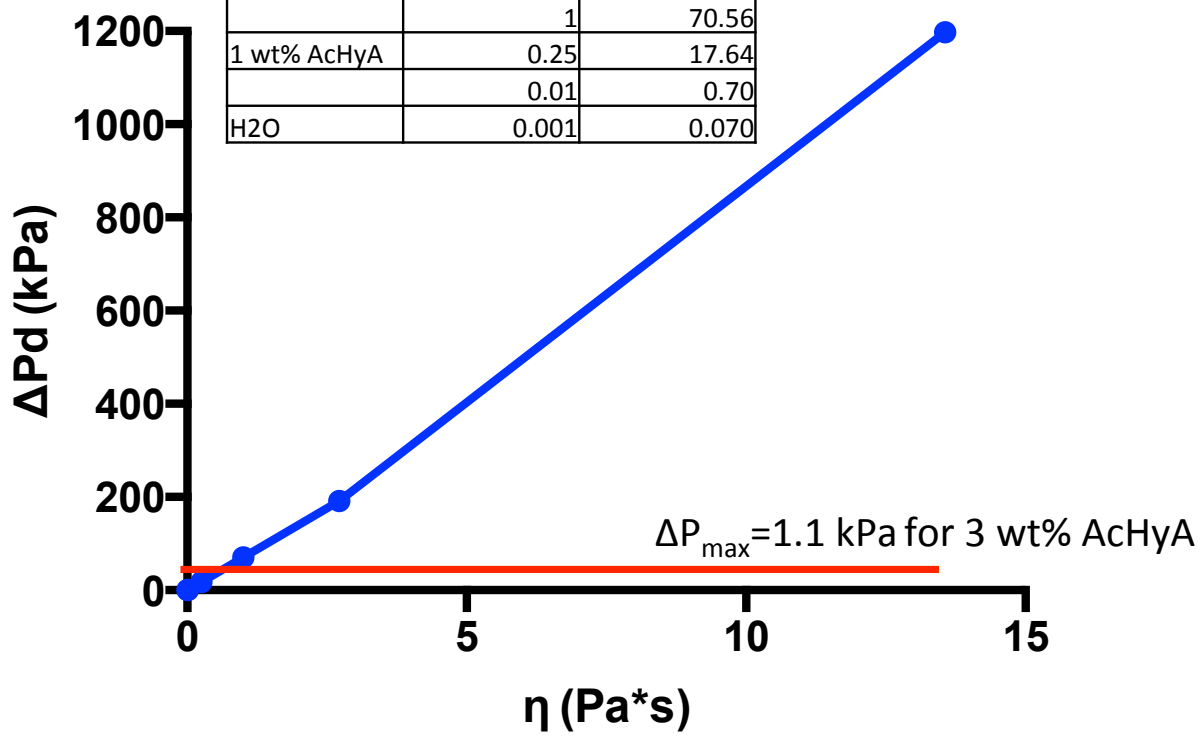

Figure 4.14. Relationship between hydrogel viscosity and driving pressure difference in CBV for v=0.21 m/s (loading time = 0.29s), w=50 um, L=60 um, h=100 um.

CHAPTER 5:
3D *IN VITRO* CARDIOVASCULAR TISSUE MODEL

5.1 Abstract

Cardiovascular disease refers to damaged, narrowed, or blocked blood vessels that can cause a stroke or myocardial infarction.[1-4] According to the 2017 Heart Disease and Stroke Statistics Update by the American Heart Association, Cardiovascular Diseases (CVD) remain the leading causes of death worldwide.[5] Numerous studies have investigated regenerative therapies for ischemic tissues involving stem cell transplantation using hydrogel scaffolds. However, these therapies have had limited success due to poor donor cell engraftment and low survival. One major contributing factor to the lack of success is the insufficient vascularization within the ischemic tissue and the scaffold.[6-11] Due to the complex mechanisms involved in angiogenesis and the unknown safety/efficacy of stem cell transplantation, much remains to be learned before ischemic tissues can be repaired with fully functioning, vascularized engineered tissues. Stem cell derived cardiovascular models present a unique platform to study the complex process of angiogenesis and CM-EC interaction in a patient-specific manner.[8,12,13] This study investigated some of these limitations by co-culturing endothelial cells and cardiomyocytes differentiated from human induced pluripotent stem cells in a tunable hyaluronic acid (HyA-850 R) scaffold to promote cell survival and maintenance of lineage-specific function.[14] The inability of the hiPSC-CMs to survive longer than a few days in the HyA gel or support hiPSC-EC tube formation highlighted the need to develop more mature cardiac lineage cells and optimized 3D culture conditions for improved cell viability.

5.2 Introduction

A myocardial infarction (MI) is the result of blood supply loss from the coronary circulatory system due to Cardiovascular Disease (CVD) that leads to ischemia in the myocardium and the death of functional, beating cardiomyocytes (CMs). [1-4] According to the 2017 Heart Disease and Stroke Statistics Update by the American Heart Association, Cardiovascular Diseases (CVD) remain the leading causes of death in in the U.S. [5] The total cost associated with CVD in 2012 was determined to be higher than any other diagnostic group in the U.S and the report estimates 92.1 million American adults currently have at least one form of CVD. As of 2011, the AHA reports that CVD accounted for about 1 in 3 deaths in the U.S. and approximately 34% of these deaths occurred in people younger than 75 years old (the current life expectancy is 78.5 years). The total cost (direct and indirect) associated with CVD in 2012 was determined to be $316.1 billion, which is higher than any other diagnostic group in the U.S. [5] Additionally, the World Health Organization cites CVD as the leading cause of death worldwide and expects the death rate to continue rising within the next 15 years regardless of socioeconomic backgrounds.[15] Overall, people in low- and middle-income countries are the most severely affected by CVD due to limited access to primary healthcare for early detection and treatment. These statistics demonstrate the need for more effective, patient-specific treatments of cardiovascular diseases.

Within the last decade, several studies in tissue engineering for repair of ischemic myocardium have demonstrated the benefit of co-culturing cardiomyocytes (CMs) with endothelial cells (ECs) to create a more physiologically relevant and effective therapy.[5,6,14,15] However, the results indicated that improvements were needed to increase CM survival and augment vascularization of the tissue construct to enhance the clinical translational ability of the proposed therapy. Current studies attempting to remedy these issues have incorporated co-cultures of harvested or stem cell derived cardiomyocytes and endothelial cells in natural or semi-synthetic scaffolds that contained cytokines to promote vascularization.[10,11,16-21] Tulloch et al studied a co-culture of hESC and iPSC derived CMs in a collagen I matrix combined with human umbilical vein endothelial cells (HUVECs) and found the ECs did not affect CM beat rate, alignment, or hypertrophy but did help increase CM viability *in vitro*. *In vivo* studies of grafts in a non-myocardial infarction rat model demonstrated that ECs anastomosed with the host vasculature and perfusion studies revealed host red blood cells in these blood vessels.[21] Bearzi et al genetically modified mouse iPSCs to produce PIGF and MMP-9, differentiated them towards a cardiac cell lineage, and encapsulated the embryoid bodies in a PEG-fibrinogen hydrogel.[16] In vivo studies of the implanted system in a mouse anterior tibialis showed formation of arteriolar-like structures and cTNNI+ cells. A mouse MI model demonstrated the implants led to an increase in angiogenesis and overall improved cardiac function. Furthermore, Ye and colleagues showed that incorporating hiPSC derived CMs, ECs, and SMCs into a fibrin scaffold containing IGF-1 improved cardiac function and caused CM hypertrophy and alignment in a porcine MI model. However, a robust vasculature did not develop after 4 weeks post MI and significant cell death was observed throughout the study.[22] More recently, Giacomelli and Mummery developed a method to simultaneously differentiate human pluripotent stem cells to cardiomyocyte and cardiac endothelial cell lineage. After lineage-specific enrichment, the CMs and ECs were co-cultured as a pellet to form an *in vitro* 3-D cardiovascular micro-tissue (MT-CMEC). Compared to the cardiomyocyte-only micro-tissue (MT-CM), the MT-CMEC demonstrated increased gene expression for cardiac ion channel proteins and exhibited a physiologically relevant dose-response to isoproterenol. [23] Many issues remain with current studies on cardiovascular tissue engineering studies, including the use of ECs and CMs obtained from primary cell lines, mouse stem cells, or commercially available immortalized cell lines. Additionally, many current studies relied on unmodified and commercially available natural scaffolds such as collagen, gelatin, fibrin, Matrigel, and decellularized matrices that do not effectively mimic the human extracellular matrix.

Consequently a therapy that can restore cardiomyocytes in the ischemic region and reconnect them with the coronary vascular network is still needed.[1,24] Numerous studies have investigated regenerative therapies involving stem cell transplantation using hydrogel scaffolds. However, these therapies have had limited success due to poor donor cell engraftment and low survival. One major contributing factor to the lack of success is the limited vascularization within the ischemic cardiac tissue and the scaffold. [6-11] Due to the complex mechanisms involved in angiogenesis and the unknown safety/efficacy of stem cell transplantation, much remains to be learned before ischemic tissues can be repaired with fully functioning, vascularized engineered tissues. Stem cell derived

cardiovascular models present a unique platform to study the complex process of angiogenesis and CM-EC interaction in a patient-specific manner.[8,12,13]

This study investigated these limitations by co-culturing endothelial cells and cardiomyocytes differentiated from human induced pluripotent stem cells in a tunable hyaluronic acid (HyA) scaffold to promote cell survival and maintenance of lineage-specific function. The CMs were differentiated from the WTC hiPSC line using the method developed by Lian and Pelacek that involves modulating the Wnt-signaling pathway.[25] The hiPSC-endothelial cells were obtained from the differentiation method described in chapter 3. The *in vitro* cardiovascular tissue model was developed by comparing the culture of hiPSC-CMs in the HyA-850 R hydrogel alone and with the hiPSC-ECs. The hiPSC-CMs demonstrated a limited ability to survive, function, and support angiogenesis within the hydrogel, which highlighted the complexity of recapitulating multi-cellular tissues *in vitro*. The results indicate the cells were not interacting in a physiologically relevant manner since cardiomyocytes and endothelial cells engage in mutually beneficial paracrine signaling in the human myocardium that promotes cell survival, viability, and angiogenesis.[26-29]

5.3 Materials and Methods

5.3.1 hiPSC-Cardiomyocyte Differentaition and Lactate Purification

The cardiomyocyte differentiation was based on the protocol developed by Lian et al where they demonstrated that the temporal modulation of beta-catenin activity during a Wnt-based differentiation led to the formation of beating cardiomyocytes (CMs) in growth factor-free medium. First, the human pluripotent stem cells were passaged onto plates coated with growth factor-reduced Matrigel (Corning) at 25,000-30,000 cells/cm^2 and fed Essential 8 Medium supplemented with 10 uM ROCK inhibitor (Day -2). The medium is replenished the next day (Day -1) without ROCK inhibitor. Differentiation is initiated on Day 0, by feeding the cells RPMI supplemented with B27 minus insulin (Thermo Fisher) and 6 uM CHIR 99021 (STEMCELL Technologies), a small-molecule inhibitor of GSK3 which inititates canonical Wnt signaling. The media is removed after 24 hours and replaced with RPMI supplemented with B27 minus insulin only. Cardiac mesoderm specification is initiated on Day 2, the cells fed RPMI supplemented with B27 minus insulin with IWP-4, a small-molecule antagonist to Wnt-signaling. The media is exchanged on Day 4 for RPMI B27 minus insulin. On Day 6 the cells are fed RPMI B27 complete and this media is exchanged every other day until the cells are ready for use. Beating sheets of cells can be observed as early as Day 7.[25] (protocol summarized in Fig 5.1)

Cardiomyocytes were isolated from the mixed population using lactate purification medium on Day 14. First, the cells were dissociated using 0.25% Trypsin with a 10 minute incubation in 37°C (5% CO_2) and quenched with EB20 medium (1:5 enzyme to EB20). One batch of EB20 was composed of 120 ml of Hyclone Fetal Bovine Serum (Fisher), 6 ml of GlutaMAX-I, 100X (Life Technologies), 6 ml of MEM NEAA 10mM (100X), 4.2 ul of β-mercaptoethanol. The cells were then centrifuged at 1000 rpm for 5 minutes. The cells were then resuspended in RPMI supplemented with B27 complete with 1 uM Rock

inhibitor and replated onto Matrigel coated TCPS plates at a split ratio of 1:2. The following day, the cells were fed 4 mM Lactate Purification medium composed of 1 M lactate in HEPES buffer, 5% Non-essential amino acid solution (1x, Thermo Fisher), 1% Glutamax (1x, Thermo Fisher) in DMEM without glucose or sodium pyruvate (Thermo). The cells were fed the lactate purification medium every other day for one week. After purification, the cardiomyocytes were maintained in RPMI supplemented with B27 complete.

5.3.2 Flow Cytometry

The unpurified cardiomyocyte differentiation population was tested for cardiac troponin (CTnT) expression with flow cytometry. The cells were dissociated from cell culture dishes as described previously. After centrifugation to remove trypsin and EB20, the cells were resuspended in PBS and centrifuged again at 1000 rpm for 5 minutes. The PBS was aspirated and the cells were resuspended in 4% paraformaldehyde (PFA), after 10 minute the PFA was removed by centrifugation . The cells were resuspended in PBS and centrifuged again to wash any residual PFA. The PBS was removed and cells were resuspended in 0.5 mL FACS buffer (50 mL DPBS, 0.5 mL FBS, 0.25 g saponin). Anti-human CTnT primary antibody (MS-295-P, Thermo Scientific) was diluted in the cell/FACS solution at 1:200 and incubated at room temperature for 30 minutes. The cells were then washed twice with centrifugation and resuspension in 0.5 mL FACS buffer. The secondary antibody (anti-mouse Alexa Fluor-488, Thermo Fisher) was diluted in cell/FACS solution at 1:200 and incubated at room temperature for 30 minutes. The cells were then washed twice in FACS buffer and once in PBS. Stained cells were then resuspended in 0.5 mL PBS and analyzed with a with a Beckman Coulter FC500 flow cytometer. The data was analyzed with Kaluza software (Beckman Coulter) and gating was based on corresponding isotype controls.

5.3.3 Immunofluorescence staining

Cells were rinsed with PBS and fixed with 4% PFA for 10 minutes. They were then permeabilized with 0.1% Triton for 5 minutes and washed with PBS twice. The samples were then blocked witn 3% FBS for 30 minutes. Samples were stained sequentially with primary and secondary antibodies in PBS for either 2 hours at room temperature or overnight at 4°C (antibodies are listed in Table 5.1). The samples were then washed twice with PBS. Fluorescent and phase contrast images were taken on a Nikon Eclipse TE300 microscope with a Hamamatsu C11440 digital camera and Zen lite software (Carl Zeiss, Thornwood, NY).

5.3.4 CTnT+ hiPSC-CMs and Co-culture hydrogel encapsulation

The gelation procedure for the HyA was described in chapter 4 and reported previously[14,30,31] Purified CTnT+ hiPSC-CMs were encapsulated into the 3 wt% HyA gel at concentrations of $1x10^6$ cells/mL , $3x10^6$ cells/mL , and $10x10^6$ cells/mL for cell viability measurements. For confocal microscopy and beat rate analysis, the purified CTnT+ hiPSC-CMs were encapsulated into the 3 wt% HyA gel at at a concentration of $3x10^6$ cells/mL Co-

culture hydrogel samples consisted of encapsulating hiPSC-ECs and hiPSC-CMs at a ratio of 1:3 respectively.

5.3.5 CTnT+ hiPSC-CMs Viability Assay

hiPSC-CM viability within the hydrogels was measured using the LIVE/DEAD™ Viability/Cytotoxicity Kit for mammalian cells (Invitrogen). Purified CTnT+ hiPSC-CMs were encapsulated within hydrogel at concentrations of $1x10^6$ cells/mL , $3x10^6$ cells/mL , and $10x10^6$ cells/mL The samples were tested 24 hours after encapsulation by removing the culture medium, rinsing 1x with PBS, and incubating with 1:1000 Calcein and 1:500 Ethidium homodimer-1 (EthD) in PBS for 30 minutes at 37°C. The samples were then rinsed 1x with PBS and imaged with a Prairie two photon/confocal microscope (Prairie Technologies, Middleton, WI).

5.3.6 Confocal microscopy

Cells encapsulated within the hydrogel were rinsed with PBS and fixed with 4% PFA for 30 minutes and permeabilized for 5 minutes with 0.1% Triton. The samples were then rinsed 3x with PBS and blocked with 3% BSA for 30 minutest. They were then stained with 1:200 primary anti-human CTnT and anti-human alpha-actinin (Table 5.1) and 1:200 Acti-stain 555 phalloidin (Cytoskeleton, Inc.) in PBS overnight at 4°C. Next, the samples were washed in triplicate with PBS. Samples were then stained with Alexa Fluor 488 goat anti-mouse and Alexa Fluor 568 goat anti-rabbit secondary antibody (1:200 in PBS) and incubated overnight at 4°C. The samples were then washed three times with PBS. Prior to imaging, cell nuclei were stained with DAPI (Invitrogen) for 5 minutes and washed 1x with PBS. Fluorescent images were taken with a Prairie two photon/confocal microscope (Prairie Technologies, Middleton, WI).

5.3.7 hiPSC-CM beat rate analysis in hydrogel samples

Videos of the beating hiPSC-CM mono- and co-culture hydrogel samples were taken for 10 seconds at Day 3, 7, and 14. Videos were taken on a Nikon Eclipse TE300 microscope with a Hamamatsu C11440 digital camera and Zen lite software (Carl Zeiss, Thornwood, NY). The beat rate and contraction velocity were measured using motion-tracking software.[32]

5.4 Results and Discussion

5.4.1 Characterization of CTnT and α-Actinin expression of hiPSC-CMs

Flow cytometry analysis of the mixed population at Day 9 of the cardiomyocyte differentiation demonstrated that approximately 62% of the cells were CTnT+ (Fig 5.2). (Note, our lab has recently optimized the protocol in terms of cell density and small-molecule treatment days to improve the output of CTnT+ cells). The beating hiPSC-CMs were lactate purified for seven days, fixed, and stained in the TCPS culture plates. Fluorescence microscopy demonstrated high levels of CTnT expression and sarcomeres could be visualized through the alpha-actinin stain. CTnT staining revealed heterogenous

cardiomyocyte morphologies and sizes in addition to disorganized arrangement of cells within the culture dish. Alpha-actinin staining demonstrated some organized sarcomeres in elongated cardiomyocytes while smaller, cuboidal cardiomyocytes had disorganized, clustered sarcomeres.

5.4.2 Viability assay of encapsulated hiPSC-CM for cell seeding density

To determine optimal seeding density for hiPSC-CMs in the acrylated hyaluronic acid hydrogel, a live/dead assay was done on samples with cell concentrations of $1x10^6$, $3x10^6$, and $10x10^6$ cells/mL (Fig. 5.3). Hydrogel samples were stained and analyzed with confocal microscopy 24 hours post-encapsulation. Stacked images demonstrate the samples with cell concentrations of $1x10^6$ and $10x10^6$ cells/mL had the most uptake of EthD, which marks the dead cells. The high cell death for the low hiPSC-CM concentration is in congruence with the arrangement of cardiomyctes in-vivo since they require cell-cell contacts for survival and proper function. The high cell death for the hydrogel with a concentration of $10x10^6$ cells/mL appears to be the result of too many cells competing with each other for nutrients and space.

5.4.3 Motion capture analysis of beat rate and contraction velocity of hiPSC-CM in Monoculture and Co-culture with hiPSC-ECs within AcHyA hydrogel

Beat rate and contraction velocities were measured using motion capture analysis of 10 second videos of mono- and co-culture hiPSC-CMs encapsulated in the HyA hydrogel on Days 3, 7, and 14. hiPSC-CM beating could only be detected on Day 3 post-encapsulation and it appeared to stop by Day 7 in both sets of samples. Figure 5.4 shows the beating velocity analysis of Day 3 samples with the motion tracking software and their corresponding heat maps depicting mean contraction. Beating was slow and slightly below the physiological range for humans and the addition of VEGFA to the co-culture appeared to reduce the average beat rate. Figure 5.5 summarizes the beat rate of these samples; no significant difference was found between beat rate of the mono and co-cultures.

5.4.4 Confocal microscopy analysis of hiPSC-CM morphology in Monoculture and Co-culture with hiPSC-ECs within AcHyA hydrogel

Mono- and co-culture hiPSC-CMs encapsulated in the HyA hydrogel were stained for CTnT and F-actin. The samples were analyzed at Day 7 with confocal microscopy and the CMs appear rounded and non-viable (Fig. 5.6). Additionally, the co-cultured samples were stained for CD31 to identify the hiPSC-ECs and no tube formation could be detected. Since the hiPSC-CMs did not appear to support EC tube formation through paracrine signaling, the culture medium (RPMI B27 complete) was supplemented with 50 ng/mL VEGFA; which is a typical concentration found in EC-specific media formulations. Tube formation was not detected, despite the addition of a potent proangiogenic growth factor. The mono- or co-cultured samples were also stained for alpha-actinin to view and quantify sarcomere arrangement and size. However, the only sarcomere formation that could be detected was in the mono-cultured CMs on Day 3 (Fig. 5.7).

5.5 Conclusions

This study demonstrates that a functional population of cardiomyocytes could be obtained by applying the Wnt pathway modulation protocol developed by Lian and Pelacek to the WTC hiPSC line. Although the hiPSC-CMs expressed alpha-actinin on visible sarcomeres in 2D culture, they did not do so in 3D encapsulation within the HyA-850 R hydrogel. Additionally, the hiPSC-CMs could not obtain a physiological beat rate with any of the applied culture conditions and contraction was not detectable after 3 days in the hydrogel. Furthermore, the hiPSC-CMs did not appear to support tube formation within the 3D matrix when co-cultured with hiPSC-ECs with or without VEGFA supplementation. This study demonstrated that the HyA-850 R hydrogel alone cannot support hiPSC-CM long-term survival and maturation. Additionally, the CM-EC co-culture does not appear to mimic physiological, mutually-beneficial paracrine signaling that occurs in the healthy human myocardium.[26-29]

5.6 References

1 Back, M. & Hansson, G. K. Anti-inflammatory therapies for atherosclerosis. *Nat Rev Cardiol* **12**, 199-211, (2015).

2 George, S. J., Johnson, Jason. *Atherosclerosis: Molecular and Cellular Mechanisms*. (Wiley-VCH Verlag GmbH & Co., 2010).

3 Chung, A. S. & Ferrara, N. Developmental and pathological angiogenesis. *Annu Rev Cell Dev Biol* **27**, 563-584, (2011).

4 Frangogiannis, N. G. The inflammatory response in myocardial injury, repair, and remodelling. *Nat Rev Cardiol* **11**, 255-265, (2014).

5 Benjamin, E. J., Blaha, M. J., Chiuve, S. E., Cushman, M., Das, S. R., Deo, R., de Ferranti, S. D., Floyd, J., Fornage, M., Gillespie, C., Isasi, C. R., Jimenez, M. C., Jordan, L. C., Judd, S. E., Lackland, D., Lichtman, J. H., Lisabeth, L., Liu, S., Longenecker, C. T., Mackey, R. H., Matsushita, K., Mozaffarian, D., Mussolino, M. E., Nasir, K., Neumar, R. W., Palaniappan, L., Pandey, D. K., Thiagarajan, R. R., Reeves, M. J., Ritchey, M., Rodriguez, C. J., Roth, G. A., Rosamond, W. D., Sasson, C., Towfighi, A., Tsao, C. W., Turner, M. B., Virani, S. S., Voeks, J. H., Willey, J. Z., Wilkins, J. T., Wu, J. H., Alger, H. M., Wong, S. S., Muntner, P., American Heart Association Statistics, C. & Stroke Statistics, S. Heart Disease and Stroke Statistics-2017 Update: A Report From the American Heart Association. *Circulation* **135**, e146-e603, (2017).

6 Ruvinov, E. S., Y.; Cohen, S. *Cardiac Tissue Engineering: Principles, Materials, and Applications*. (Morgan and Claypool Publishers Inc., 2014).

7 Laflamme, M. A. & Murry, C. E. Heart regeneration. *Nature* **473**, 326-335, (2011).

8 Cahill, T. J., Choudhury, R. P. & Riley, P. R. Heart regeneration and repair after myocardial infarction: translational opportunities for novel therapeutics. *Nat Rev Drug Discov*, (2017).

9 Coulombe, K. L., Bajpai, V. K., Andreadis, S. T. & Murry, C. E. Heart regeneration with engineered myocardial tissue. *Annu Rev Biomed Eng* **16**, 1-28, (2014).

10 Kraehenbuehl, T. P., Ferreira, L. S., Hayward, A. M., Nahrendorf, M., van der Vlies, A. J., Vasile, E., Weissleder, R., Langer, R. & Hubbell, J. A. Human embryonic stem cell-derived microvascular grafts for cardiac tissue preservation after myocardial infarction. *Biomaterials* **32**, 1102-1109, (2011).

11 Thomson, K. S., Korte, F. S., Giachelli, C. M., Ratner, B. D., Regnier, M. & Scatena, M. Prevascularized microtemplated fibrin scaffolds for cardiac tissue engineering applications. *Tissue Eng Part A* **19**, 967-977, (2013).

12 Lalit, P. A., Hei, D. J., Raval, A. N. & Kamp, T. J. Induced pluripotent stem cells for post-myocardial infarction repair: remarkable opportunities and challenges. *Circ Res* **114**, 1328-1345, (2014).

13 Nsair, A. & MacLellan, W. R. Induced pluripotent stem cells for regenerative cardiovascular therapies and biomedical discovery. *Adv Drug Deliv Rev* **63**, 324-330, (2011).

14 Jha, A. K., Tharp, K. M., Ye, J., Santiago-Ortiz, J. L., Jackson, W. M., Stahl, A., Schaffer, D. V., Yeghiazarians, Y. & Healy, K. E. Enhanced survival and engraftment of transplanted stem cells using growth factor sequestering hydrogels. *Biomaterials* **47**, 1-12, (2015).

15 WHO. *Global Atlas on cardiovascular disease prevention and control*. (2011).

16 Bearzi, C. G. C. PlGF–MMP9-engineered iPS cells supported on a PEG–fibrinogen hydrogel scaffold possess an enhanced capacity to repair damaged myocardium. *Cell Death and Disease* **5**, 1-9, (2012).

17 Garzoni, L. R., Rossi, M. I., de Barros, A. P., Guarani, V., Keramidas, M., Balottin, L. B., Adesse, D., Takiya, C. M., Manso, P. P., Otazu, I. B., Meirelles Mde, N. & Borojevic, R. Dissecting coronary angiogenesis: 3D co-culture of cardiomyocytes with endothelial or mesenchymal cells. *Exp Cell Res* **315**, 3406-3418, (2009).

18 Habib, M., Shapira-Schweitzer, K., Caspi, O., Gepstein, A., Arbel, G., Aronson, D., Seliktar, D. & Gepstein, L. A combined cell therapy and in-situ tissue-engineering approach for myocardial repair. *Biomaterials* **32**, 7514-7523, (2011).

19 Laflamme, M. A., Chen, K. Y., Naumova, A. V., Muskheli, V., Fugate, J. A., Dupras, S. K., Reinecke, H., Xu, C., Hassanipour, M., Police, S., O'Sullivan, C., Collins, L., Chen, Y., Minami, E., Gill, E. A., Ueno, S., Yuan, C., Gold, J. & Murry, C. E. Cardiomyocytes derived from human embryonic stem cells in pro-survival factors enhance function of infarcted rat hearts. *Nat Biotechnol* **25**, 1015-1024, (2007).

20 Sekine, H. S., T.; Hobo, K. Endothelial Cell Coculture Within Tissue-Engineered Cardiomyocyte Sheets Enhances Neovascularization and Improves Cardiac Function of Ischemic Hearts. *Circ Res* **118**, S145-S152, (2008).

21 Tulloch, N. L., Muskheli, V., Razumova, M. V., Korte, F. S., Regnier, M., Hauch, K. D., Pabon, L., Reinecke, H. & Murry, C. E. Growth of engineered human myocardium with mechanical loading and vascular coculture. *Circ Res* **109**, 47-59, (2011).

22 Ye, L., Chang, Y. H., Xiong, Q., Zhang, P., Zhang, L., Somasundaram, P., Lepley, M., Swingen, C., Su, L., Wendel, J. S., Guo, J., Jang, A., Rosenbush, D., Greder, L., Dutton, J. R., Zhang, J., Kamp, T. J., Kaufman, D. S., Ge, Y. & Zhang, J. Cardiac repair in a porcine model of acute myocardial infarction with human induced pluripotent stem cell-derived cardiovascular cells. *Cell Stem Cell* **15**, 750-761, (2014).

23 Giacomelli, E., Bellin, M., Sala, L., van Meer, B. J., Tertoolen, L. G., Orlova, V. V. & Mummery, C. L. Three-dimensional cardiac microtissues composed of cardiomyocytes and endothelial cells co-differentiated from human pluripotent stem cells. *Development* **144**, 1008-1017, (2017).

24 Libby, P., Ridker, P. M. & Hansson, G. K. Progress and challenges in translating the biology of atherosclerosis. *Nature* **473**, 317-325, (2011).

25 Lian, X., Hsiao, C., Wilson, G., Zhu, K., Hazeltine, L. B., Azarin, S. M., Raval, K. K., Zhang, J., Kamp, T. J. & Palecek, S. P. Robust cardiomyocyte differentiation from human pluripotent stem cells via temporal modulation of canonical Wnt signaling. *Proc Natl Acad Sci U S A* **109**, E1848-1857, (2012).

26 Brutsaert, D. L. Cardiac endothelial-myocardial signaling: its role in cardiac growth, contractile performance, and rhythmicity. *Physiol Rev* **83**, 59-115, (2003).

27 Tirziu, D., Giordano, F. J. & Simons, M. Cell communications in the heart. *Circulation* **122**, 928-937, (2010).

28 Leucker, T. M., Bienengraeber, M., Muravyeva, M., Baotic, I., Weihrauch, D., Brzezinska, A. K., Warltier, D. C., Kersten, J. R. & Pratt, P. F., Jr. Endothelial-cardiomyocyte crosstalk enhances pharmacological cardioprotection. *J Mol Cell Cardiol* **51**, 803-811, (2011).

29 Tousoulis, D., Kampoli, A. M., Tentolouris, C., Papageorgiou, N. & Stefanadis, C. The role of nitric oxide on endothelial function. *Curr Vasc Pharmacol* **10**, 4-18, (2012).

30 Jha, A. K., Mathur, A., Svedlund, F. L., Ye, J., Yeghiazarians, Y. & Healy, K. E. Molecular weight and concentration of heparin in hyaluronic acid-based matrices modulates growth factor retention kinetics and stem cell fate. *J Control Release* **209**, 308-316, (2015).

31 Jha, A. K., Tharp, K. M., Browne, S., Ye, J., Stahl, A., Yeghiazarians, Y. & Healy, K. E. Matrix metalloproteinase-13 mediated degradation of hyaluronic acid-based matrices orchestrates stem cell engraftment through vascular integration. *Biomaterials* **89**, 136-147, (2016).

32 Huebsch, N., Loskill, P., Mandegar, M. A., Marks, N. C., Sheehan, A. S., Ma, Z., Mathur, A., Nguyen, T. N., Yoo, J. C., Judge, L. M., Spencer, C. I., Chukka, A. C., Russell, C. R., So, P. L., Conklin, B. R. & Healy, K. E. Automated Video-Based Analysis of Contractility and Calcium Flux in Human-Induced Pluripotent Stem Cell-Derived Cardiomyocytes Cultured over Different Spatial Scales. *Tissue Eng Part C Methods* **21**, 467-479, (2015).

5.7 Tables

Table 5.1. Antibodies for immunofluorescence staining (IF) and flow cytometry (FC).

Antibody		Application
CD31	ThermoFisher, Mouse IgG1 Clone: WM59 Cat: MA1-26196	1:100 (IF)
CTnT	ThermoFisher, Mouse IgG1 Clone: 13-11 Cat: MS-295-P1	1:200 (IF, FC)
Alpha-actinin	Sigma Aldrich, Mouse IgG1 Clone: EA-53 Cat: A7811	1:100 (IF)
F-Actin	Cytoskeleton Inc., Acti-stain 555 phalloidin Cat: PHDH1-A	1:200 (IF)

5.8 Figures

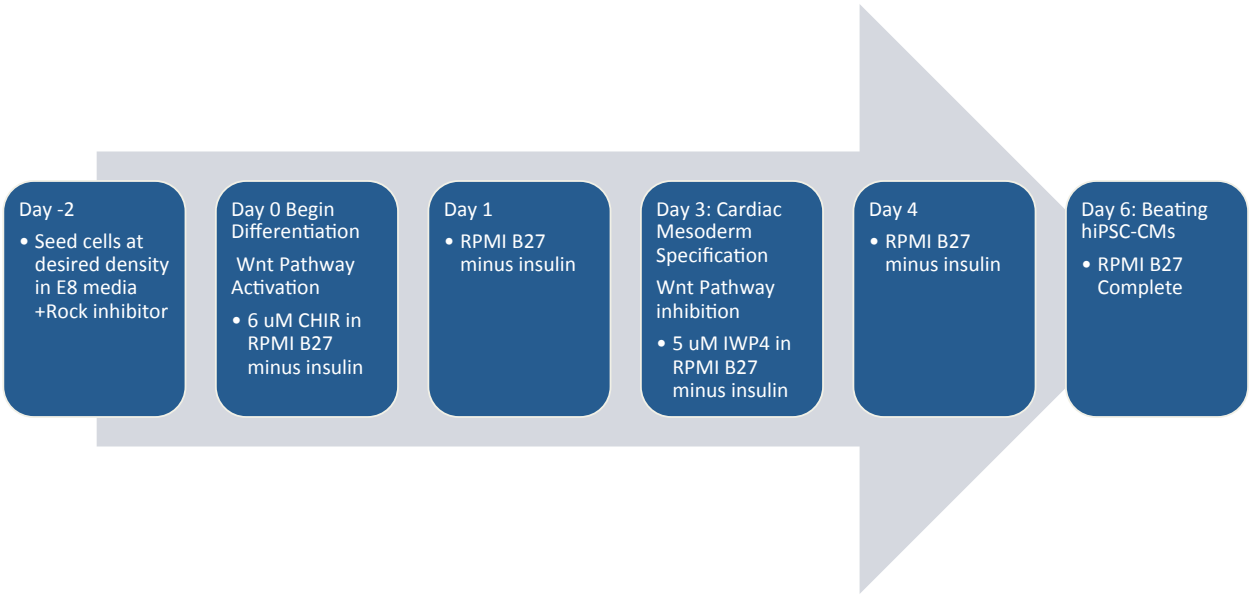

Figure 5.1. Schematic of the hiPSC-CM directed differentiation protocol.[25]

(a)

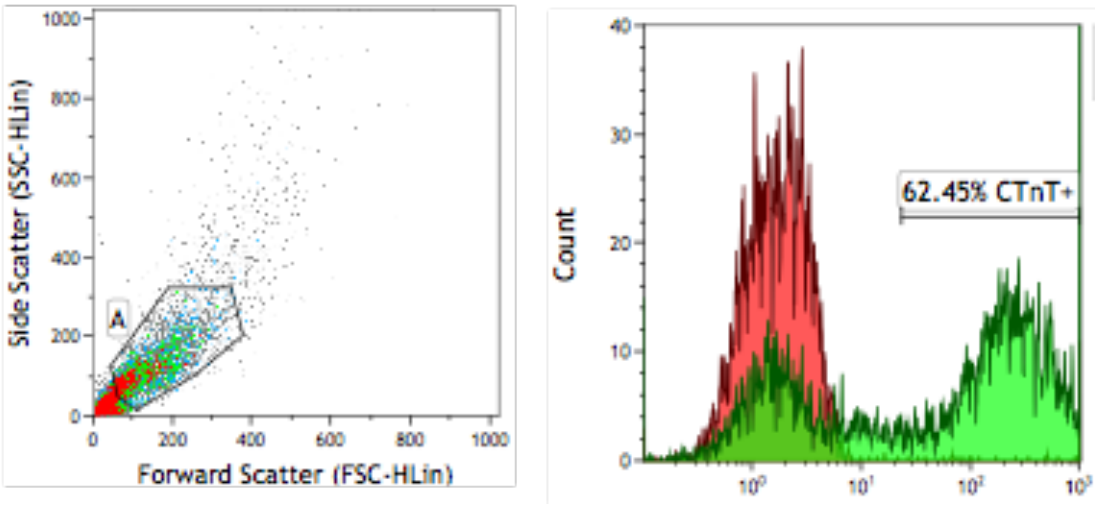

(b)

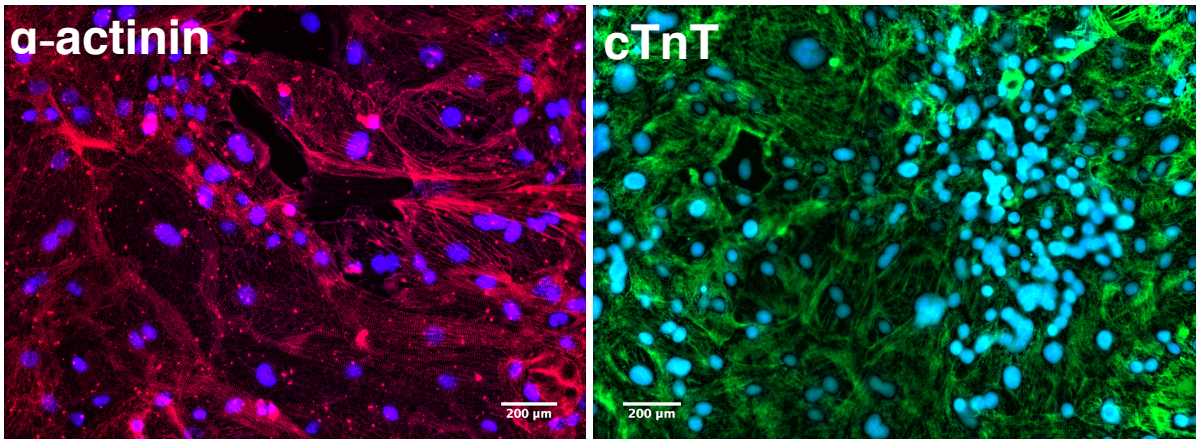

Figure 5.2. (a) flow cytomtometry analysis of unpurified WTC hiPSC-CM on Day 9 of differentiation for cardiac troponin T (cTnT) expression (a) fluorescence microscopy images of lactate purified hiPSC-CMs stained in 2D TCPS plate for sarcomeric alpha-actinin and cTnT.

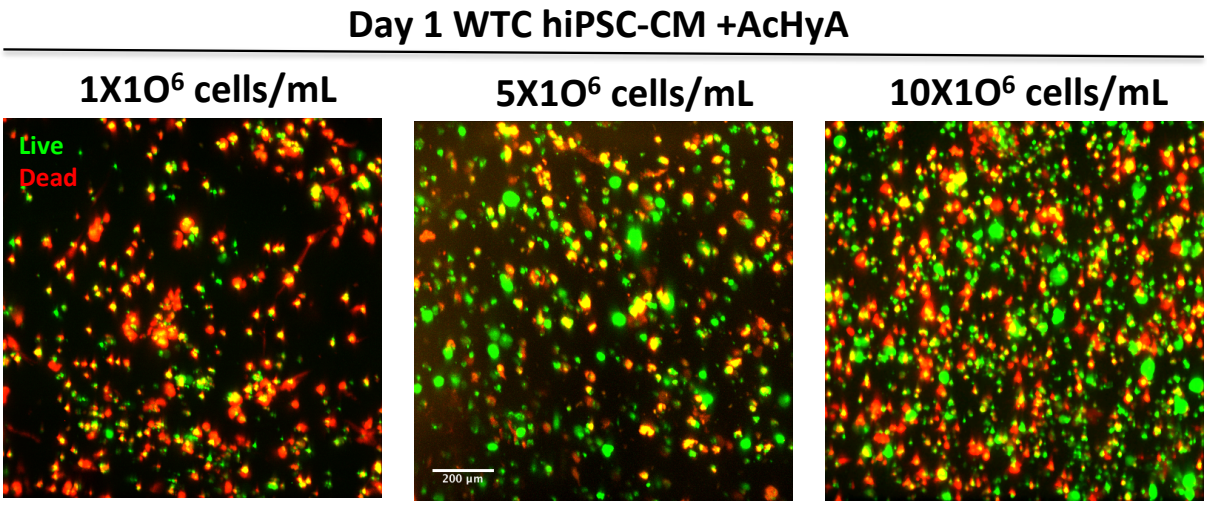

Figure 5.3. Representative confocal images of Live/Dead assay for hiPSC-CMs 24 hours after encapsulation in the AcHyA hydrogel at varying cell densities.

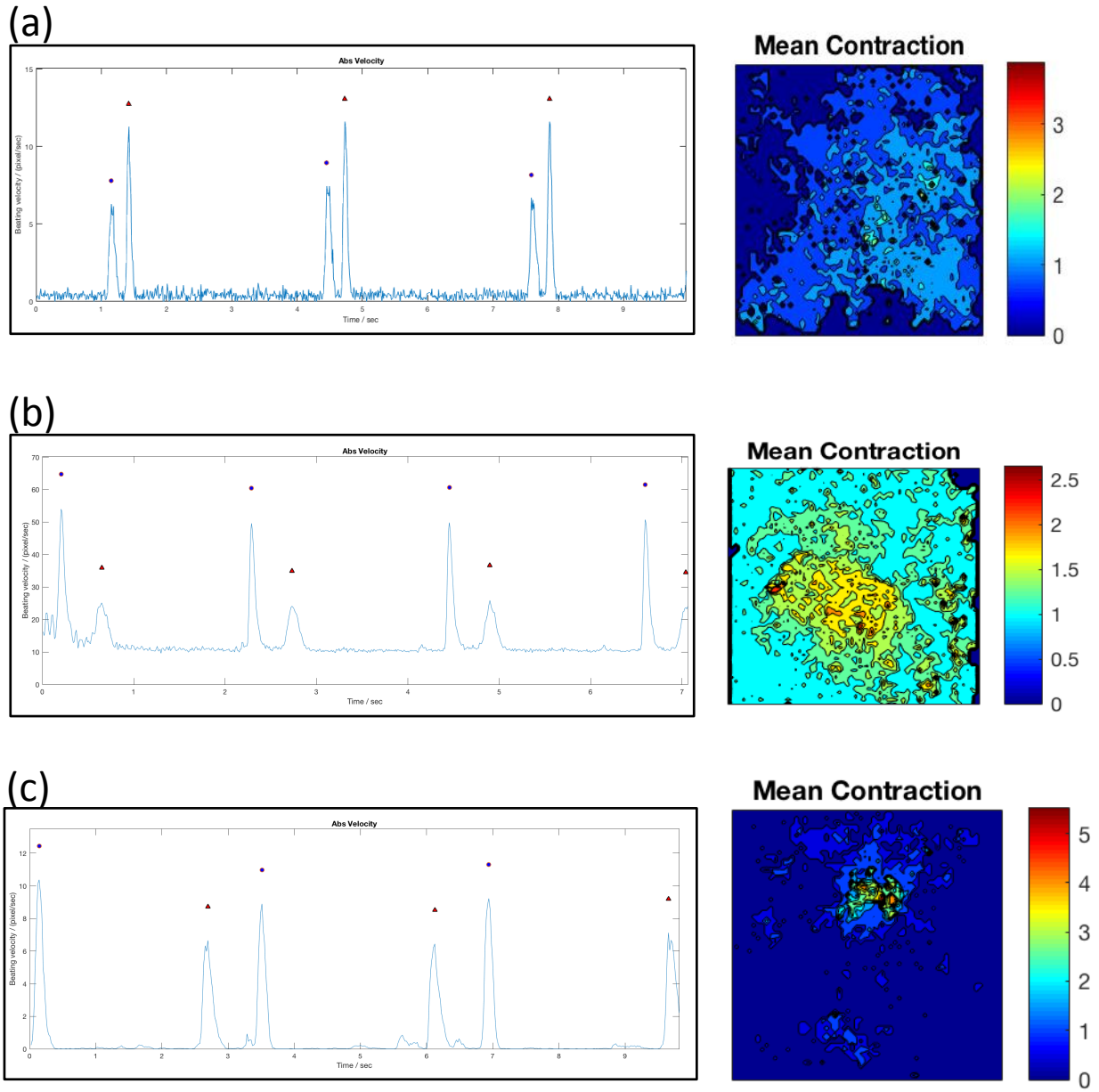

Figure 5.4. Day 3 post-encapsulation beating velocity of CM only and co-culture hydrogel samples with corresponding heat map depicting mean contraction obtained from video motion tracking analysis (a) hiPSC-CM only (b) Co-culture without VEGFA (C) Co-culture with VEGFA.

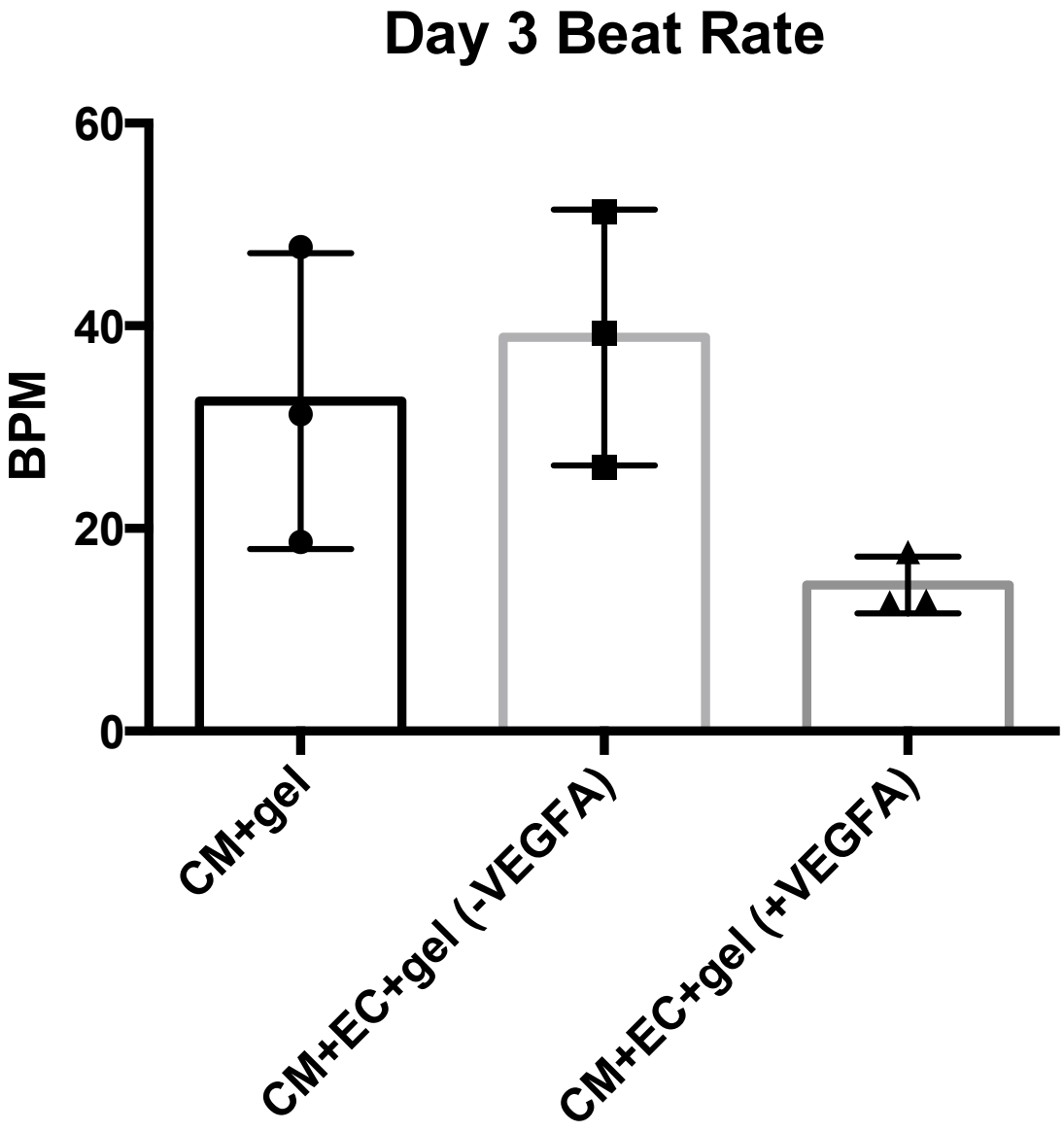

Figure 5.5. Summary of Day 3 post-encapsulation beat rate (bpm=beats per minutes) of CM only and co-culture hydrogel samples obtained from video motion tracking analysis.

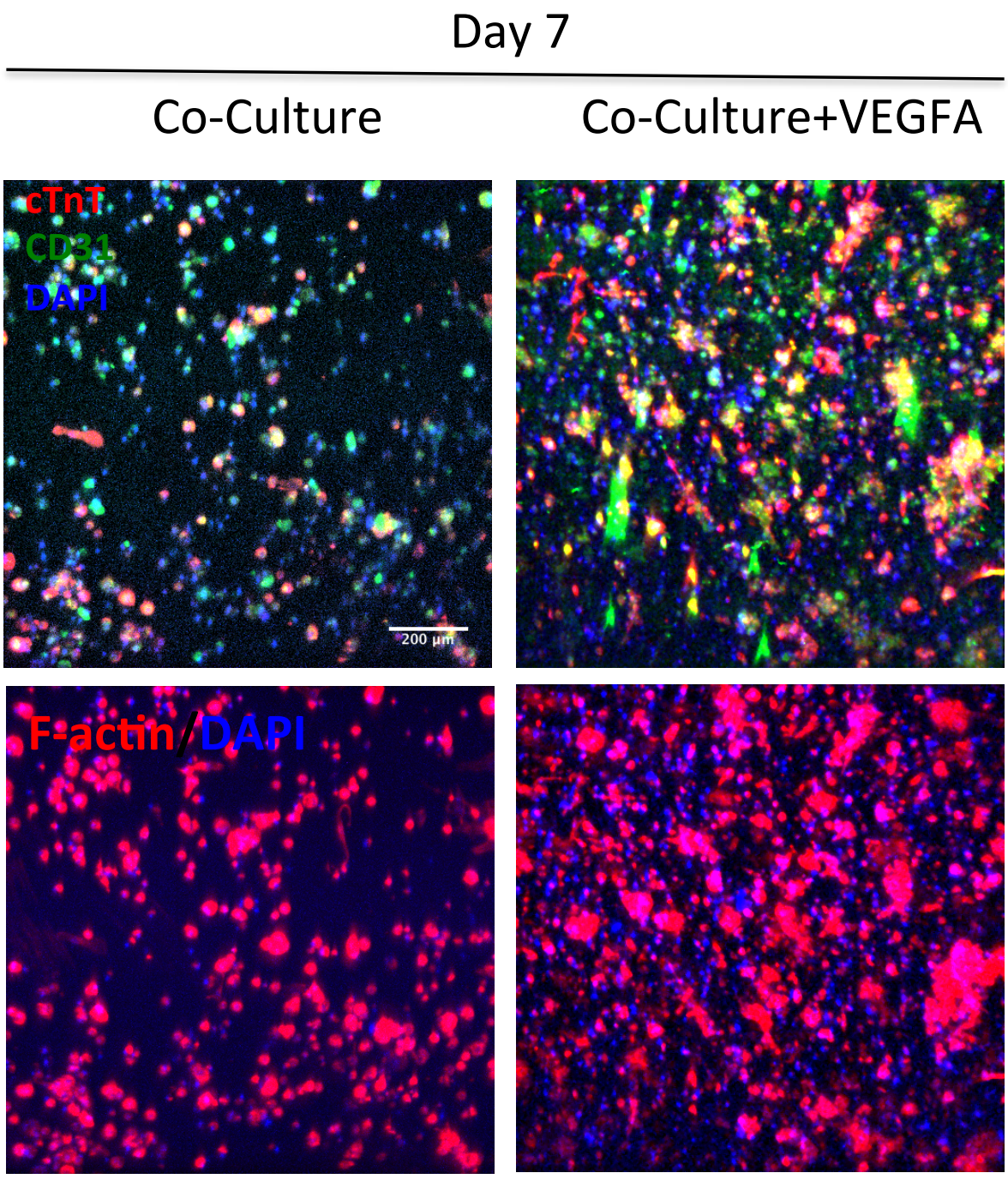

Figure 5.6. Representative confocal images of immunofluorescently stained co-culture hydrogel samples with or without VEGFA loading (top row: red=cTnT, green=CD31, blue=DAPI; bottom row: red=F-actin, blue=DAPI).

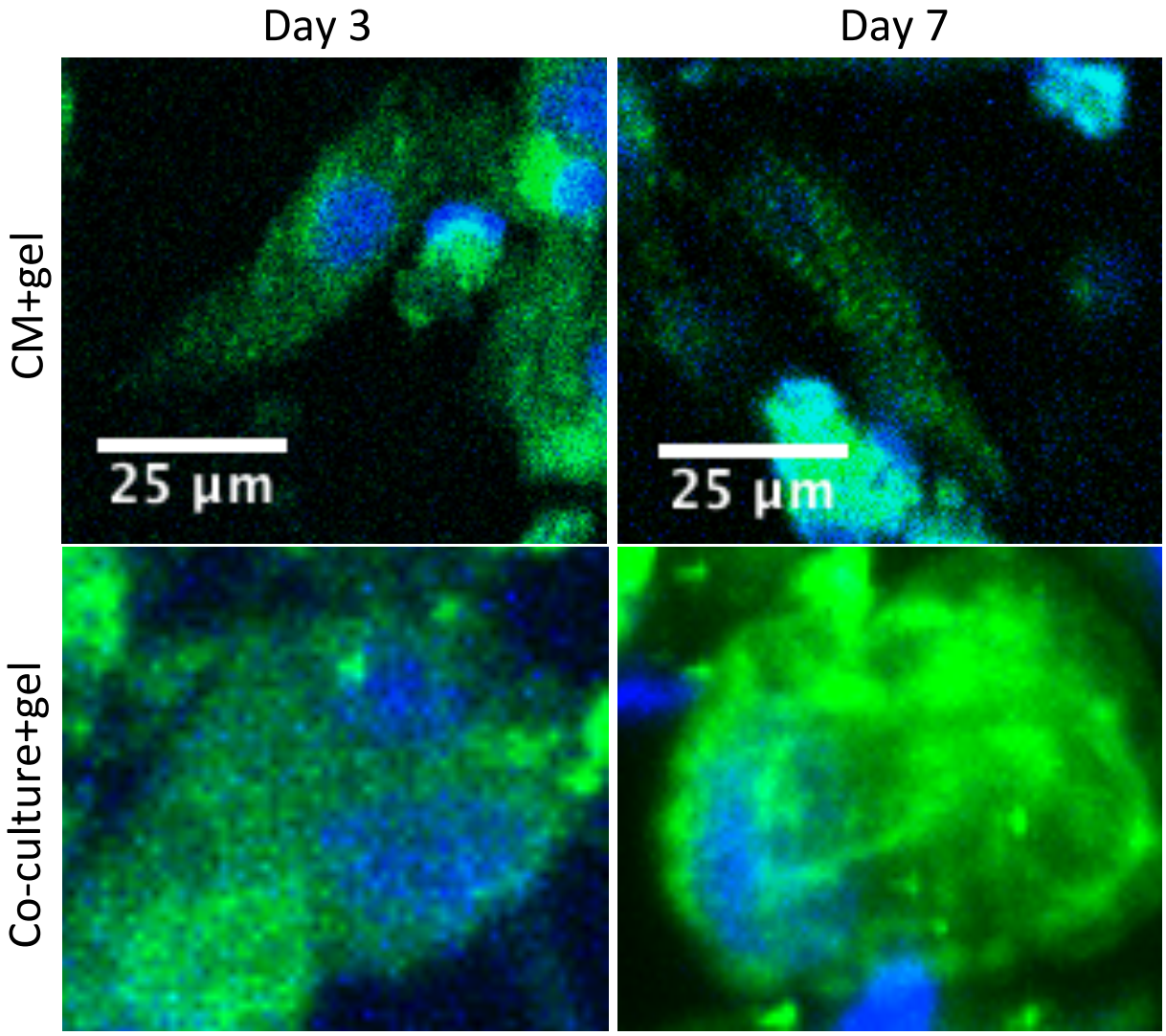

Figure 5.7. Representative confocal images of immunofluorescently stained hiPSC-CM only and Co-culture hydrogel samples for sarcomeric alpha-actinin.

CHAPTER 6:
CONCLUSIONS AND FUTURE DIRECTIONS

6.1 Conclusions

This dissertation presented a novel method for obtaining a CD31+ endothelial cell population from pluripotent stem cells that is validated through phenotype characterization, gene expression studies, and lineage-specific function assays. Further validation of the isolated hiPSC derived endothelial cells was demonstrated through a bioengineering-based approach by encapsulating the hiPSC-ECs in a bioinspired hyaluronic acid matrix. Finally, the effect of co-culturing the hiPSC-ECs with hiPSC-CMs was investigated by development and characterization of an in vitro cardiovascular tissue model.

Chapter 3 presented the validation of a 5-day hiPSC-EC differentiation protocol using a defined medium (E8) supplemented with proangiogenic factors. This method incorporated the Wnt, SMAD, and MEK/MAPK pathways that regulate embryonic vasculogenesis and angiogenesis. The differentiation protocol resulted in an endothelial cell population that expressed lineage-specific markers at earlier time points compared to previously reported methods, which was demonstrated by flow cytometry and RT-qPCR analysis. The early expression of EC markers likely occurred since the cells were already supplemented with TGF-β1 and bFGF from the complete E8 maintenance media prior to differentiation. This allowed the SMAD and MEK/MAPK pathways to be enhanced and directed to promote the endothelial cell lineage with the addition of BMP4, VEGF-A, and SB431542. The decreased expression of VEGFR2/KDR on day 7 could signify a shift to a more quiescent state through contact inhibition by the endothelial cell population as they became more confluent, and demonstrated that continuation of the differentiation process beyond day 5 was not necessary. Due to the sustained expression of endothelial lineage markers, the terminally differentiated population could be purified based on CD31+ expression. After a week of expansion, the sorted hiPSC-ECs took up Ac-LDL and formed stable networks in a Matrigel angiogenesis assay for up to three days, unlike HUVECs that typically regress within 12-24 hours. The purified population also maintained CD31/CD34 expression, increased VCAD and KDR expression, and diminished expression of CD45 and CD90. The hiPSC-EC's ability to perform lineage-specific functions and maintain endothelial marker expression shortly after sorting demonstrated a maturation stage after differentiation was not necessary, significantly reducing the duration of the protocol.

Chapter 4 verified the endothelial cells derived from this differentiation method could be used in a physiologically relevant *in vitro* angiogenesis model. The hiPSC-ECs ability to respond to biochemical and biophysical cues within a bioinspired matrix was demonstrated with dynamic, and corresponding changes in tube formation and nitric oxide production. First, it was confirmed that without proangiogenic signals, the encapsulated hiPSC-ECs did not sprout or self-assemble into capillary-like networks (HyA-850 R). The EC's ability to form stable networks once the system was cultured in the growth factor-rich endothelial growth medium, EGM2, (HyA-850 E) showed that like physiological

angiogenesis, the encapsulated hiPSC-ECs were dependent on proangiogenic signaling. Pathological angiogenesis could also be modeled with this system by loading the HyA hydrogel with excessively high concentrations of VEGF-A and TGF-β1 similar to a tumor microenvironment. During tumor angiogenesis, the upregulation of VEGF-A causes the formation of an unstable, high-density vasculature, which occurred in the HyA-850 EV. The HyA-850 ET system demonstrated stable capillary-like network formation, which modeled late-stage tumor progression where TGF-β1 promotes high-density angiogenesis. Our results are in agreement with a previous study that demonstrated TGF-β1 loaded in the HyA hydrogel promoted capillary-like network formation of mouse cardiac progenitor cells. Next, I demonstrated the encapsulated ECs responded to changes in matrix rigidity in a physiologically relevant manner that is in congruence with several published studies where slower, but more stable tube formation was seen in the stiffer matrix (HyA-850 E) compared to the softer matrix (HyA-170 E). The Griess assay further validated the system's physiologically relevant behavior, since higher NO production was detected in the HyA-850 E compared to the hydrogels loaded with high concentrations of proangiogenic growth factors (HyA-850 EV and HyA-850 ET), suggesting similarities with a tumor microenvironment for the latter. The dependence of tube formation on proangiogenic signaling and the potential for this angiogenesis model to be used in preclinical toxicology testing was further demonstrated by treating the HyA-850 E system with a small-molecule inhibitor of VEGFR2/FGFR (SU5402). As expected, the tube formation was responsive to inhibitor dosage and provided the calculation of an IC_{50} value that is in agreement with previous reports. Finally, tube patency and perfusion was demonstrated by loading the HyA-850 E in a microfluidic device that allowed fluid flow within the vascular network, consistent with a recent report using a modified differentiation protocol and fibrin as the matrix. The demonstrated sensitivity to microenvironmental changes and 3D capillary-like structure makes this system a physiologically relevant in vitro angiogenesis model for pre-clinical development and screening of anti-angiogenic or cardiovascular drugs.

Additionally, in Chapter 4, an analysis of the capillary burst valve that connects the media channels and main chambers in the tri-chamber microfluidic device was discussed and provided insight on why the 3 wt% HyA hydrogel (HyA-850) consistently "burst" through the CBV during loading. The analysis demonstrated that because the HyA is more viscous than water, it has a greater driving pressure difference at its leading edge during loading which exceeds the maximum pressure difference at the CBV to maintain a pinned meniscus. Furthermore, in order to keep the HyA from bursting the CBV, it needs to be loaded 10^4 times slower than water. Additionally, the analysis demonstrated that reducing the driving pressure difference during loading by changing the dimensions of the capillary burst valve also decreases the maximum hydrostatic pressure difference at the CBV. This indicates the 3wt% HyA hydrogel will continue to burst through the CBV regardless of the dimensional changes. Based on this study, and previous publications, which use gels with viscosities similar to water, it can be concluded that this microfluidic device design does not appear to be suitable for high viscosity liquids.

Chapter 5 presented the development of an *in vitro* cardiovascular tissue model that consisted of culturing hiPSC-CMs in the HyA-850 R hydrogel alone and with the hiPSC-ECs. A functional population of cardiomyocytes was obtained by applying the Wnt pathway

modulation protocol developed by Lian and Pelacek to the WTC hiPSC line. Although the hiPSC-CMs expressed alpha-actinin on visible sarcomeres in 2D culture, they did not do so in 3D encapsulation within the HyA-850 R hydrogel. The hiPSC-CMs could not obtain a physiological beat rate with any of the applied culture conditions and contraction was not detectable after 3 days in the hydrogel. Furthermore, the hiPSC-CMs did not appear to support tube formation within the 3D matrix when co-cultured with hiPSC-ECs with or without VEGF-A supplementation. From this study it can be concluded that the HyA hydrogel alone could not support hiPSC-CM long-term survival and maturation. Additionally, the CM-EC co-culture does not appear to mimic the physiological, mutually beneficial paracrine signaling that occurs in the healthy human myocardium.

6.2 Future Directions

The future directions of this research should aim to examine the following topics:

- The novel differentiation protocol developed in this study focused on producing, characterizing, and isolating a robust and functional endothelial cell population. It would be interesting to further characterize the CD31-/CD34+ and CD31-/CD45+ populations that are present at the end of the differentiation since this phenotype expression is indicative of hematopoietic stem cell or endothelial progenitor cell lineages. It may be possible these populations are the same group and could be further differentiated to monocyte/macrophage, lymphocyte, or smooth muscle cell lineages.
- Additionally, the field of vascular tissue engineering is moving toward identifying arterial and venular endothelial cell subtypes from the directed differentiation protocols. The EC differentiation protocol described in this study could be producing a specific EC subtype that may be ideal for tissue-specific studies such as developing multicellular *in vitro* constructs with hiPSC-CM or hiPSC-hepatocytes.
- Furthermore, culturing the hiPSC-ECs in the HyA hydrogel with the addition of exogenous growth factors may also influence the subtype lineage and make the system more effective as an *in vitro* drug toxicity screening platform or organ-specific regenerative therapy.
- This study demonstrated the encapsulated hiPSC-ECs could form stable, perfusable capillary tubes in an engineered matrix. *In vivo* studies could move this system from being an *in vitro* angiogenesis model to a regenerative therapy for ischemic tissues. However, since the encapsulate hiPSC-ECs cultured in EGM2 showed the most stable long-term tube formation, it would be beneficial to determine which components and growth factors in this media are most effective and which ones are unnecessary in order to limit the amount of exogenous factors used *in vivo*.
- The study to develop a cardiovascular tissue model demonstrated that hiPSC-CMs and hiPSC-ECs derived from the same stem cell source were not interacting in a physiologically relevant manner. Several factors could be affecting this and need to be further investigated before this model can be functional. These factors include cell lineage maturity, stromal cell addition, matrix degradation rate, and culture media components.